

**Identifying Opportunities for Increasing the Milling Efficiency
of a Bushveld Igneous Complex (BIC) Upper Group (UG) 2
Ore**

Gwiranai Danha

**A Thesis submitted to the Faculty of Engineering and the Built
Environment, University of the Witwatersrand, in fulfilment of the requirements
for the Doctor of Philosophy in Engineering**

Johannesburg, 2013

DECLARATION

I hereby declare that the work set out in this thesis is the result of my own original research, and that it has not been submitted for another degree at any other university or institution.

Signed:

Gwiranai Danha

Date: 18/10/2013

ABSTRACT

The aim of this thesis was to identify opportunities to increase the milling efficiency of a UG2 ore. In order to achieve this task, we first characterized the feed material using a simple method that relies only on the breakage kinetic data and knowledge of basic process modelling skills. The initial results obtained from our test work partially validated the hypothesis that the material was made up of at least two components (heterogeneous), since the results could not eliminate the possibility of the presence of weaker particles in the feed. A heterogeneous and a homogeneous (single component) ore containing weaker particles have similar breakage behaviour, because in both cases the 'softer' or weaker particles break first, followed by the 'harder' or stronger.

We then employed a more direct method of characterization in which we used an Atomic Absorption Spectrometer (AAS) to analyze the concentration of the element copper. Copper was used as a tracer element for the rich mineral phase of platinum group metals (PGMs), because the mode of occurrence of PGMs is such that they are associated with base metals. The results of this investigation confirmed the presence of a 'soft' mineral phase that does not contain much copper. We also found that the concentration of copper in the larger-sized particles increases with grinding time, which provides evidence of the presence of another, 'harder' mineral phase that contains copper and hence PGMs. By using this method we confirmed that the feed material was heterogeneous.

After establishing the nature of the ore's composition, we tested the further hypothesis that it may be possible to mill selectively, to retain the desired mineral phase and discard the undesired. The anticipated benefits of achieving selective milling are that it would reduce the amount of energy required by the mill; require a smaller mill size; and greatly improve overall mineral recoveries, as only material of value would be processed. For the particular ore and conditions tested here, we evaluated an average value for the fraction of the soft component in the feed to be 0.5620. If this fraction is successfully separated out, then the secondary or subsequent mill size can be reduced by 56.2%. Our experimental results proved that it is possible to achieve selective milling by varying the slurry density and the grinding period in a mill.

We then used the Attainable Region (AR) method to find ways of reducing the grinding period and grinding energy required to achieve a specific result; and also of maximizing the amount of material in the desired size range. No work on utilizing the AR technique to optimize the size reduction of a real industrial ore in slurry has been published as yet, although researchers have used the method for comminution carried out under dry conditions and on test material. Although the investigation reported in this thesis is not intended to set out ideal operating parameters for industrial mills, it aims to show how the AR technique can be used to develop some ways of improving mill performance. The experimental results we obtained proved that this method could be successfully applied to identifying opportunities for higher efficiency in milling a typical industrial ore. A solids concentration of 33% by mass, milled for between 15–30 minutes, gave us the maximum amount of material in the intermediate size class.

An AR plot is dependent on set cut-off points, so if the set points change, a cumbersome manual process has to be undertaken to come up with a new AR plot. For this reason, we then proposed, developed and demonstrated an AR programme that allows changes to be made by simply re-entering new product set points. The results show that the software saves the user a considerable amount of time and labour (we estimate the time saving involved in using the software in place of the manual procedure at about 90%).

ACKNOWLEDGEMENTS

I would like to express my sincere gratitude to my academic supervisors, Professors Diane Hildebrandt and David Glasser, for their inspired guidance, patience and motivation throughout this work. A big thank you.

Special mention goes to Pippa Lange, Dr. Metzger, Professor Bwalya and Professor Moys for their helpful suggestions and the numerous corrections they recommended to earlier drafts of the thesis.

To all members of COMPS, staff and students alike, thank you for your support and the different roles you played for the duration of my studies at WITS. Communion guys: I could not have done it without your positive attitude and good team work during the weekly group meetings.

I would also like to acknowledge the debt I owe to my family and friends, especially Clayton, Pheneas, Tirivaviri, Joshua and Evans, who were always there for me. Your presence in my life is a blessing.

CONTENTS	PAGE
DECLARATION.....	ii
ABSTRACT	iii
ACKNOWLEDGEMENTS	vi
LIST OF FIGURES.....	xi
LIST OF TABLES.....	xvi
1 INTRODUCTION	1
1.1 Objectives of this thesis	4
1.2 Thesis outline	5
2 BACKGROUND AND LITERATURE REVIEW.....	9
2.1 Mineral and ore	9
2.2 Mineral processing	10
2.3 Comminution in the mineral processing industry.....	11
2.3.1 Mineral liberation	13
2.4 Mineral beneficiation approach	15
2.4.1 Wet grinding	17
2.5 Particle Size Distribution (PSD) representation methods.....	25
2.5.1 Graphical representation of sizing analyzes	27
2.5.2 The Attainable Region (AR) Method.....	31
2.6 The characteristics of the feed material	37
2.7 Mineralogical analysis	42
2.8 References.....	43
3 THE LABORATORY EQUIPMENT USED.....	48
3.1 Sample preparation equipment.....	48
3.1.1 Jones Riffle Splitter.....	48

3.1.2	Cone and quartering	49
3.2	Milling equipment	50
3.2.1	Tumbling ball mill	50
3.3	Size analysis equipment	54
3.3.1	Test sieves	54
3.3.2	Mastersizer 2000MU	58
3.4	Filtration equipment.....	60
3.4.1	Buchner funnel	60
3.5	Analytical equipment.....	61
3.5.1	Atomic Absorption Spectrometer (AAS).....	61
3.6	References.....	63
4	EXPERIMENTAL SET- UP AND PROCEDURE.....	64
4.1	Sample preparation.....	66
4.2	Milling.....	66
4.2.1	Mill calibration.....	68
4.2.1.1	Torque calibration procedure	70
4.2.1.2	Speed calibration procedure	73
4.3	Particle size analysis and classification.....	76
4.3.1	Particle size analysis	76
4.3.2	Classification	78
4.4	Atomic Absorption Spectrometer (AAS) calibration.....	79
4.4.1	AAS analysis	80
4.5	References.....	81
5	LABORATORY SCALE APPLICATION OF BREAKAGE KINETICS DATA TO CHARACTERIZE AN UPPER GROUP (UG) 2 ORE.....	82

5.1	Introduction	82
5.1.1	Mineral processing circuits	83
5.1.2	Process modelling	84
5.1.3	Particle size classification	86
5.2	Kinetic approach to grinding.....	86
5.3	Experimental procedure	92
5.4	Discussion of experimental results.....	92
5.4.1	Results for the intermediate size class material.....	104
5.5	Conclusion	107
5.6	References.....	109
6	USE OF THE ATOMIC ABSORPTION SPECTROMETER ANALYSIS TO CHARACTERIZE THE UG2 ORE.....	111
6.1	Introduction	111
6.1.1	The atomic absorption spectrometer (AAS) characterisation technique ..	112
6.2	Experimental procedure	113
6.3	Analysis and discussion of results based on the AAS technique	115
6.4	Conclusion	127
6.5	References.....	128
7	A LABORATORY SCALE APPLICATION OF THE ATTAINABLE REGION TECHNIQUE ON UG2 ORE.....	129
7.1	Introduction	129
7.1.1	Size reduction of ores	130
7.1.2	The Attainable Region (AR) analysis method	131
7.2	Experimental procedure	131
7.3	Analysis and discussion of results according to the AR technique.....	132
7.4	Conclusion	146

7.5	References.....	148
8	DEVELOPMENT AND DEMONSTRATION OF A PROPOSED ATTAINABLE REGION PROGRAMME	150
8.1	Introduction	150
8.2	Particle population grouping.....	151
8.3	Describing grinding as a reaction process	152
8.4	Demonstration of the current AR procedure.....	153
8.5	Preparation of data for AR analysis.....	159
8.5.1	Mill power	159
8.6	Demonstration of the proposed AR programme.....	162
8.7	Conclusions.....	164
8.8	References.....	165
9	CONCLUSIONS	166
10	RECOMMENDATIONS	169
	APPENDIX A: CLASSIFICATION OF PRODUCT MATERIAL INTO THREE SIZE CLASSES.....	170
	APPENDIX B: COMPARISON OF HETEROGENEOUS AND HOMOGENEOUS MODEL PARAMETERS.....	176
	APPENDIX C: PARTICLE SIZE DISTRIBUTION (PSD) AND ATOMIC ABSORPTION SPECTROMETER (AAS) RESULTS	184
	APPENDIX D: MILL ENERGY CONSUMPTION DURING MILLING	189
	APPENDIX E: THE AR PROGRAMME OPERATING PROCEDURE	191
	APPENDIX F: DATA SOURCE FILE.....	196

LIST OF FIGURES

Figure 2.1: Liberation of valuable minerals by size reduction.....	11
Figure 2.2: Typical Mineral Beneficiation Flow-sheet	16
Figure 2.3: Mode of operation of a ball mill	20
Figure 2.4: Gates/Gaudin/Schumann	27
Figure 2.5: A typical Rosin Rammler plot	28
Figure 2.6: Typical log probability plots	29
Figure 2.7: A typical Attainable Region Plot of mass fraction of material in the intermediate size class versus mass fraction of material in the feed size class (this graph was obtained from Chapter 7, section 7.3, Figure 7.7).....	36
Figure 2.8: Typical PGM flowchart	38
Figure 2.9: A typical PGM plant milling/concentrator circuit	39
Figure 3.1: Jones Riffle Splitter	49
Figure 3.2: Cone and quartering (www.nzdl.org).....	50
Figure 3.3a: Rear view of the tumbling ball mill equipment in the Mineral Processing laboratory at the University of the Witwatersrand.....	52
Figure 3.3b: Front view of the ball mill charged with a slurry and grinding media	53
Figure 3.4: Stacked sieves used for a size test.....	54
Figure 3.5: The Malvern particle size analyzer.....	58
Figure 3.6: Atomic Absorption Spectrometer (AAS)	61
Figure 4.1: Experimental programme flowchart.....	65
Figure 4.2: Torque calibration section of the mill equipment	69
Figure 4.4: Plot of the relationship between the speed settings on the mill and the actual speed of rotation of the mill.	75
Figure 4.5: A typical frequency plot from the Mastersizer.....	77

Figure 4.6: A typical cumulative plot from the Mastersizer	77
Figure 5.1: The particle size distribution (PSD) of the feed material used for the experiments. The size ranges of the feed size class (class 1), the intermediate size class (size class 2) and the fines (size class 3) are shown on the Figure.	93
Figure 5.2: Mass fraction of feed size class material with different solid contents versus grinding time.....	94
Figure 5.3: A log plot of the ratio of the mass fraction of material remaining in the feed size class after grind time, t , compared with the mass fraction of the material in the feed size class before grinding, versus grinding time, with different percentages of solids in the slurry.	95
Figure 5.4: Comparison of a single–component and a two–component model, against experimental data for mass fraction of feed size class material remaining after a grind time t , under dry milling conditions	98
Figure 5.5: Comparison of a single–component and a two–component model, against experimental data for mass fraction of feed size class material remaining after a grind time t , with a 50% solids content.	99
Figure 5.6: Comparison of homogeneous versus heterogeneous models, against experimental data for mass fraction of feed size class material remaining after a grind time t , with a 33% solids content.	99
Figure 5.7: Comparison of a single–component and a two–component model against experimental data for mass fraction of feed size class material remaining after a grind time t , with a 25% solids content.	100
Figure 5.8: Comparison of homogeneous and heterogeneous models against experimental data for mass fraction of feed size class material remaining after a grind time t , with a 20% solids content.	100
Figure 5.9: Specific rates of breakage of soft and hard components of the ore, versus percentage solids content.	102
Figure 5.10: General block diagram of mill set-up used to achieve selective grinding and separation of the soft component from the harder component.	104

Figure 5.11: A typical comparison of homogeneous and heterogeneous models against experimental data for the mass fraction of intermediate size class material remaining after a grind time t , with 20% solids content.	105
Figure 5.12: Specific rates (S_{2A} , S_{2B}) of breakage of the soft and hard components of the ore in the intermediate size class, versus percentage solids content.	106
Figure 6.1: Plot of the mass percentage of material retained on each sieve against sieve size for the feed material and after 10 and 30 minutes of grinding.....	115
Figure 6.2: The cumulative mass percentage of material passing a sieve size against the sieve size for the feed material, after 10 and 30 minutes of grinding	115
Figure 6.3: Mass of the sample digested against sieve size for the feed material and after 10 and 30 minutes of grinding. The mass is measured to the accuracy of the scale, namely 0.01g	117
Figure 6.4: Plot of the concentration of copper in a digested sample against sieve size for the feed material and after 10 and 30 minutes of grinding	117
Figure 6.5: The percentage by mass of copper in a digested sample against particle size for the feed material and after 10 and 30 minutes of grinding.....	118
Figure 6.6: Plot of the mass of copper in a sample retained on each sieve against that sieve size for the feed material and after 10 and 30 minutes of grinding	118
Figure 6.7: The percentage by mass of copper in a sample retained on a sieve against that sieve size for the feed material and after 10 and 30 minutes of grinding.....	119
Figure 6.8: Change in mass percentage of copper against particle size for the feed material and after 10 and 30 minutes of grinding	119
Figure 6.9: Natural logarithm of the ratio of mass of copper remaining on the largest sieve size (425 μ m) after a certain grinding time to that initially on that sieve against grinding time.....	120
Figure 6.10: Plot of the measured mass fraction of copper on largest sieve (425 μ m) versus predicted mass percentage of the hard component in the largest size class...	120

Figure 7.2: Mass fraction of material in the feed size class versus grinding time for different solid concentrations.....	133
Figure 7.3: Mass fraction of material in the intermediate size class versus grinding time for different solid concentrations.	133
Figure 7.4: Mass fraction of material in the intermediate size class versus grinding time for 33% solids concentration.	134
Figure 7.5: Mass fraction of material in the fines size class versus grind time for different solid concentrations.....	134
Figure 7.6: Mass fraction of material in the intermediate size class versus the mass fraction of material in the feed size class for different solids concentrations.	137
Figure 7.7: Mass fraction of material in the intermediate size class versus the mass fraction of material in the feed size class for 33% solids concentration.....	138
Figure 7.8: Mass fraction of material in the fines size class versus the mass fraction of material in the feed size class for different solids concentrations.....	138
Figure 7.9a: Mass fraction of material in the fines size class versus the mass fraction of material in the feed size class for 33% solids concentration.	139
Figure 7.9b: Flow sheet development including a by-pass stream in order to maximize fines production or minimize production of intermediate sized particles for a given mass% feed material in the product.	141
Figure 7.10: Grinding energy versus grinding time for different concentrations of solids	142
Figure 7.11: Grinding energy versus mass fraction of material in feed size class for different concentrations of solids.....	142
Figure 7.12: Grinding energy versus mass of material in intermediate size class for different concentrations of solids.....	143
Figure 7.13: Grinding energy versus mass of material in intermediate size class for 33% solids concentration.....	143

Figure 7.14: Grinding energy versus mass fraction of material in fines size class for different concentrations of solids.....	144
Figure 8.1: A cumulative mass % of material passing a particle size versus particle size for different dry grinding periods (this graph is obtained from Appendix A, Figure A1).	153
Figure 8.2: Cumulative mass % of material passing a particle size versus particle size. We redefined the size classes to make size class 1 above 75 μ m, size class 2 to be between 45-75 μ m and size class 3 below 45 μ m.....	155
Figure 8.3: Example of an AR plot of the mass fraction of material in the intermediate size class versus the mass fraction of material in the feed size class. In the red curve size class 2 lies between 15-45 μ m while in the blue curve size class 2 is between 45-75 μ m.	157
Figure 8.4: Comparison of actual energy measured against model prediction, for a 50% by mass solids concentration.	162
Figure 8.5: The user interface of the AR programme	163
Figure A 1: A plot of volume percentage of material below a particle size vs particle size for different dry grinding times.....	170
Figure A 2: A plot of volume percentage of material below particle size vs particle size for different grinding times with 50% solids content.	171
Figure A 3: A plot of volume percentage of material below particle size vs particle size for different grinding times with 33% solids content.	172
Figure A 4: A plot of volume percentage of material below particle size vs particle size for different grinding times with 25% solids content.	173
Figure A 5: A plot of volume percentage of material below particle size vs particle size for different grinding times with 20% solids content.	174
Figure E 1: Userform1 inter-phase	193
Figure E 2: Mill details inter-phase	194
Figure E 3: Userform1 inter-phase with selected samples to be processed.....	195

LIST OF TABLES

Table 4.1: Mill and experimental specifications	68
Table 4.2: Relationship between the torque and voltage for cumulative masses	71
Table 4.3: Relationship between the speed settings and actual speed of the mill.....	74
Table 5.1: Size classes specification.....	93
Table 5.2: Model parameter values for model described by Equation 5.7.....	96
Table 5.3: Model parameter values with fixed ϕ for model described by Equation 5.7..	97
Table 5.4: Model parameter values, described by Equation 5.7.....	97
Table 5.5: Model parameter values for model described by Equation 5.10.....	106
Table 6.1: Relationship between the predicted mass fraction of the hard component and the measured mass fraction of copper in the largest size class	126
Table 8.1: Attainable Region data	154
Table 8.2: AR data	156
Table A 1: Size classification based on Figure A1	170
Table A 2: Size classification based on Figure A2	171
Table A 3: Size classification based on Figure A3	172
Table A 4: Size classification based on Figure A4	173
Table A 5: Size classification based on Figure A5	174
Table A 6: Ratio of the natural logarithm of the mass fraction of material remaining in the feed size class after grinding time t, to the initial, with different solids content	175
Table B 1: Excel solver estimated parameters for heterogeneous and homogeneous models for the feed size class with 100% solids content.....	176
Table B 2: Excel solver estimated parameters for heterogeneous and homogeneous models for 50% solids content	176

Table B 3: Excel solver estimated parameters for heterogeneous and homogeneous models for 33% solids content	177
Table B 4: Excel solver estimated parameters for heterogeneous and homogeneous models for 25% solids content.	177
Table B 5: Excel solver estimated parameters for heterogeneous and homogeneous models for 20% solids content.	178
Table B 6: Excel solver estimated parameters for heterogeneous and homogeneous models for the intermediate size class with 20% solids content.....	179
Table B 7: Excel solver estimated parameters for heterogeneous and homogeneous models for the intermediate size class with 25% solids content	180
Table B 8: Excel solver estimated parameters for heterogeneous and homogeneous models for the intermediate size class with 33% solids content.....	181
Table B 9: Excel solver estimated parameters for heterogeneous and homogeneous models for the intermediate size class with 50% solids content.....	182
Table B 10: Excel solver estimated parameters for heterogeneous and homogeneous models for the intermediate size class with 100% solids content.....	183
Table C 1: PSD data for the feed sample.....	184
Table C 2: PSD data for the sample after 10mins of grinding	184
Table C 3: PSD data for the sample after 30mins of grinding	185
Table C 4: AAS results for the feed samples.....	186
Table C 5: AAS results for the samples after 10 minutes of grinding	187
Table C 6: AAS results for the samples after 30 minutes of grinding	188
Table D 1: Energy used for grinding with 50% solids content	189
Table D 2: Energy used for grinding with 33% solids content	189
Table D 3: Energy used for grinding with 25% solids content	190
Table D 4: Energy used for grinding with 20% solids content	190

CHAPTER 1

1 INTRODUCTION

Mechanical size reduction of solids (comminution) is a unit operation that is basic to many industries involved in the processing of solid materials. The fundamental objectives of comminution in mineral processing are not merely to reduce the particle size but to 'free' the constituent minerals that make up an ore, so that valuable components can be separated from the waste.

The current trend in mineral processing is towards the exploitation of low grade ores as the high grade ones become depleted. The effective liberation of values from these low grade ores remains one of the major challenges for mineral processors. Comminuting the ore to fine particle sizes has been proposed as a possible solution to this problem, but it has disadvantages in terms of high energy and milling costs, and low recoveries due to high mineral losses in subsequent processes. In downstream separation processes, for example in froth floatation, the fine material does not attach properly to the rising air bubbles, and hence does not float well. It is our hypothesis in this work that efficient size reduction and liberation from low grade ores (as exemplified by UG2) can be achieved by designing/retrofitting and operating comminution circuits in a way that will convert the maximum of energy input into selective grinding, in this way producing an optimum amount of the desired size of fragments.

In South Africa, there are broadly three ore bodies containing basic Platinum Group Metals (PGMs), namely, the Merensky Reef, the UG2 Reef and the Platreef. Initially the Merensky Reef was the major source of PGMs, but as the deposits at or near the surface have become depleted, the attention of the mining industry has turned increasingly to the lower-grade UG2 Reef. We obtained the material used in this study from Anglo Platinum's Amandelbult UG2 plant.

We characterized the material using breakage kinetics data, in order to test the hypothesis that the ore possesses multiple components, each of a different hardness. After inferring the heterogeneity of the ore, we ran a few samples of the ore on the Atomic Absorption Spectrometer (AAS) to check for the presence of more than a single component in the ore. After characterizing the ore as heterogeneous, we then applied an Attainable Region (AR) optimization method to the milling data. Within the limits of the experimental investigation, we were able to specify the optimum slurry density for our objective of maximizing the amount of material in the intermediate size range for this PGM ore.

In many industrial operations, the desired product lies in an intermediate particle size range. Processing a feed size range is normally associated with low mineral recoveries, as most of the values remain locked up in the particles. Although the intention may be to reduce the size of the feed material, excessive comminution to break the material into the fine size class presents many difficulties. These include increased cohesion of smaller particles and inhalation concerns because of the increased likelihood of their

becoming entrained. In addition, grinding beyond the desired size class results in over-grinding, which is a waste of time and energy and therefore inefficient. For all these reasons, an intermediate size is the best choice for many downstream operations.

It is known from laboratory and industrial tests that the rate of breakage of a material is faster in wet than in dry milling, hence the choice of wet milling for this investigation. The best milling conditions are produced by an optimum slurry density that is high enough to fill the active breakage regions with material, yet low enough to prevent the fluid slurry from adhering to the walls of the mill. Tangsathitkulchai and Austin (1985) set this optimum at 45 volume percent solids for quartz, coal and copper ore. However, there is no quantitative rule to predict optimum slurry density (Tangsathitkulchai, Austin 1985), because optimal conditions depend on the physical properties; mineralogical composition; degree of heterogeneity and fineness of grind. Moreover, no optimal slurry densities have been reported for the PGM ore used in this study. We propose the AR described in research as a method that can be used to predict or specify optimum slurry conditions for this ore.

The AR is a fundamental approach that is equipment-independent and used in the field of comminution to describe breakage processes (Khumalo et al., 2006, 2007, 2008). A complete Attainable Region analysis requires us to describe the set of all possible outputs for a system (Khumalo et al. 2008). Previous researchers, Metzger et al. (2009) and Khumalo et al. (2007) have used the AR method only for comminution carried out under dry conditions. Both of these studies investigated the application of the approach

to the milling of a test material, silica sand for the former and silica sand and quartzite for the latter. No work has been reported to date on utilizing the AR to optimize the size reduction of a real ore from the mineral processing industry. The novelty of the research described in this thesis lies in the application of the AR optimization method in a situation where we carried out comminution under wet conditions and on a typical industrial ore, in order to determine optimal operating conditions that produce a maximum amount of material of intermediate size. To apply the results of the investigation, we developed a user-friendly AR programme that saves about 90% of the time that it would otherwise take to plot the AR curves manually.

1.1 Objectives of this thesis

The aim of our work was to identify opportunities for increasing the milling efficiency of the Bushveld Igneous Complex (BIC) Upper Group (UG) 2 ore. This aim would be achieved by following the objectives below:

- i. to test the hypothesis of heterogeneity of the ore;
- ii. to determine the optimum slurry density that meets a required objective;
- iii. to apply the AR optimization technique to laboratory grinding data;
- iv. to develop an AR programme that simplifies and accelerates the construction of AR curves; and
- v. to propose a modification of the current UG2 ore comminution circuit.

1.2 Thesis outline

CHAPTER 2

This chapter presents the background context of mineral processing, liberation, comminution and Attainable Region theory, with the aim of providing a framework for the research reported in this thesis. It also reviews the literature available on these subjects. The reader is taken through the stages of a typical mineral processing approach, from run-of-mine to the final concentrate. Because comminution was performed wet in this study, the factors that affect wet milling are also described. The AR technique is explained and discussed, and the ore used in the experimental programme is fully described.

CHAPTER 3

This chapter is devoted to the most important pieces of laboratory equipment we used to carry out the experimental programme described in the thesis. The apparatus we used are grouped under the headings; milling; size analysis; filtration and analytical equipment. Discussion of pieces of laboratory equipment used is necessary to the account of our investigation, because the rationale behind the experiments was dictated by the strength and the limitations of the standard equipment commonly used in mineral processing laboratories.

CHAPTER 4

In this chapter, we set out a detailed description of the experimental procedure we followed to obtain the laboratory scale results that form the basis of discussion in the

subsequent chapters. In order to make our description easy to follow, we make use of a block diagram that summarizes the experimental programme.

CHAPTER 5

This chapter presents the first series of experimental wet milling batch tests and the results obtained from milling an UG2 ore feed in a laboratory-scale ball mill. The purpose of these experiments was to test the hypothesis that it may be possible to grind so as to make it possible to separate components of feed material that is apparently heterogeneous, and retain the valuable and discard other components of no value. The results obtained in this chapter give partial credence to our hypothesis that the feed material is made up of at least two components. The general conclusion of this chapter is that the two-component parallel first-order model offers a better approximation to the experimental data, possibly because of the heterogeneous nature of the material.

CHAPTER 6

In this chapter, we give an account of our use of an alternative and perhaps more direct approach to characterizing the feed sample, in order to see if we could obtain any evidence that would confirm or falsify the initial hypothesis that the material is heterogeneous. Since the mode of occurrence of PGMs is that they are associated with base metals, we used the Atomic Absorption Spectrometer (AAS) to analyze the concentration of copper, and used that information to infer the presence of more than a single mineral phase in the feed material. The results described in this chapter confirm that the feed material is heterogeneous.

CHAPTER 7

The content of this chapter concerns the application of the AR method to the feed material grinding data. The effects of slurry density, grinding time and grinding energy on the grindability of a UG2 ore in a laboratory scale batch tumbling ball mill are investigated. Because we found that by regulating energy input and slurry density, we could fulfil specific objectives, we saw an opportunity to optimize the amount of energy input required for a given amount of breakage by adjusting the operational parameters such as the slurry density and grinding time while increasing grinding selectivity.

CHAPTER 8

In this chapter we review the current AR approach, and propose a new and more flexible application of AR to comminution. We do this by introducing a software programme developed to extend the capabilities of AR analysis, and demonstrating what the programme can do.

CHAPTER 9

This chapter reviews the work reported in the previous ones, and shows that the objectives we set out at the beginning of this investigation were accomplished successfully. It also sums up the possibilities our research has opened up for increasing the efficiency of milling a UG2 ore.

CHAPTER 10

In this chapter we give recommendations on how efficient size reduction and liberation of valuable minerals from low grade ores (as exemplified by the UG2) should be

achieved. This short chapter lays the foundation for future work, which should focus on establishing a mill-set up and flow-sheet that can achieve selective grinding of any heterogeneous ore.

CHAPTER 2

2 BACKGROUND AND LITERATURE REVIEW

In this chapter, we provide not only an account of the nature and process of comminution, but a brief history of the technological research that has formed the basis of the methods used today. This will provide a context within which the descriptions of the actual processes commonly followed at present can be described in detail, and will establish points of reference that will enable the reader to understand to what degree the innovations suggested by the experimental findings of the authors offer substantial advantages.

2.1 Mineral and ore

By definition, a mineral is a natural inorganic substance possessing a definite chemical composition and atomic structure. In a much more extended sense, we use the term 'mineral' to include anything of economic value that is extracted from the earth. 'Ore' is a term we use to describe an aggregate of minerals from which a valuable constituent, especially a metal, can be profitably mined and extracted. Most rock deposits contain metals or minerals, but when the concentration of valuable minerals or metals is too low to justify mining, it is considered a waste or gangue material. Within an ore body, valuable minerals are surrounded by gangue and it is our primary objective in mineral processing to liberate and concentrate those valuable minerals.

2.2 Mineral processing

Mineral processing or beneficiation is the science and art of extracting desirable metals from their ores in order to produce a valuable commercial end product. It is a process in which ore particles are first reduced in size (*comminution*) and then separated on the basis of their physical and/or chemical properties. Our objective in mineral beneficiation is to split the material being processed into two or more process streams. The intention is that the minerals of interest be diverted into one stream, the concentrates, while the other minerals present are diverted into a second stream, the tails. Sometimes when the minerals are difficult to separate, a third stream called the middling is produced. This has a mineral content that is intermediate between that of a concentrate and a tails.

Mineral processing is done for the following reasons.

- **To extract a valuable mineral**

Most minerals of commercial value naturally occur associated with gangue, and extraction of these minerals involves separating them from this gangue.

- **To remove undesirable impurities**

Deleterious materials, which reduce the value of the ore, can be removed by the use of mineral beneficiation techniques.

- **To produce a concentrate**

The objective here is to enrich the material (concentrate) by discarding as much of the gangue as possible.

- **To separate two or more valuable minerals**

It is common for a valuable ore to contain more than one desirable mineral. In this situation it is not only necessary to extract the concentrate and discard the gangue, but also to process the remaining values in the gangue.

2.3 Comminution in the mineral processing industry

Comminution is the most important unit operation in the beneficiation of ores (Wills 1990). The primary objective of carrying out comminution in the mineral processing industry is not merely to reduce the particle size of the feed material, but also to free (liberate) the constituent minerals that make up an ore so that valuable minerals can be separated from the minerals of little value, as illustrated by Figure 2.1. However, this process is generally performed relatively poorly, and at a considerable expense in terms of operational costs.

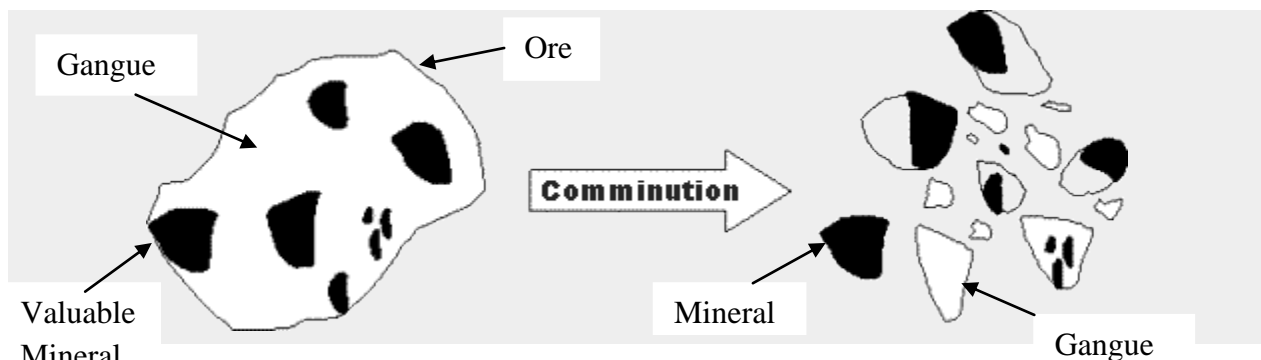


Figure 2.1: Liberation of valuable minerals by size reduction

The importance of mineral beneficiation is today taken for granted, but it is interesting to reflect that less than a century ago, ore concentration was often a fairly crude operation, involving relatively simple gravity and hand sorting techniques performed by the mining

engineers. Over the subsequent years, however, mineral beneficiation has developed into an important professional discipline. Without modern processing techniques, the concentration of many ores would be hopelessly uneconomic (Wills, Atkinson 1991).

In conventional practice, the comminution of mineral ores is performed by crushing, followed by grinding. Crushing reduces the size of particles to a level at which grinding can be carried out to liberate the valuable minerals (Pearse 1986). Crushing, which is usually a multiple-stage dry process, is accomplished by compression of the ore against rigid surfaces, or by impact against surfaces in a rigidly constrained motion path.

Examples of commonly used crushers are:

- jaw crushers;
- gyratory crushers;
- cone crushers; and
- impact crushers.

Grinding is the last stage in the process of comminution, and is also the most important part of the process of liberating valuable minerals from gangue. Grinding has changed very little in the past 50 years, and continues to be carried out in tumbling mills. It is well known that these are extremely energy-inefficient and have other limitations. The reasons that conventional mills have been used for so long are that they are relatively simple devices, and are continuous, high-throughput machines that can be fairly easily controlled to produce the desired product particle size distribution.

2.3.1 Mineral liberation

Apart from being relatively wasteful of energy, tumbling mills are also inefficient with regard to mineral liberation because of the indiscriminate nature of the grinding force. Ideally, comminution forces should be directed at the mineral crystal boundaries. Accordingly, engineers have made efforts to use tensile forces in an attempt to draw existing fractures further apart. One of the earlier versions was the Snyder process (Cavanaugh, Rogers 1974), which was a method of comminuting material by applying air, gas or steam under pressure in a pressure chamber. The material is broken by the stresses induced when the sudden release of that pressure causes the material to be ejected along a duct and into a receiving chamber. This process was believed to improve the liberation of minerals at generally coarser sizes.

The next attempt to bring about selective liberation of minerals from an ore entailed a novel noncontact comminution process concept (Parekh, Epstein & Goldberger 1984). This process involved the application of electric and ultrasonic energy in order to separate minerals from gangue particles. A third attempt at enhancing the preferential liberation from an ore introduced a new idea developed at the Royal School of Mines in London (Anon 1986). This comminution process reversed traditional assumptions by causing rocks to fragment from the inside rather than fracturing them by compressive forces. This method utilized high voltage pulses to generate plasma in the rocks and hence explode them from within.

The fourth attempt was based on an idea developed at the Camborne School of Mines in England (Wills, Parker & Binns 1987), and entailed heat treatment of the crushed ore prior to conventional grinding. A hard-rock tin ore was heated to 600°C before being quenched in water. The differential expansion and contraction promoted intergranular fracturing, and a significant reduction in grinding resistance was achieved owing to the micro-cracks produced in the ore minerals. This resulted in greatly improved liberation of the cassiterite.

The fifth attempt at encouraging preferential breakage and liberation of valuable minerals was also developed at the Camborne School of Mines in England (Clarke, Wills 1989), where preliminary test-work had shown that high pressure roller comminution may improve the liberation of cassiterite from its gangue minerals. Much interest has recently been focused on the high-pressure roller press, which was developed in Germany. This press is essentially a highly sophisticated type of rolls crusher capable of generating very high inter-particle pressures. There is evidence to show that liberation can be improved by using these devices, which are currently being used successfully to comminute cement and limestone, and it is expected that they will find a use in the grinding of industrial ores.

Unfortunately, the first four of the above attempts have not been adopted by the relatively conservative mineral processing industry, mainly because of the high energy and operational costs involved as well as their lack of practicality in industrial-scale applications.

The effective liberation of material of value remains one of the major challenges in treating modern ores which, due to the increasing complexity and smaller grain sizes of these ores, requires finer grinding to achieve the necessary degree of liberation (Veasey, Wills 1991). Vizcarra et al. (2010) agree, and state that a means to liberate minerals from the surrounding phases effectively would be a significant advance in minerals processing technology, as the degree of liberation determines the efficiency of both the comminution and subsequent units in a beneficiation process. Regrettably, efforts to address this liberation problem by way of fine and ultrafine milling have led to higher energy utilization, because both the valuable (mineral) and valueless (gangue) components are indiscriminately milled. Tomanec and Milovanovic (1994) estimated that milling alone accounts for more than 30–50% of the total power used in the concentration process, but this can rise to as high as 70% for hard or finely dispersed and inter-grown ores.

2.4 Mineral beneficiation approach

Mineral beneficiation begins when an ore is delivered from a mine to a processing facility. At this point, the ore is called ‘run-of-mine’ material, because it has not been treated in any way. In broader terms, mineral beneficiation consists of two functions, as illustrated by Figure 2.2. First, it involves the preparation and ‘liberation’ of the valuable from gangue minerals (comminution stage) and second, the separation of these valuable minerals from gangue minerals to produce concentrates and tailings respectively (mineral extraction stage). Our laboratory scale research focus is concentrated on the former stage.

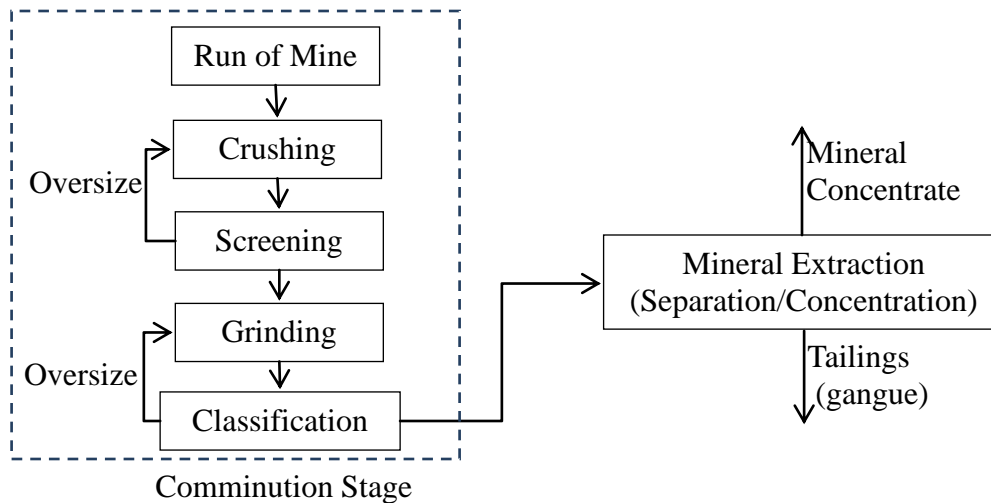


Figure 2.2: Typical Mineral Beneficiation Flow-sheet

Laboratory and industrial grinding tests have shown that grinding aides can influence the process of size reduction significantly (Klimpel, Austin 1982). It is generally known that water is the most common grinding aid, and that slurry density plays an important role in the size reduction process. The density of slurry determines the distribution of solid charge in the mill, with migration of particles from the tumbling zone to the mill periphery as the solid concentration is increased (Tangsathikulchai, Austin 1989). The changes in the circulation path of the mill charge in wet grinding lead to variations in the grinding performance and mill's power consumption. The amount of water that has to be added to the mill charge to maximize the breakage process is important. Tangsathikulchai and Austin (1985) reported a maximum in breakage rates at a slurry density of about 45 volume percent solids in water. However, the optimum slurry density changes in accordance with the specific objectives of a particular grinding process, and the mineralogical composition and physical properties of the ore.

The advantage of wet over dry grinding lies in the manner water has of bringing and keeping particles into positions advantageous to breakage. Other benefits of wet grinding are;

- Lower power consumption per ton of product
- Higher capacity per unit mill volume
- Makes possible the use of wet screening or classification for close product control
- Elimination of the dust problem
- Makes possible the use of simple handling and transport methods such as pumps and piping

We performed the laboratory scale experiments in a ball mill filled with different amounts of water. In the following section we discuss the wet grinding process and the factors that affect its efficiency.

2.4.1 Wet grinding

Wet grinding is performed in tumbling mills where the grinding medium comminutes the ore particles. The grinding medium can be steel rods, or balls, the ore itself (autogenous grinding) or a combination of the ore and balls (semi-autogenous grinding). Grinding is a random process subject to the laws of probability and the degree of grinding of an ore particle depends on the probability of it being caught between the grinding medium. Grinding can take place by several mechanisms, including impact or compression, due to forces applied almost normally to the particle surface; chipping due to oblique forces,

and abrasion due to forces acting parallel to the surfaces. Wet grinding is influenced by a number of factors namely;

- mill power;
- mill type;
- mode of operation;
- rotational speed;
- product quality;
- mill conditions; and
- screening

1. Mill power

The power demand (kW) of a conventional ball mill is a function of its known dimensions and basic operating conditions. As part of our experimental programme we measured the power drawn by the ball mill during the experiments and under different slurry conditions.

2. Mill type

The most common type of mill for grinding is a tumbling ball mill. A ball mill is a retention mill in which a reservoir of particles is acted on repeatedly. It is simple, relatively easy to construct, reliable, easy to control and maintain, and has low energy requirements per ton of product. A ball mill is an all-purpose mill that uses steel balls as grinding media. It is particularly suitable for fine grinding, for the following reasons.

- Ball mills have greater breakage forces than rod mills of the same diameter. This is because ball-on-ball contact occurs at a point, while rod-on-rod contact occurs along a line. Thus, for the same diameter and mass of grinding medium, the area of contact is less with balls than it is with rods. Greater breakage forces result in a greater degree of size reduction.
- In ball mills, the presence of large particles does not impede the breakage of small particles in the manner it does in rod mills
- In fine grinding, the number of particles to be ground is enormous. A larger number of contact points should therefore increase the grinding capacity. In ball milling, this can be achieved by the use of small balls.

3. Mode of operation

The mode of operation of a tumbling ball mill (Figure 2.3) is as follows. The rotation carries balls and granular material round the mill and as the balls tumble down, they strike particles nipped against other balls. In addition the general movement of the balls in the bed will rub particles between them. The three types of size reduction which can occur are caused by fracture, chipping, abrasion or attrition. The measured values of the primary progeny fragment distribution are the total of the fragments produced by each mechanism. At low rotational speed the balls have a relatively gentle tumbling action, but as the speed increases the tumbling action converts to a cascading state. At higher rotational speeds, a cataract of balls is formed.

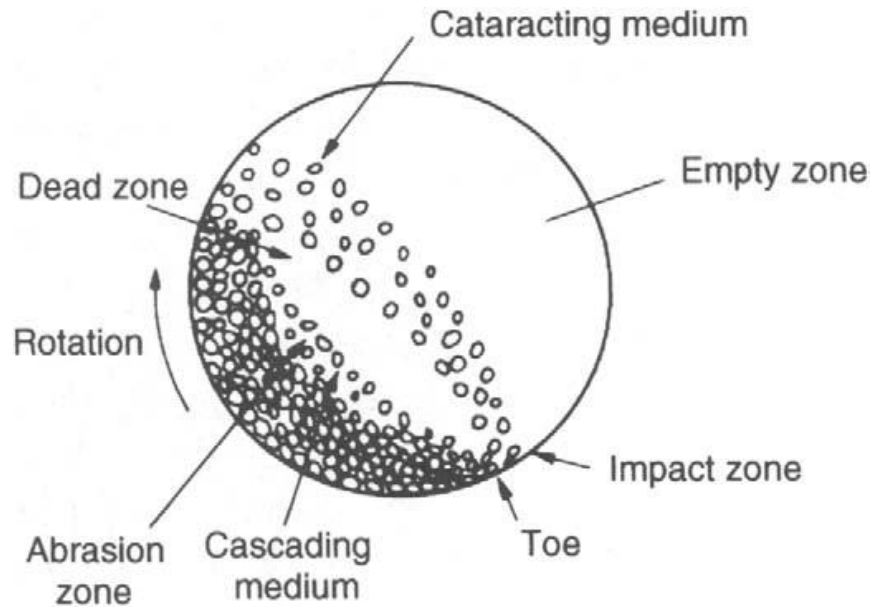


Figure 2.3: Mode of operation of a ball mill

4. Rotational speed

The tumbling action in a mill is a result of the rotation of the mill about its axis. The rates and modes of particle (powder) breakage vary with the mill speed. At low rotational speeds, the components of the load remain in contact with one another, and the tumbling action is called 'cascading'. The dominant size reduction in this mechanism is attrition. At high speeds, the components of the load are ejected into free flight before impacting on the mill liners. This tumbling action is called 'cataracting' and the dominant size reduction is by impact. The net power required to turn a mill is also a function of rotational speed.

5. Product quality

The quality of the product obtained from the grinding circuit is often specified by one or more of the following measurements: the weight fraction of product passing one or two

of preselected sieve sizes, the specific surface area, or the achievement of a preselected degree of liberation of valuable material from a larger mass of rock. It is sometimes desirable to give an approximate indication of the extent of size reduction accomplished or desired. A term often used is the reduction ratio, which is the ratio of the maximum particle size in the feed to that in the product. To calculate the reduction ratio, it is necessary to characterize the size of the feed and size of the product by single numbers. This ratio is commonly taken to be the ratio of 80% passing sizes of feed to product. The product specifications chosen in a given situation depend on which characteristic is most easily correlated to the desired performance of the end product.

6. Mill conditions

Changing mill conditions is the same as changing the temperature in a chemical reactor. Briefly discussed below are some of the mill conditions that need to be specified in order to address the question of grinding efficiency.

6.1 Critical speed

The critical speed of the mill is defined as the rotational speed at which the balls have stopped tumbling and have just started to centrifuge on the mill case.

$$\text{Critical speed, rpm} = 42.2/\sqrt{D - d}$$

: Where D is the internal mill diameter and d the maximum ball diameter.

The maximum power drawn by a mill occurs at different fractions of critical speed from one mill to another, depending on the mill diameter, ratio of ball to mill diameter and the

ball and powder filling conditions. This maximum is usually found in the range of 70–80% of critical speed. The rotational speed of the mill is normally specified by the fraction of the critical speed (ϕ_c).

6.2 Ball filling

The rate of breakage depends on how much of the mill volume is filled with balls. The fractional ball filling, J , is usually expressed as the fraction of the mill filled by the ball bed at rest. It is conventional to define constant formal bed porosity for all calculations. Using a formal bed porosity of 0.4:

$$J = \text{mass of balls} / (\text{ball density} \times \text{mill volume}) \times 1.0 / 0.6.$$

6.3 Ball diameter

The power required by the mill varies with the ball diameter, and an incorrect choice of ball diameter results in direct inefficiency. A charge of balls that are too small causes a slumping in the charge, a low power draw, plus excessive wear rates of the balls. A different ball diameter allows one to have the same mass of grinding media in the mill, but will achieve a different extent of grinding and power draw. The optimum choice of ball size depends on the feed size distribution, the desired product size, and the balance between energy and steel costs.

6.4 Mill filling

It has been established that for a given ball loading, it is undesirable to either under- or overfill the mill with powder. In the case of a low filling, much of the energy of the

tumbling balls is taken up in steel-to-steel contact, while at high filling the powder cushions the breakage action. Mill filling by feed is expressed as the fraction of mill volume filled by the feed bed:

$$f_c = \text{mass of feed} / (\text{feed density} \times \text{mill volume}) \times 1.0/0.6.$$

In order to relate the particle loading to the ball loading, the formal bulk volume of powder is compared with the formal porosity of the ball bed:

$$U = f_c / 0.4J,$$

where $U = 0.6$ to 1.1 is a good feed/ball loading ratio to give efficient ball loading in the mill, and

U is the fraction of the spaces between the balls at rest which is filled with feed.

6.5 Slurry density

Slurry density is defined by the fraction by weight of solids in the mixture. The rheological properties of a slurry are better defined by the volume fraction of solids, c :

$$c = (w_s / \rho_s) \times 1 / \{ (w_s / \rho_s) + [(1 - w_s) / \rho_l] \},$$

where w_s , is the weight fraction of solid, ρ_s and ρ_l are the densities of the solid and the liquid.

The solids to liquids ratio in a wet grinding process has a strong influence on the operation of the mill because it affects the viscosity of the slurry, and hence the rate at which it flows through the mill. This in turn affects the period during which the solids are resident in the mill, and thus the extent to which they are milled. The solids to water

ratio also affects the grinding action in the mill. A slurry that is too dilute leads to excessive contact between the components of the medium, which gives high rates of wear. Conversely, too high a solids concentration results in a cushioning of the medium, which reduces the grinding capacity. Hence, the slurry density has to be within an optimum range, usually quoted at 45 % by volume.

7 Screening

Screening of material is extensively used in the minerals industry, and is generally carried out on relatively coarse material, as the efficiency decreases as the fineness increases. Fine screens are expensive, very fragile, and tend to become blocked with retained material. Screening is therefore usually limited to material above about 38 μ m in size (Austin, Rogers 1985), while finer sizing is normally done by classification or laser diffraction. Screening can be performed wet or dry; but even in dry screening, wet washing is required. The main purposes of screening in the mineral processing industry are:

- to prepare a closely sized end product, because the final product specification usually provides information that is important to subsequent processes;
- to prevent oversize material from passing to the next stage in crushing and grinding operations; and
- to increase the capacity and efficiency of crushing machines by preventing the entry of undersize material.

7.1 Types of screens

A screen is a surface having a number of apertures of given dimensions. There are many types of screens, which are broadly classified as either stationary or moving. Given below are some examples.

➤ **Stationary screens**

- sieve bends; and
- the grizzly

➤ **Moving screens**

- revolving screens;
- shaking screens;
- reciprocating screens;
- gyratory screens; and
- vibrating screens.

2.5 Particle Size Distribution (PSD) representation methods

After particles have been comminuted and screened, the next step in the process is size analysis. The concept of defining particle size in mineral processing is ambiguous because ore particles do not have definite shapes, like spheres and cubes. Instead the size of a spherical particle is defined by its diameter; and a cubical particle by the length of a side. Even for particles of regular shape, particle size does not have a unique meaning. In mineral processing an indirect measure of size is used, and the size of a particle is defined as the smallest whole opening in a square mesh screen through which a particle will fall. As previously noted, if the particles are too small to be

measured using sieves, other methods like laser diffraction can be used for the purpose.

It is often necessary to divide the particle population into groups, each identified by the smallest and largest size in the group. Screening using mesh sizes in geometric series is normally used to achieve this classification. The concept of particle groups or classes allows for the description of the behaviour of classes of particles rather than that of individual particles. A representative size is associated with each particle size class, and it is assumed that all particles in the class will behave as if they had a size equal to the representative size.

Particle size distribution can be measured experimentally using sieves (21 cm in diameter) of the kind found in a laboratory. The data obtained by screening is normally presented in tabular form that shows mesh size against the fraction smaller than that mesh. Graphical representations are generally preferred because of their convenience in assessing and comparing particle size distributions. A variety of different graphical coordinate systems have become popular, some with a view of making the particle size distribution function plot a straight line or close to a straight line. In some of these graphical plots, the particle size axis is plotted on a logarithmic coordinate scale, and various options are used for the ordinate scale. In other graphical plots, specially ruled graph papers are available for PSD plots.

2.5.1 Graphical representation of sizing analyzes

Shown below are some of the different methods of charting sizing tests.

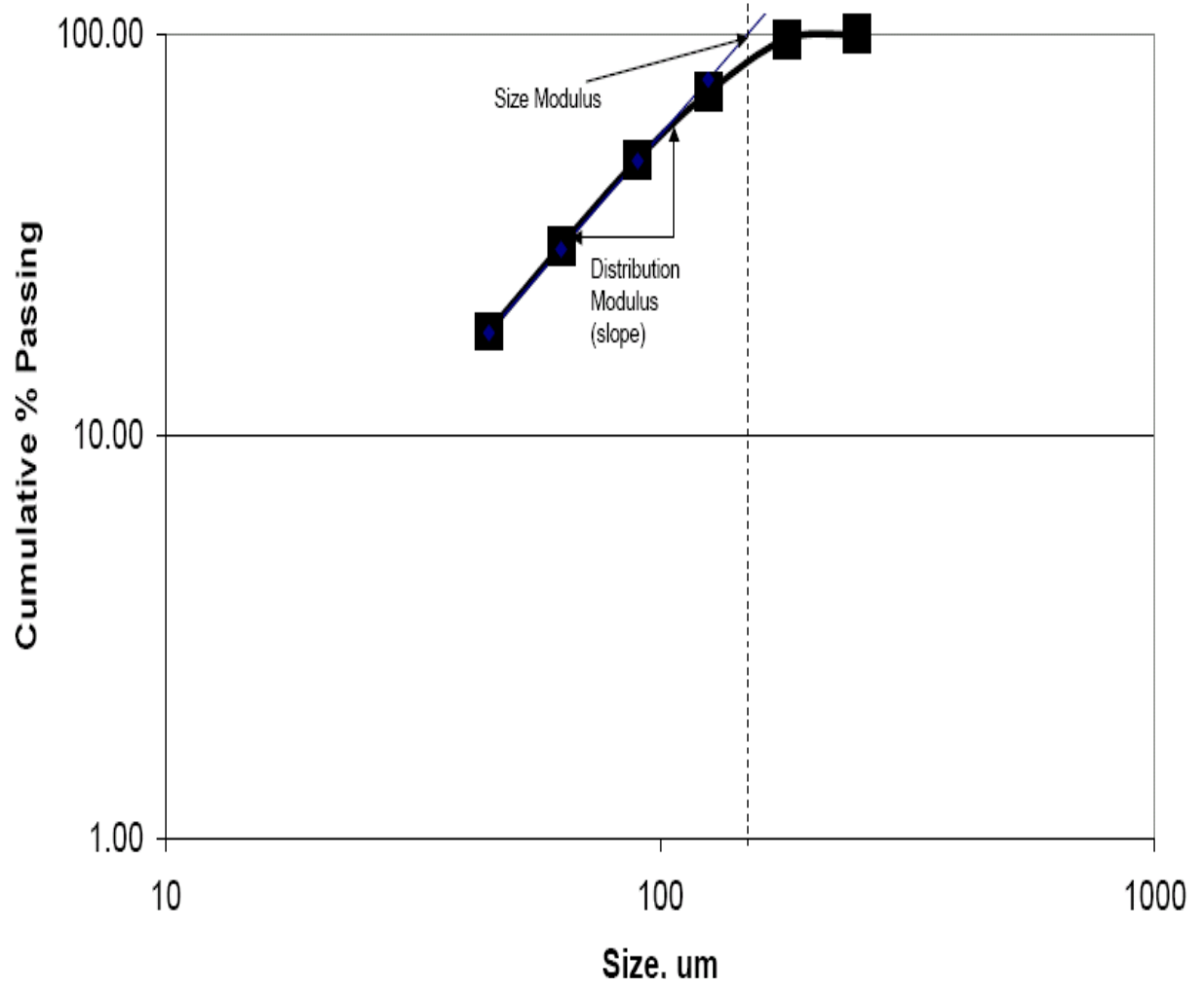


Figure 2.4: Gates/Gaudin/Schumann Plot

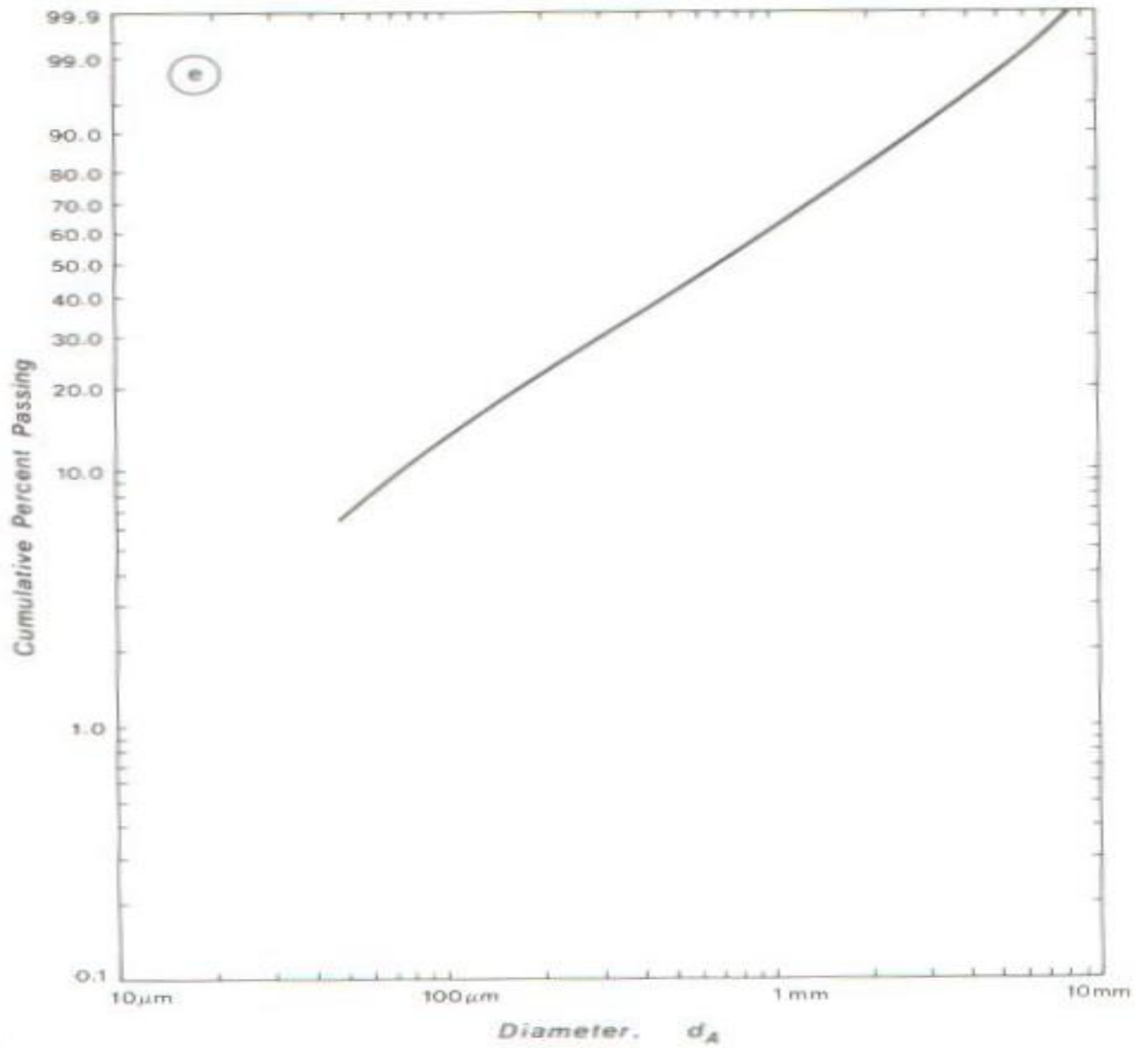


Figure 2.5: A typical Rosin Rammler plot

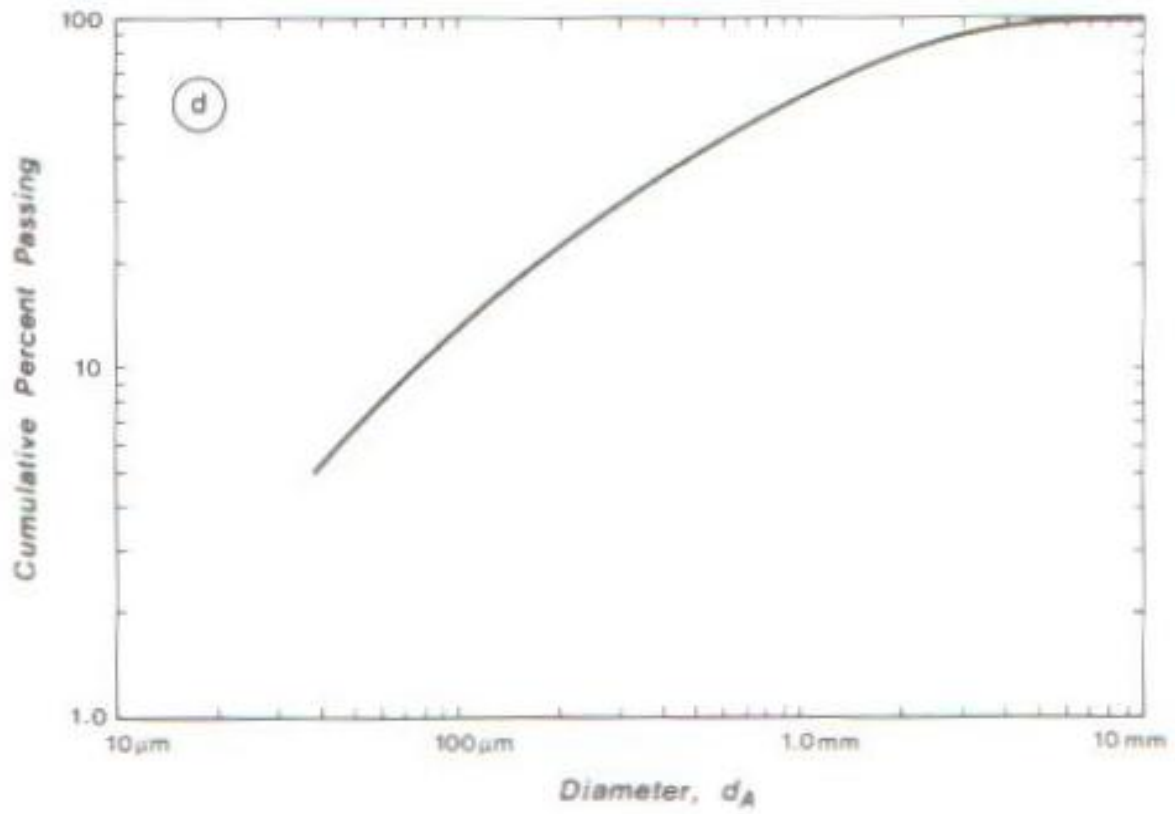
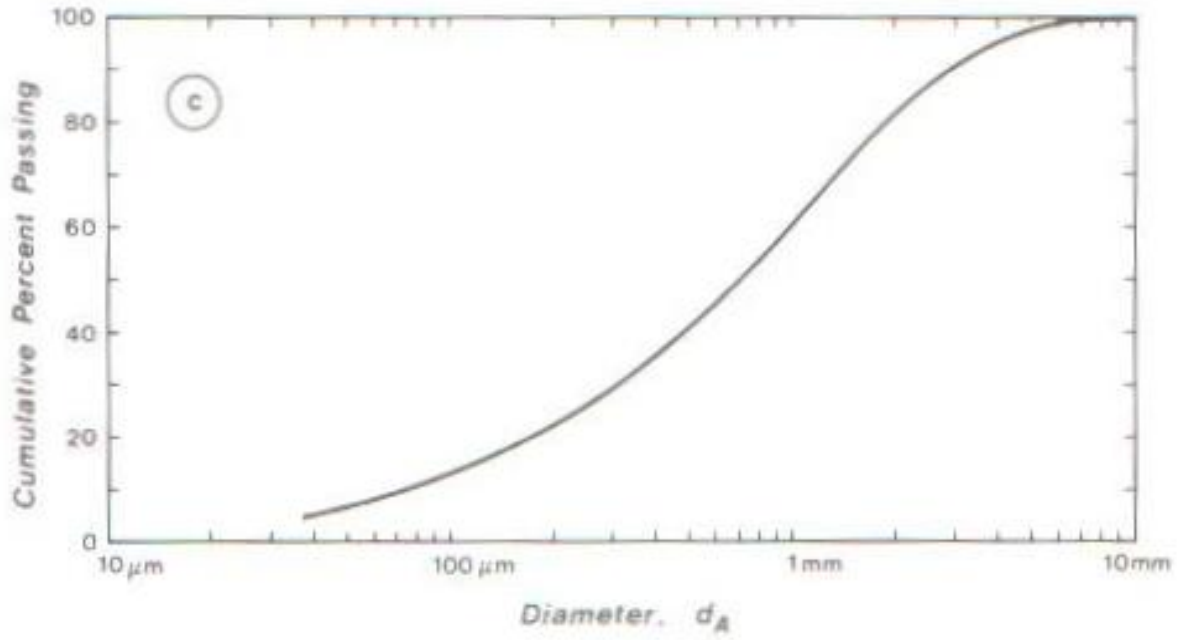


Figure 2.6: Typical log probability plots

Figure 2.4 shows the Gates–Gaudin–Schumann plot, which is a graph of the cumulative percentage of material passing a sieve size versus the sieve size. In this type of plot, both axes are in the logarithmic scale, and most of the data points should lie in a straight line. The equation for the straight line section of the plot is given by;

$$y = (x/k)^a \quad (2.1),$$

where y is the cumulative % passing,

x is the particle size,

k is the size modulus, and

a is the distribution modulus.

If we take logs on both sides of Equation 2.1, it converts to a straight line given by Equation 2.2;

$$\log y = a \times \log(x) - a \times \log(k) \quad (2.2),$$

where a is the slope of the line, and $-a \times \log(k)$ the y -intercept.

The size modulus is a measure of how coarse the size distribution is, and can be determined from the graph by extrapolating the straight–line section of the plot up to the 100% passing mark and finding the corresponding size value. The distribution modulus is a measure of how broad the distribution is, and can be obtained by calculating the slope of the straight–line section of the plot.

Figure 2.5 shows a typical Rosin–Rammler plot that is frequently used to describe the PSD of powders of various types and sizes. The function is particularly suited to

representing particles generated by grinding, milling and crushing operations. The conventional Rosin–Rammler function is described by Equation 2.3.

$$R = \exp \left[- \left(\frac{D}{D_m} \right)^n \right] \quad (2.3),$$

where R is the retained weight fraction of particles with a diameter greater than D,

D is the particle size,

D_m the mean particle size, and

n is a measure of the spread of particle sizes.

Figure 2.6 shows PSDs in the form of log probability plots. The graphs show the cumulative mass percent of material passing a sieve size versus the sieve size. All the above PSD representation methods are limiting in that they do not provide connectivity between the different states of a grinding process. The Attainable Region method, which is briefly discussed in the next section, was developed at the Centre of Material and Process Synthesis (COMPS), University of the Witwatersrand, South Africa, to adequately represent the state of dynamic grinding systems.

2.5.2 The Attainable Region (AR) Method

The AR method has been successfully applied in the field of chemical reactor engineering for choosing and optimizing reactor configurations (Glasser, Hildebrandt & Crowe 1987). It was first proposed as a novel approach to the problem of reactor synthesis by Horn (1964), who addressed the issue of finding the optimal reactor structure for a given set of competing reactions and associated kinetics. He noted that for given kinetics and feeds, it might be possible to find the set of all possible output

concentrations from all possible reactor systems. He called the set of all possible products the Attainable Region (Horn, 1964). There are two reasons why all the possible products have to be found.

- If an objective function is complicated, it might not be known where the optimum will occur.
- One of the products may be an intermediate that is required to produce the optimum. It will not be known what the global optimum is until all the possible intermediate products have been found.

What follows covers some of the terminology that is frequently used in the description, analysis and understanding of the AR technique.

- State variable

A state variable is one of the parameters that are used to describe the mathematical "state" of a dynamical system. Intuitively, the state of a system describes enough about the system to determine its future behaviour.

- The objective function

The objective function is the function that needs to be optimized. This may be the maximizing of a given product, the minimizing of some amount of energy utilized or any other state variables.

- The characteristic vector

The listed co-ordinates of a point that specify the product of a system are termed the characteristic vector. From vector mathematics, we know that the coordinates of a point can also be considered as a vector from the origin. The characteristic vector characterizes the state (or composition) of a stream, and must contain sufficient variables to describe fully the reaction kinetics and the objective function.

- The reaction vector

The reaction vector contains the rates of formation of the components and thus the kinetics of all the reactions. The reaction vector gives the instantaneous change in state of a mixture when it undergoes a batch reaction.

- The mixing vector

The only other process that may occur in any given system is mixing, which can occur in two modes, on its own or inside a reactor. The former occurs when two process streams combine to form a single process stream. Mixing, like reaction, is represented by a vector that points from the stream being considered to the stream it is being mixed with.

Finding the AR requires an iterative construction process. However, there are a set of necessary conditions or "rules" that allow one to check whether all the possible products have been found to help one construct the region. The next step, finding the optimum, entails the relatively simple procedure of looking for the point on the boundary where

the objective function is optimized. This will usually be found where one of the lines of constant value for the objective function just touches the boundary of the AR. In most cases the objective function will be at a tangent to the boundary it touches. After that, based on knowledge of the processes that are required to reach the optimal point, the engineer can determine an optimal flowsheet.

Since milling can also be considered a rate process in which the various size classes break from the larger sizes to the smaller in a manner analogous to reactor systems, the AR approach has been extended and successfully applied to comminution (Khumalo et al. 2006). The power of the AR approach is that it describes the behaviour of different size classes throughout the milling process, and can represent particle size distributions (PSDs) as single points in space (Khumalo et al. 2006, 2007, 2008). This allows the connectivity of the points to be used for process description and optimization purposes.

The AR is a fundamental approach that is equipment-independent and can be used in the field of comminution to describe breakage processes (Khumalo et al., 2006). A complete AR analysis requires us to describe the set of all possible outputs for a system (Khumalo et al. 2007). The work already done by researchers (Khumalo et al. 2006, 2007, 2008) and (Metzger et al. 2008, 2009) used the AR method to optimize comminution processes carried out under dry conditions only. Both Khumalo and Metzger investigated the application of the approach to the milling of a test material, silica sand for the former and silica sand and quartzite for the latter. No work has been reported to date on utilizing the AR to optimize the size reduction of a real ore from the

mineral processing industry. The objective of the research set out in this thesis was to apply the AR optimization method to a situation in which comminution is carried out under wet conditions, and on a typical industrial ore.

One assembles an AR plot by focusing on the essential features of the process, what is desired, and what is currently available. These can include, but are not limited to, grinding energy, grinding time and mass fraction of different size classes. Any number of size classes can be considered, but typically three are used, grouped as:

- (i) the feed size class, is taken as the top size class or size class 1;
- (ii) the middle size class, which is the result of a moderate extent of breakage and is termed size class 2; and
- (iii) the fines size class, which is the result of a relatively large extent of breakage and is termed size class 3.

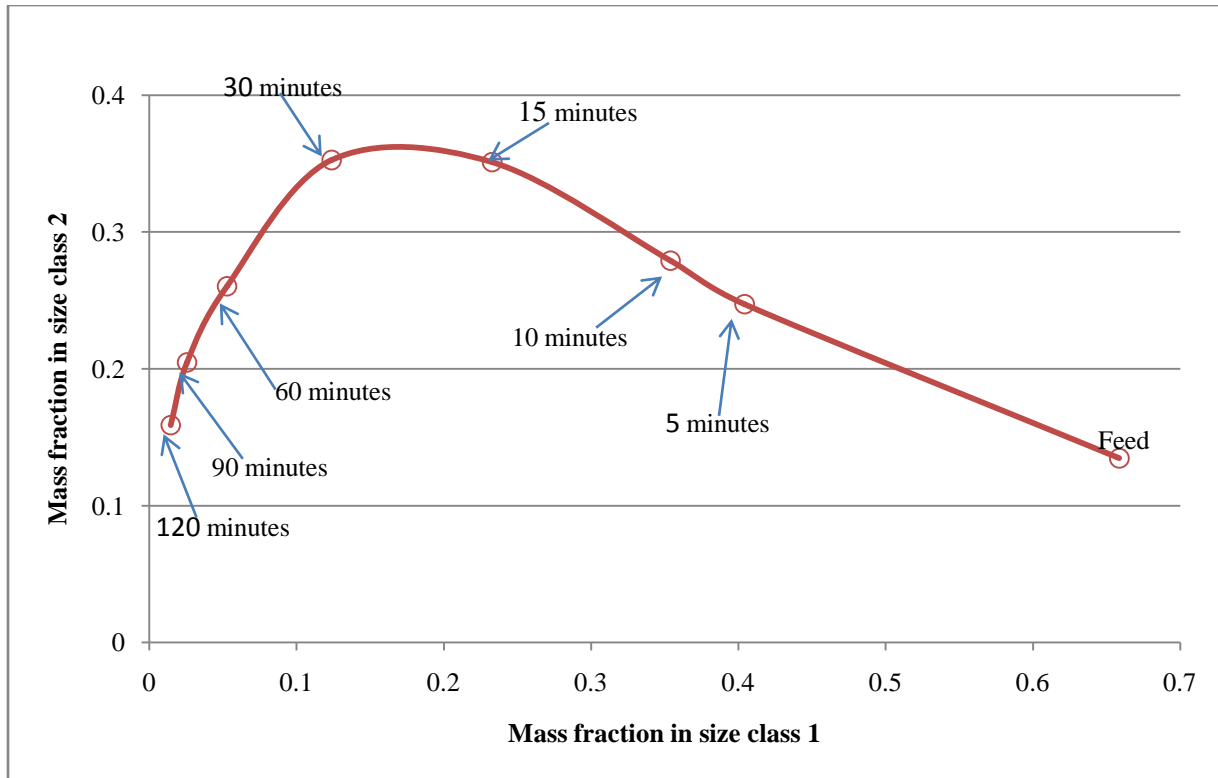


Figure 2.7: A typical Attainable Region Plot of mass fraction of material in the intermediate size class versus mass fraction of material in the feed size class (this graph was obtained from Chapter 7, section 7.3, Figure 7.7)

An example of an AR plot is presented in Figure 2.7. It is constructed by following the procedure outlined by Khumalo et al. (2007) and Metzger et al. (2009), and shows the mass fraction of material in size class two and size class one in size class 2 versus size class 1 phase space. Each point on the graph corresponds to a different duration of mill operation, starting from a single feed point. This simple plot provides some very important information on the process, including the following.

1. The boundary curve describes the processes used, and can be interpreted in terms of pieces of equipment, implicitly identifying the optimal equipment required.

2. The turning point of the curve isolates an optimum solution when the objective is to maximize the mass in the intermediate size class. This solves the optimization problem and provides the process control policy needed to fulfil that objective, in other words the run time required to achieve that optimum.

2.6 The characteristics of the feed material

We obtained the feed material from Anglo Platinum Amandelbult Plant's Upper Group 2 (UG2) primary cyclone underflow section. South Africa dominates world PGM production because of the massive resource base contained in the Bushveld Igneous Complex (BIC), which underlies an area of approximately 40,000 km² in the central region of the country (Hochreiter et al., 1985). The BIC is the largest known source of Platinum Group Metals (PGMs), and, taken in conjunction with the Great Dyke in Zimbabwe, contains something like 90% of the known PGM reserves in the world (Cramer, 2008). The BIC is a platinum-rich layered mafic intrusion in which slow cooling has allowed the PGMs and base-metal sulphides to coalesce and concentrate into three commercially exploited layers known as the Merensky, the plat-reef and the UG2 reefs.

The production of PGMs from UG2 ores poses a number of technical challenges (Cramer 2001), owing to the fact that these ores have low counts of PGMs (ranging between 1–7 ppm) and the PGMs are tightly interlocked with the silicate matrix. However, there is economic value in exploiting the low-grade UG2 reef because the high-grade Merensky reef is becoming depleted.

Generalized PGM Process

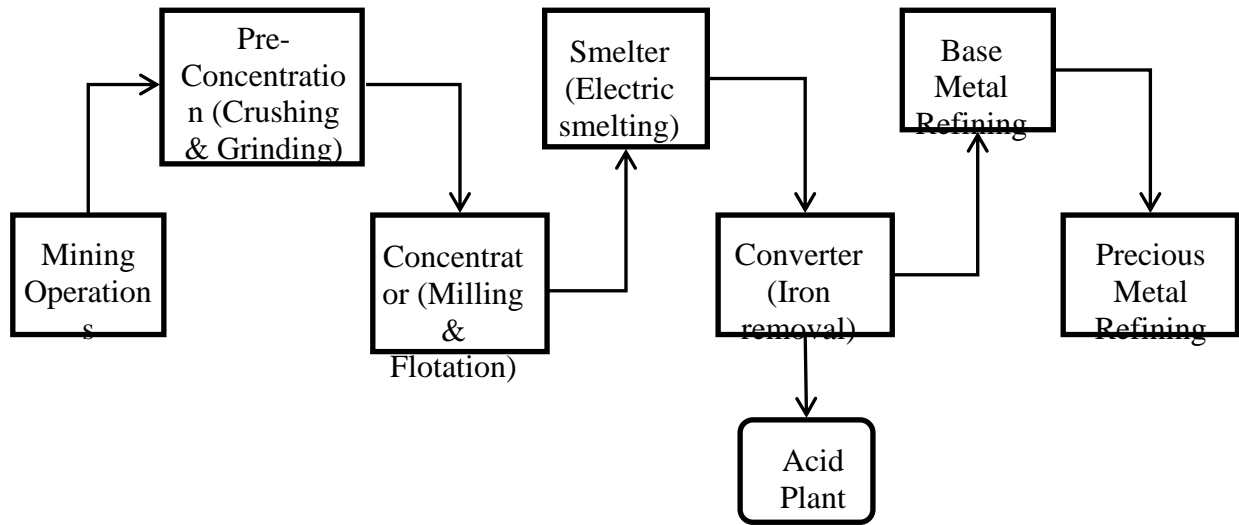


Figure 2.8: Typical PGM flowchart

Figure 2.8 shows the general unit operations used in processing PGM from run-of-mine. Typically, an ore delivered from the mining operations contains between 1–6ppm PGMs. The ore is subsequently reduced in size and concentrated through crushing, grinding, milling and flotation operations. The grade is increased after pre-concentration, typically to between 4–12ppm. This is further raised after the concentration stage to between 80–400ppm, and after furnace smelting to between 500–800ppm (Cramer, 2008). Smelting is done to remove as gangue impurities, silicates, aluminates, magnesia and iron in the form of slag. The furnace matte is converted in order to eliminate by oxidation, sulphur and iron to sulphur dioxide and slag respectively. The sulphur dioxide gas is used in the acid plant to produce sulphuric acid, which is sold to the fertilizer manufacturers. The converter matte contains up to 1200ppm PGM, and after base metal refining, the PGM concentration in the feed to the precious metal refining stage lies between 50–60% by mass.

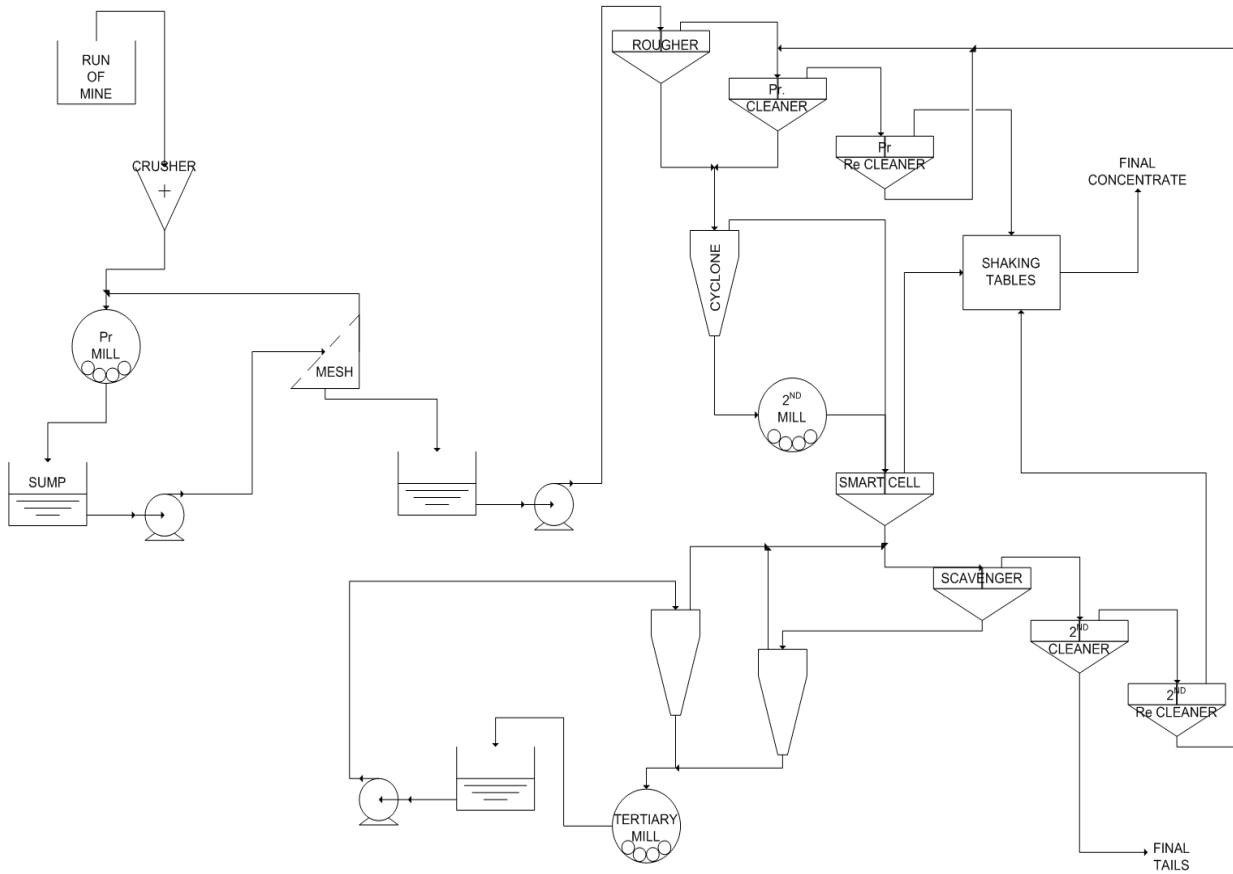


Figure 2.9: A typical PGM plant milling/concentrator circuit

Figure 2.9 shows a typical concentrator circuit used in the PGM industry. The flow-sheet is characterized by milling and flotation units. Crushed run-of-mine ore is directly fed to a first set of grinding (primary) mills, usually of the Semi-Autogenous (SAG) type and operated at above 80% by mass solids content. After primary milling, the product is diluted to below 50% by mass solids content in the reservoir tank before being pumped into a set of primary flotation cells where the liberated PGM concentrate is separated from the tailings. The tailings from the primary flotation cells are charged into a second set of grinding (secondary) mills, usually of the ball mill type. The PGM concentrates in the mill product are separated from the tailings in secondary flotation cells, while the tails are sent

to a third set of mills (tertiary mills). All the concentrate streams are joined to form the final concentrate, while the tails from the secondary floatation mills become the final tails.

This description covers the general operation of current milling circuits. The research we undertook aimed to raise the efficiency of such concentrator circuits.

The mode of occurrence of PGMs ranges from being predominantly associated with base-metal sulphides (either locked within, or at the grain boundaries of, sulphide minerals) to being predominantly associated with gangue minerals (locked in silicate, or at grain boundaries of chromite and silicate grains) (Penberthy, Oosthuyzen and Merkle., 2000). The mode of occurrence of the values in PGM ores will therefore influence the design of the mineral processing circuit (Bryson 2004) because it is important to mill the ore in such a way that the small PGM particles are not detached from the larger sulphide mineral in the primary milling circuit. Bryson (2004) states that the objective of these milling circuits is to apply sufficient milling energy in the primary milling stage to liberate sulphide minerals from the gangue while preventing the application of excessive milling that may lead to a reduction of PGM values from valuable material that has been removed from the sulphide minerals. At the same time, by milling only to a grain size of the main mineral phase in the primary circuit, the engineer saves the energy costs associated with milling the mineral rather than the rock.

Because PGM minerals also occur as partially-locked and totally locked particles in silicate minerals, the use of fine milling techniques in the secondary milling circuits is important to

the liberation of this material. The secondary mill is used to liberate those PGM values locked in silicate phase by means of size reduction. The milling of silicate rather than chromite phase is important in secondary milling, and energy savings may be considerable. The effectiveness of these secondary mills is generally not as good as could be desired because only the mineral phase and not the rock phase should be ground to reduce energy usage. One area of focus in the current research aimed at improving milling performance is how the varying degrees of hardness of minerals in the ore can be effectively exploited when liberating PGMs (Bryson 2004).

Apart from attempting to increase the effectiveness of the comminution process in liberating and extracting minerals from ores, researchers are well aware that milling is a highly energy-intensive process. This has significant bearing on the operating cost of mineral processing plants. The amount of electrical energy consumed by comminution processes across the world is 3-4% of the total produced (Matijašić et al. 2009). It follows that energy efficiency is increasingly an area of focus in the mineral processing industry. The various South African platinum producers have invested significant time and resources in investigating energy efficient milling technology and processing flow sheets, in order to improve energy usage in the extraction of PGMs (Rule 2009). The findings suggest that this can be done if comminution circuits are operated under optimal conditions and design configurations that bring about the best possible recovery and grade of the PGMs being extracted, at the lowest possible operating cost.

2.7 Mineralogical analysis

A great deal of information about an ore is required to enable the engineer to understand and predict its behaviour during processing. Techniques such as particle sizing, elemental, diffraction and image analysis are means of obtaining the information required.

Some of the methods we could have used to provide the quantitative data about mineral composition, association and liberation of the sample material are petrographic and image analysis. Imaging and image analysis are fundamental to mineral liberation analysis, and a high resolution image is a prerequisite for mineral identification and quantification (Fandrich, etl., 2007). Optical image analysis systems are capable of differentiating between mineral species on the basis of the distinctive reflectivities of different species. Simple Scanning Electron Microscope (SEM) back-scatter colour image analysis can acquire images rapidly, but falls short in that it cannot identify the actual mineral species or quantify them (Benvie, 2007), which is why it is normally used in combination with an energy dispersive spectrometer equipped scanning electron microscope EDS-SEM to ensure accurate discrimination between mineral species. Back Scattered Electrons (BSE) image analysis, in which a series of BSE images are collected and processed to produce liberation data, is the most basic liberation analysis tool.

Unfortunately, this researcher was unable to obtain the equipment described above to characterize the ore, and therefore used the equipment available at The University of Witwatersrand's Mineral Processing laboratory.

2.8 References

Anon 1986, "NEW IDEAS IN MINERALS PROCESSING.", *World mining equipment*, vol. 10, no. 6, pp. 14, 16, 18-19.

Austin, L.G. & Rogers, R.S.C. 1985, "Powder technology in industrial size reduction", *Powder Technology*, vol. 42, no. 1, pp. 91-109.

Austin, L.G., Klimpel, R.R. & Luckie, P.T. 1984, "Process engineering of size reduction: ball milling", pp 234-247

Bryson, M.A.W. 2004, "Mineralogical control of minerals processing circuit design", *Journal of The South African Institute of Mining and Metallurgy*, vol. 104, no. 6, pp. 307-309.

Cavanaugh, W.J. & Rogers, D.J. 1974, "APPLICATIONS OF THE SNYDER PROCESS.", , pp. 91-122.

Clarke, A.J. & Wills, B.A. 1989, "Technical note Enhancement of cassiterite liberation by high pressure roller comminution", *Minerals Engineering*, vol. 2, no. 2, pp. 259-262.

Cramer, L.A. 2001, "The extractive metallurgy of South Africa's platinum ores", *JOM*, vol. 53, no. 10, pp. 14-18.

Cramer, L.A . 2008, "What is your PGM concentrate worth"? Third International Platinum Conference 'Platinum in Transformation', *The South African Institute of Mining and Metallurgy*.

- Deal, M., Kappes, R. & Lee, J. 2011, "The applicability of alternative particle size analysis methods in laboratory testing", *SME Annual Meeting and Exhibit and CMA 113th National Western Mining Conference 2011*, pp. 579.
- Glasser, D., Hildebrandt, D. & Crowe, C. 1987, "A geometric approach to steady flow reactors: The attainable region and optimization in concentration space", *Industrial and Engineering Chemistry Research*, vol. 26, no. 9, pp. 1803-1810.
- Hochreiter, R.C., Kennedy, D.C., Muir, W. & Wood, A.I. 1985, "Platinum in South Africa", *South African Institute of Mining and Metallurgy*, vol. 85, no. 6, pp 165-185
- Horn, F. 1964, "Attainable and non attainable regions in chemical reaction technique", *3rd European Symposium on 'Chemical Reaction Engineering'*, Pergamon Press Ltd, Great Britain,
- Khumalo, N., Glasser, D., Hildebrandt, D. & Hausberger, B. 2008, "Improving comminution efficiency using classification: An attainable region approach", *Powder Technology*, vol. 187, no. 3, pp. 252-259.
- Khumalo, N., Glasser, D., Hildebrandt, D. & Hausberger, B. 2007, "An experimental validation of a specific energy-based approach for comminution", *Chemical Engineering Science*, vol. 62, no. 10, pp. 2765-2776.
- Khumalo, N., Glasser, D., Hildebrandt, D., Hausberger, B. & Kauchali, S. 2006, "The application of the attainable region analysis to comminution", *Chemical Engineering Science*, vol. 61, no. 18, pp. 5969-5980.

- King, R.P. 2001, "Modeling & Simulation of Mineral Processing Systems", *Butterworth-Heinemann, UK*, pp 144-151
- Klimpel, R.R. & Austin, L.G. 1982, "Chemical additives for wet grinding of minerals", *Powder Technology*, vol. 31, no. 2, pp. 239-253.
- Matijašić, G., Žižek, K., Sofilić, U., Mandić, V. & Skopal, H. 2009, "Wet comminution kinetics of dolomite at laboratory scale", *Chemical Engineering and Processing: Process Intensification*, vol. 48, no. 4, pp. 846-851.
- Metzger, M.J., Glasser, B.J., Glasser, D., Hausberger, B., Hildebrandt, D. & Khumalo, N. 2008, "Use of the attainable region (AR) analysis to optimize particle agglomeration and breakage operations", *AIChE Annual Meeting, Conference Proceedings*.
- Metzger, M.J., Glasser, D., Hausberger, B., Hildebrandt, D. & Glasser, B.J. 2009, "Use of the attainable region analysis to optimize particle breakage in a ball mill", *Chemical Engineering Science*, vol. 64, no. 17, pp. 3766-3777.
- Parekh, B.K., Epstein, H.E. & Goldberger, W.M. 1984, "NOVEL COMMUNITION PROCESS USES ELECTRIC AND ULTRASONIC ENERGY.", *Mining Engineering*, vol. 36, no. 9, pp. 1305-1309.
- Pearse, G. 1986, "CRUSHERS AND GRINDING MILLS.", *Mining Magazine*, vol. 154, no. 4.

- Penberthy, C.J., Oosthuyzen, E.J. & Merkle, R.K.W. 2000, "The recovery of platinum group elements from the UG 2 chromitite, Bushveld Complex – a mineralogical analysis", *Mineralogy and Petrology*, vol 68, pp 213-222.
- Rule, C.M. 2009, "Energy considerations in the current PGM processing flowsheet utilizing new technologies", *SAIMM - Journal of The South African Institute of Mining and Metallurgy*, vol. 109, no. 1, pp. 39-46.
- Tangsathitkulchai, C. & Austin, L.G. 1989, "Slurry density effects on ball milling in a laboratory ball mill", *Powder Technology*, vol. 59, no. 4, pp. 285-293.
- Tangsathitkulchai, C. & Austin, L.G. 1985, "The effect of slurry density on breakage parameters of quartz, coal and copper ore in a laboratory ball mill", *Powder Technology*, vol. 42, no. 3, pp. 287-296.
- TOMANEC, R. & MILOVANOVIC, J. 1994, "Mineral liberation and energy saving strategies in mineral processing", *Fizykochemiczne Problemy Mineralurgii*, vol 28, pp. 195-205
- Veasey, T.J. & Wills, B.A. 1991, "Review of methods of improving mineral liberation", *Minerals Engineering*, vol. 4, no. 7-11, pp. 747-752.
- Vizcarra, T.G., Wightman, E.M., Johnson, N.W. & Manlapig, E.V. 2010, "The effect of breakage mechanism on the mineral liberation properties of sulphide ores", *Minerals Engineering*, vol. 23, no. 5, pp. 374-382.

Wills, B.A. 1990, "Comminution in the minerals industry - An overview", *Minerals Engineering*, vol. 3, no. 1-2, pp. 3-5.

Wills, B.A. 1992, "Mineral processing technology", *5th edition*, pp 181-216

Wills, B.A. & Atkinson, K. 1991, "The development of minerals engineering in the 20th century", *Minerals Engineering*, vol. 4, no. 7-11, pp. 643-652.

Wills, B.A., Parker, R.H. & Binns, D.G. 1987, "THERMALLY ASSISTED LIBERATION OF CASSITERITE.", *Minerals and Metallurgical Processing*, vol. 4, no. 2, pp. 94-96.

CHAPTER 3

3 THE LABORATORY EQUIPMENT USED

This chapter contains a summary of the most important pieces of laboratory equipment used to carry out the experimental programme described in the thesis. This is relevant to the investigation, because the rationale behind the experiments was dictated by the strength and the limitations of the standard equipment commonly used for comminution. All the equipment listed below was available in the Mineral Processing laboratory at the University of Witwatersrand, and was in good working condition, having been serviced and calibrated before the experiments were carried out.

3.1 Sample preparation equipment

3.1.1 Jones Riffle Splitter

After a gross sample has been obtained from a supplier, it is necessary to reduce it to a size suitable for processing. Large samples may be reduced to test sample size by one or more passes through a sample splitter, commonly known as a Jones Riffle (Figure 3.1). This will divide the contents of a sample in half, while maintaining the particle size distribution of the original sample. Repeated passes allow the sample to be split into quarters, eighths, and so on until the size of the sample desired for a test run is obtained.



Figure 3.1: Jones Riffle Splitter

3.1.2 Cone and quartering

Cone and quartering is another method of splitting a gross sample into representative smaller sizes, using a manual technique. The researcher arranges a pile of the gross sample in a rough cone shape, scrapes the material up round the edges and deposits it on top, allowing it to run down equally in all directions, thus mixing the sample thoroughly (see A in Figure 3.2). The sample is then flattened into a circle with a shovel, and gradually spread to a uniform thickness (B). The researcher marks the flat pile into quarters, and rejects two opposite quarters (C). The rejected quarters are returned to

the stock. After that the two quarters remaining can be mixed into a conical pile created by taking alternate shovel-fuls from each. This process of piling, flattening and rejecting two quarters is continued until the sample is reduced to the required size.

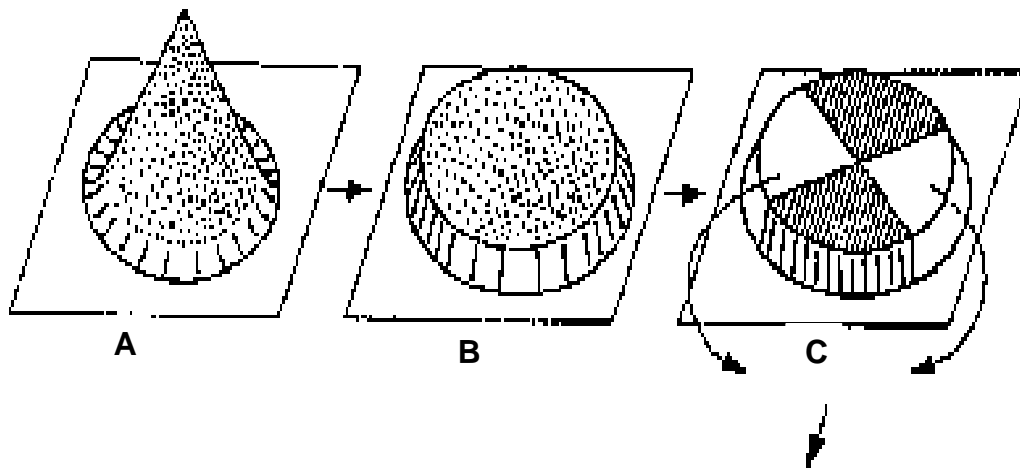


Figure 3.2: Cone and quartering (www.nzdl.org)

3.2 Milling equipment

3.2.1 Tumbling ball mill

The ball mill is a grinding mill used to reduce the size of ore particles by a combination of impact and abrasive forces. The grinding medium used usually takes the form of steel balls that are free to move inside the mill to crush the feed material by impact and attrition. Mill rotation carries both the grinding medium and the feed material round the interior of the mill. As the balls tumble down, they strike the feed material particles nipped against other balls or mill surface. In general, the movement of balls in the mill will rub the powder particles between them, breaking down the ore further.

The rotation speed of the mill has a strong bearing on the tumbling action occurring within it. At low rotational speeds the balls tumble gently, while as the speed increases the tumbling action accelerates, and the ball bed appears like an inclined surface from which balls rebound, roll down and re-encounter the surface. At higher rotational speeds the balls attach themselves to the interior surface, and rotate at the mill's speed, a condition known as centrifuging. The fraction of critical speed at which this occurs is a function of the mill filling, the size of the grinding medium and the design of the mill itself.

Although ball mills have been designed to a high degree of mechanical efficiency in achieving size reduction, they are extremely wasteful in terms of energy. This is mainly because in general the feed material is broken as a result of repeated, random impacts, which fragment liberated as well as un-liberated particles. At present, there is no practical way to ensure that these impacts are directed at the interfaces between the grains, which would greatly improve liberation.

In mineral processing, all ores have to be reduced to a desired/specified size range for efficient downstream processing. It is the purpose of all size reduction equipment, including a ball mill, to produce this size range. Correct grinding is often said to be the key to good mineral processing. Under-grinding the ore results in a product that is too coarse, with a low degree of liberation, while over-grinding wastes energy, reduces the particle size of the already liberated gangue, and may also reduce the particle size of the liberated mineral value to one below that required for efficient separation. Part of the

aim of the experiments described in the chapters that follow is to find ways to achieve the desired degree of grinding on a batch basis.

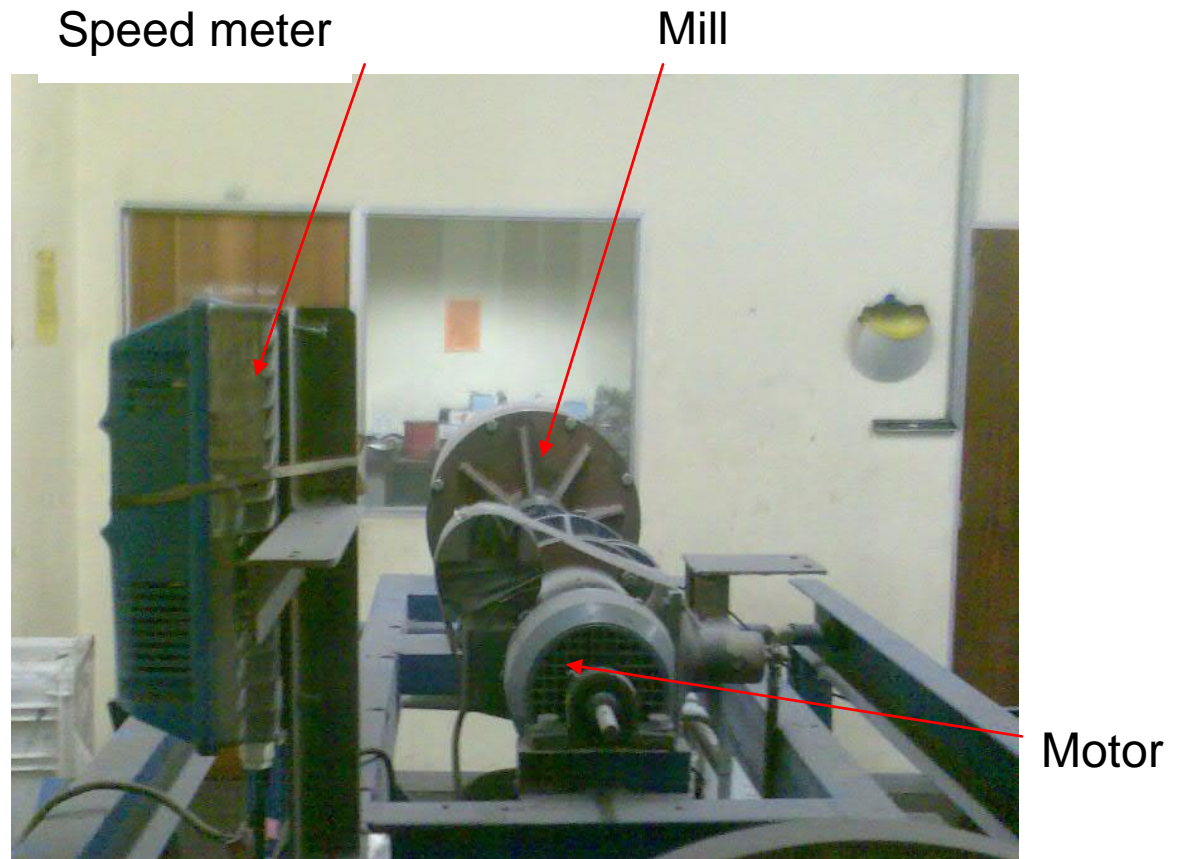


Figure 3.3a: Rear view of the tumbling ball mill equipment in the Mineral Processing laboratory at the University of the Witwatersrand.

Figure 3.3a shows the tumbling ball mill equipment we used in the experimental set-up. The 30.2 x 29.5 cm mill is a standard laboratory test mill fitted with eight rectangular prism liners. The mill is driven by a 2.5 kW motor and has an adjustable speed meter, which reads the speed of rotation in settings that can be adjusted to revolutions per minute (RPM) using a speed calibration procedure. The voltage drawn by the mill was

measured and this reading was converted to the torque on the mill, as explained in Chapter 4.



Figure 3.3b: Front view of the ball mill charged with a slurry and grinding media

Figure 3.3b shows the front view of the tumbling ball mill equipment we used in the experimental set-up, charged with a slurry and 10mm balls as grinding media.

3.3 Size analysis equipment

3.3.1 Test sieves



Figure 3.4: Stacked sieves used for a size test

Sieving is the physical separation of fine from coarse material by means of a perforated vessel, or as in this case, a series of vessels in a stack (Figure 3.4), arranged in order of the size of the mesh, the coarsest sieve at the top and the finest at the bottom. The general practice is to use the fourth or square root of two series rule to regulate the sizes. The bottom sieve has the finest mesh openings; the sieve above it has openings four or two times larger than the one beneath it; and so on for the other sieves in

the stack. The use of sieves in this sequential order allows for better data presentation and a more meaningful analysis of the test results. Another consideration is the quantity of material. There is a natural (but incorrect) tendency to use a large sample of material when sieving, but a smaller sample allows for a more accurate analysis. If the sample is too large, there is a smaller opportunity for each of the particles to contact the screen surface. On the other hand, there is a limit to a lesser mass of material in a sample. Too low an amount will result in an inaccurate measurement when the amount that rests on the sieve is weighed, because the measuring equipment used cannot weigh masses below two decimal places. Generally a 25–100 g sample size sieved for time intervals of between 10–20 minutes is recommended (www.advantechmfg.com). The exact experimental conditions and methods used for sieving are given in Chapter 4.

Sieving is easy, inexpensive and produces results rapidly, which is why sieves are widely used in particle size analysis work. However, sieves are fabricated of a woven mesh material, and variations in the weave are common. This may hinder the reproducibility of test results between sieves. Also, because of the variation in size of the openings, some smaller than normal and some larger, the time intervals at which the sieve analyzes take place also become extremely important.

Some of the terminology used in sieving is listed below.

i. Agglomeration

Agglomeration is the sticking together of particles to one another. This condition commonly occurs in materials possessing high moisture content. In order to

prevent agglomeration from occurring, materials are normally dried in an oven before sieving.

ii. Blinding

Blinding is the obstruction of the sieve apertures with particles. This is usually caused by either working with particles that are exactly the same size as the screen opening or by the build-up of a number of fine particles on the wire mesh that eventually closes off the openings. Blinding can also result from sieving agglomerated material or working with a sample quantity too large for the sieve.

iii. Electrostatic charges

Electrostatic charges result from an accumulation of electrical charges on the particles and sieve components. These cause agglomeration of the material and blinding of the sieves. This condition is frequently seen in materials with a large fraction of particles that are finer than 25 μm .

iv. Test sieve

A test sieve is a mesh screening medium with openings of uniform size and shape, mounted on a rigid frame. Normally it is used for laboratory testing or for small scale production applications.

v. Wet sieving

Wet sieving involves separation by means of a testing sieve of fines from the coarser portion of the sample. Usually a gentle spray of water is used to break down any agglomerates that may have formed and also lubricate near-size particles so they can pass through the mesh. After the fines have been washed through the sieve, the remaining material is oven-dried and analyzed.

vi. Pan

A pan is a vessel that receives the materials passing through the finest sieve. Most pans have an extended rim with a skirt that is designed as a nest for a sieve stack in order to make it easy to mount on a mechanical shaker.

vii. Skirt

A skirt is a section of a test sieve below the sieve mesh that allows for the sieves to be nested in a test stack.

3.3.2 Mastersizer 2000MU



Figure 3.5: The Malvern particle size analyzer

The Mastersizer 2000MU (Figure 3.5) is a piece of equipment for laser diffraction particle sizing that relies on the fact that the diffraction angle of light is inversely proportional to the particle size of the sample being measured (Deal, Kappes & Lee 2011). The Mastersizer is an instrument designed to measure the particle size distribution of wet and dry samples, using Hydro 2000MU and Scirocco 2000A cells respectively. The instrument has the advantages of a wide measuring range (from 0.02–2000 microns) and rapid data production. This is desirable in industrial cases where product quality controllers are expected to give rapid feedback to plant operators for process adjustment purposes.

The Mastersizer 2000MU consists of:

- **A source of light**

A laser is used to provide a coherent intense light beam on a fixed wavelength.

- **A suitable sample dispersion detector**

The key to a quality particle size measurement technique is the ability to present a well-dispersed homogeneous sample to the laser beam at an appropriate concentration and with a minimum of bias.

- **A light detector**

Light scattered by the sample is focused onto a photosensitive silicon detector, which is made up of a large number of discrete elements. The optical system is optimized to ensure that the signal from each element is directly proportional to the amount of light on it.

- **A means of passing the sample through the laser beam.**

A dry powder can be blown through the beam by means of pressure, and then sucked into a vacuum cleaner to prevent dust being sprayed into the environment. Particles in suspension can be measured by recirculating the sample in front of the laser beam, using water as a dispersant.

- **Data collection and analysis**

Hundreds of thousands of particles will pass through the laser beam every second. The light falling onto the detectors is measured and integrated 500 times each second. This makes it possible to obtain a statistically significant scattering pattern of the widest distributions within a few seconds. Microsoft Windows-based software can be used to capture and analyze the results, which can then be exported to basic

Excel. The exact experimental conditions and methods used in the Malvern analysis are given in Chapter 4.

3.4 Filtration equipment

3.4.1 Buchner funnel

A Buchner funnel is a device that separates insoluble solids from liquids, so that the useful part (the solids) can be processed. These filters generally work in a "batch" manner. They are loaded with slurry before undergoing a filtering cycle that produces a batch of solid filtered material, called the filter "cake". Water is used to create a venturi effect that lowers the pressure, forcing the water to flow through the filter cake. This is more efficient than filtration using a funnel and paper, which utilizes the low pressure caused by the weight of the liquid on the filter paper to carry out the separation. The solid is removed, the filter re-loaded with slurry, and the batch cycle repeated. The Buchner funnel used in these experiments was 22 cm in diameter.

3.5 Analytical equipment

3.5.1 Atomic Absorption Spectrometer (AAS)



Figure 3.6: Atomic Absorption Spectrometer (AAS)

Atomic Absorption Spectroscopy is a technique for determining the amount (concentration) of a particular metal element in a sample. The chemical composition of a sample may be used to give some indication of the proportion of values contained in the ore. If the mineral phase of interest contains an element that is found only in one phase, the AAS (Figure 3.6) identifies its presence and quantity, which is important if it

is a valuable mineral. Chemical analyzes can normally be used reliably as a first indication of the mineralogical composition of the ore. This information is vital to drawing up an optimum flow sheet for processing the material. In general, elemental analysis can be done accurately, reasonably fast and at a relatively low cost. Other and more accurate means of mineralogical analysis of samples take longer and are very expensive. Because chemical analysis is cheaper than mineralogical, it is the former that is most widely used in the design and control of processes.

The AAS technique can be used to analyze the concentration of many different metals in a solution. The technique makes use of absorption spectrometry to assess the concentration of a component in a sample. The electrons of the atoms in the atomizer can be promoted to higher orbitals for a short period by absorbing a set quantity of energy (that is, light of a given wavelength). This amount of energy (or wavelength) is specific to a particular electron transition in a particular element. In general, each wavelength corresponds to only one element. This gives the technique its elemental selectivity. As the quantity of energy per unit time (power) put into the flame is known, and the quantity remaining on the other side (the AAS detector) can be measured, it is possible to calculate how many of these transitions have taken place, and thus get a signal that is proportional to the concentration of the element being measured.

3.6 References

Austin, L.G., Klimpel, R.R. & Luckie, P.T. 1984, "Process engineering of size reduction: ball milling", pp 234-247

Deal, M., Kappes, R. & Lee, J. 2011, "The applicability of alternative particle size analysis methods in laboratory testing", *SME Annual Meeting and Exhibit and CMA 113th National Western Mining Conference 2011*, pp. 579.

Hogg, R. & Fuerstenau, D.W. 1972 "Power Relations for tumbling Mills", *Trans, SME-AIME*, vol.252, pp. 418-432.

Wills, B.A. 1992, "Mineral processing technology", *5th edition*, pp 181-216

Test Sieving: *Principles and Procedures* (www.advantechmfg.com).

<http://www.nzdl.org>

<http://www.galbraith.com/spectroscopy.htm>

CHAPTER 4

4 EXPERIMENTAL SET- UP AND PROCEDURE

This chapter contains a summary of the experimental programme we followed in order to obtain the laboratory scale results that form the subject of discussion in the later sections of the thesis (see Figure 4.1 below). In this chapter we will give a detailed description of the procedure followed for each 'shaded' task in the experimental programme flowchart. The AR and the breakage kinetics analysis sections of the flowchart in Figure 4.1 will be discussed in detail in the subsequent chapters.

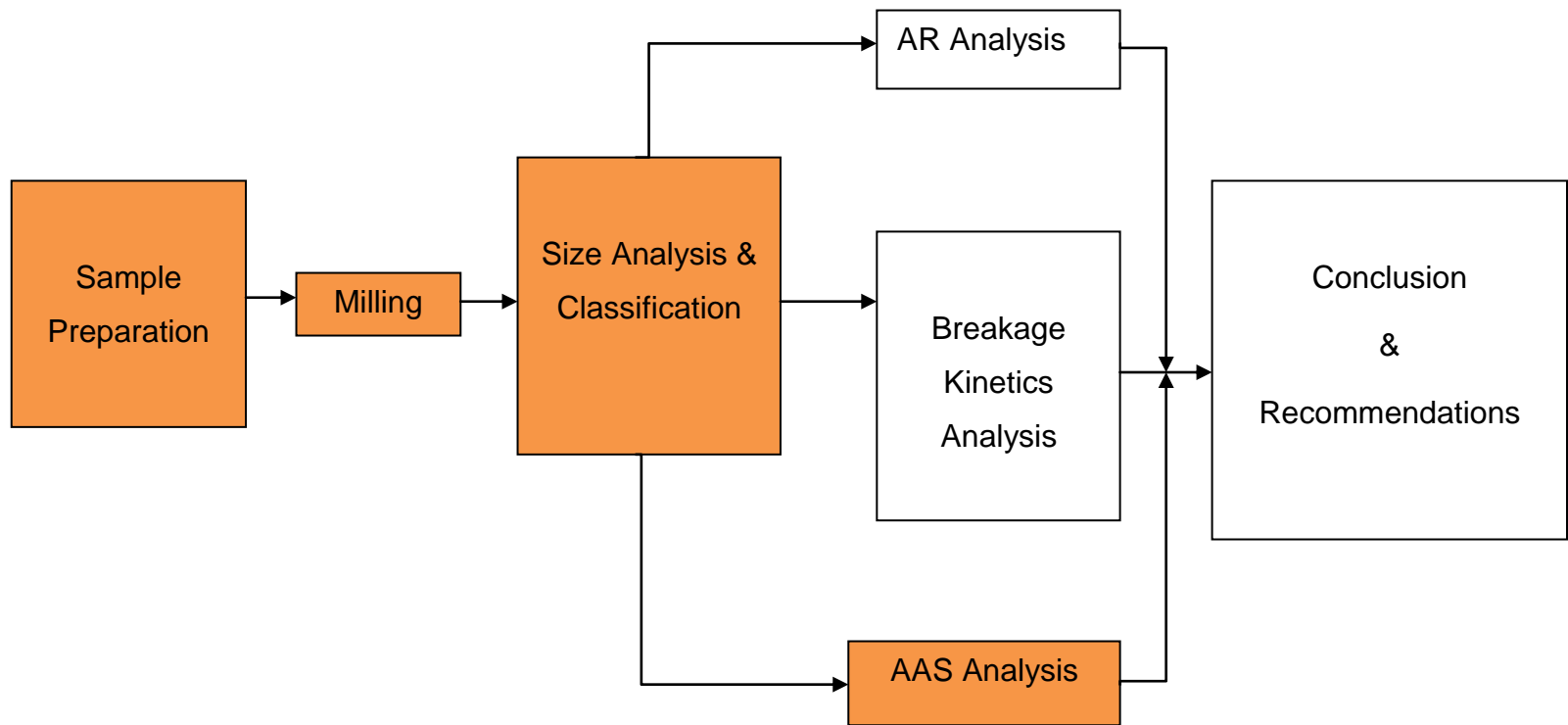


Figure 4.1: Experimental programme flowchart

4.1 Sample preparation

We obtained two 200 kg drums of dry UG2 material from Anglo Platinum's Amandelbult mine. The first task was to prepare this mineral ore in order to obtain smaller representative samples to be used as feed material for the subsequent milling tests. This we did by manually sieving the material, in fairly large amounts, through a 45 cm diameter 600 micrometer sieve, retaining the under-sized particles and returning the coarser pieces to the drums, so that at the end of this operation, we had a drum-full each of particles below 600 μm and those above. We then emptied the drum containing the former onto a 4 \times 4 square m piece of plastic paper spread on the laboratory floor. Using shovels, we mixed the material together thoroughly, and used the cone and quartering method to reduce the material sample quantity to about 25 kg. The discarded material was reserved for later use. We then used the Jones Riffle Splitter to obtain samples weighing about 500 g each, which we stored in separate polythene bags. These samples were used as feed material for the milling tests.

4.2 Milling

After sample preparation, we started the batch wet milling experiments on the ore samples. For each batch test, we charged a feed sample weighing 500g of platinum ore into the 30.2 \times 29.5 cm tumbling laboratory scale ball mill. The grinding medium consisted of 7.8 kg of single-sized 10 mm stainless steel balls. The effect of ball size was not considered in this work, and so the ball size was kept constant in all the experiments. We then added varying measured amounts of distilled water to the samples in the mill in order to obtain different slurry densities. Distilled water was used

in place of tap water because we wanted to eliminate the possibility of size reduction occurring as a result of any known or unknown chemical effects.

From the mill control room, we started and activated the wave-view software that records the voltage supply to the mill, and on the mill rig we set the speed of rotation of the mill at 68 revolutions per minute (RPM), so that we could use the voltage supplied and the speed of rotation of the mill to calculate the power drawn during milling. The effect of mill speed was not considered in this work, and so the mill speed was kept the same in all experiments. The mill was then run for grinding times ranging between 5–120 minutes for the different slurry densities. After each specific test grind period, we emptied the mill contents and separated the product slurry from the grinding media on a wire mesh. We retained the product slurry in a pan, and washed the balls so that they would be clean for the next batch test. Table 4.1 summarizes the specifications of the ball mill and the experimental parameters we employed in this investigation.

Table 4.1: Mill and experimental specifications

<i>Mill</i>	
Length (m)	0.302
Diameter (m)	0.295
% Critical speed (ϕ_c)	87.44
<i>Liners</i>	
Length (cm)	27.5
Width (cm)	2.5
Height (cm)	1.0
<i>Grinding Media</i>	
Material	Stainless steel balls
Diameter (m)	0.01
Fractional ball filling (J) %	8.2
<i>Powder Charge</i>	
Material	UG2 Ore
Density (kg/m ³)	3200
Particle size	-600 μ m
Fraction of voids filled with powder (U)	0.5
Slurry concentration (mass% solids)	20–50

4.2.1 Mill calibration

Before we used the ball mill in any milling tests, we carried out a torque and speed calibration. These calibrations are necessary because they enable us to calculate the power drawn P (in Watts) by the mill during operation (Equation 4.1), and also help us

to relate the settings on the speed-meter to the actual speed of rotation of the mill in RPMs.

$$P(W) = \frac{2 * \pi * [Speed(RPM) * Torque(N.m)]}{60} \quad (4.1)$$

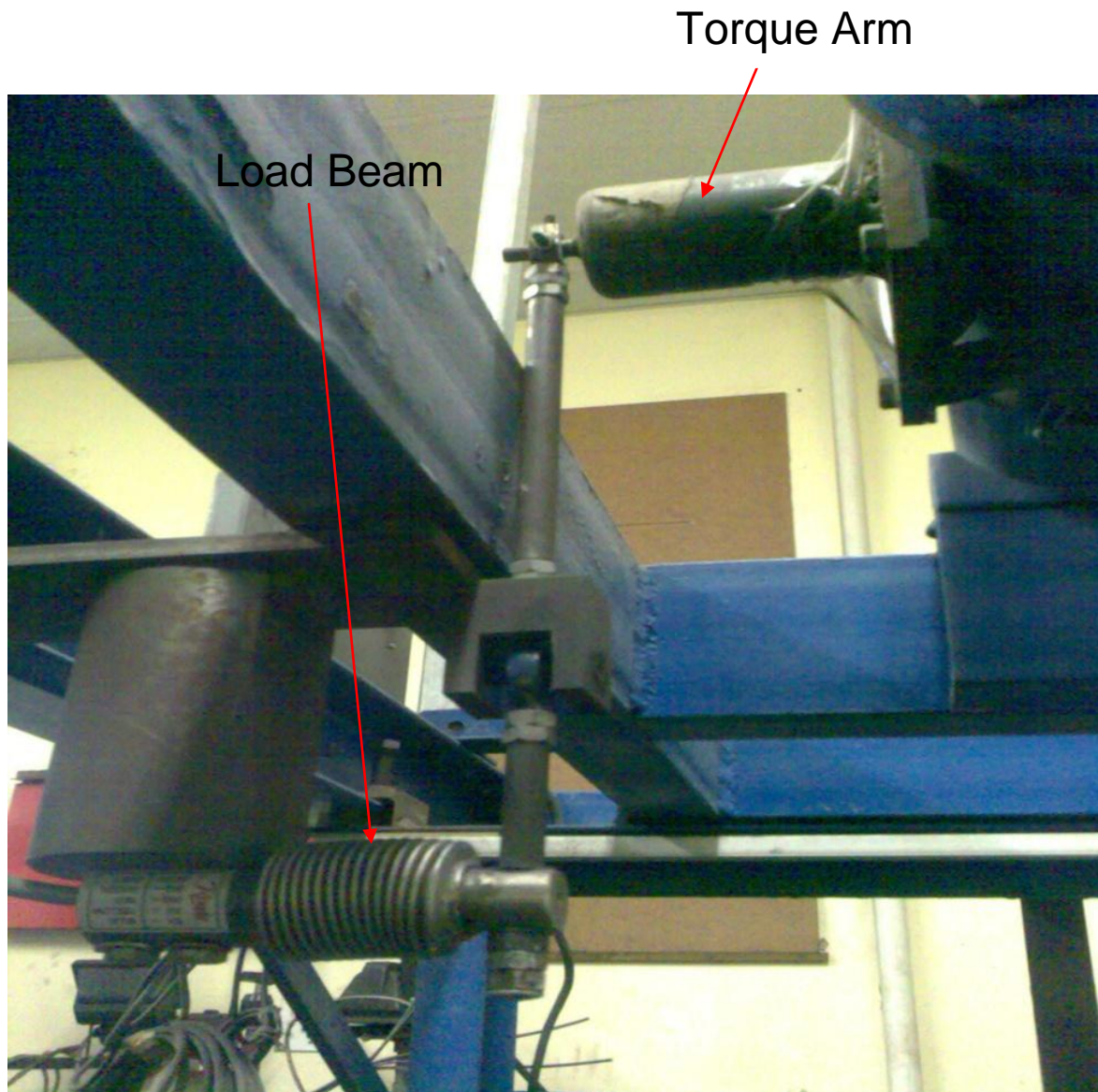


Figure 4.2: Torque calibration section of the mill equipment

Figure 4.2 is a photograph of the torque calibration part of a laboratory-scale tumbling ball mill. A series of set weights are hung from the load beam to assist the torque calibration procedure. Wave-view Microsoft Windows-based software was used to control the computer hardware, to acquire and to process the data recorded during an operation. By combining the output from the torque calibration, the voltage used and the actual rotation speed of the mill, the researcher is able to evaluate the power consumption of the mill during operation.

4.2.1.1 Torque calibration procedure

The torque calibration is carried out when the mill is empty. In order to warm it and eliminate variations in power drawn by the mill owing to friction, we start by running the empty mill for about 10 minutes before beginning the procedure. In torque calibration, we suspend a series of known weights, supported in a bucket, from the end of the load beam. We then run the empty mill at a selected speed for 60 seconds, and record the average voltage supply to the mill, using the wave-view programme. Each suspended weight has a corresponding output voltage.

The torque can then be evaluated using Equation 4.2:

$$T(N.m) = mgx \tag{4.2},$$

where m is the mass of the suspended (cumulative) masses in kg,

g is the acceleration due to gravity, in ms^{-2} , and

x is the distance from the centre of the mill to the end of the lever arm, in meters.

Table 4.2 shows a typical relationship between the suspended masses, the voltage drawn and the torque calculated by means of a calibration procedure. We used a total of six masses and a bucket as weights, and made every effort to ensure that the suspended masses were motionless before carrying out the procedure.

Table 4.2: Relationship between the torque and voltage for cumulative masses

	Individual mass (g)	Individual mass (kg)	Cumulative mass (kg)	x (m)	g (m/s^2)	Measured Voltage (v)	Evaluated Torque (N.m)
Bucket	227.70	0.23	0.23	0.22	9.81	3.45	0.50
Mass 1	2161.55	2.16	2.39	0.22	9.81	2.42	5.16
Mass 2	2179.73	2.18	4.57	0.22	9.81	1.37	9.86
Mass 3	2188.41	2.19	6.76	0.22	9.81	0.24	14.59
Mass 4	2195.84	2.20	8.96	0.22	9.81	-0.86	19.33
Mass 5	2200.37	2.20	11.16	0.22	9.81	-1.93	24.09
Mass 6	2191.33	2.19	13.35	0.22	9.81	-2.99	28.81

The relationship between the evaluated torque and the measured voltage is then plotted, as shown in Figure 4.3. The reason for doing this is to try and find a

mathematical equation (model) that can link these two parameters, after which it can be used during normal mill operation to evaluate the torque, and hence the power drawn by the mill during operation.

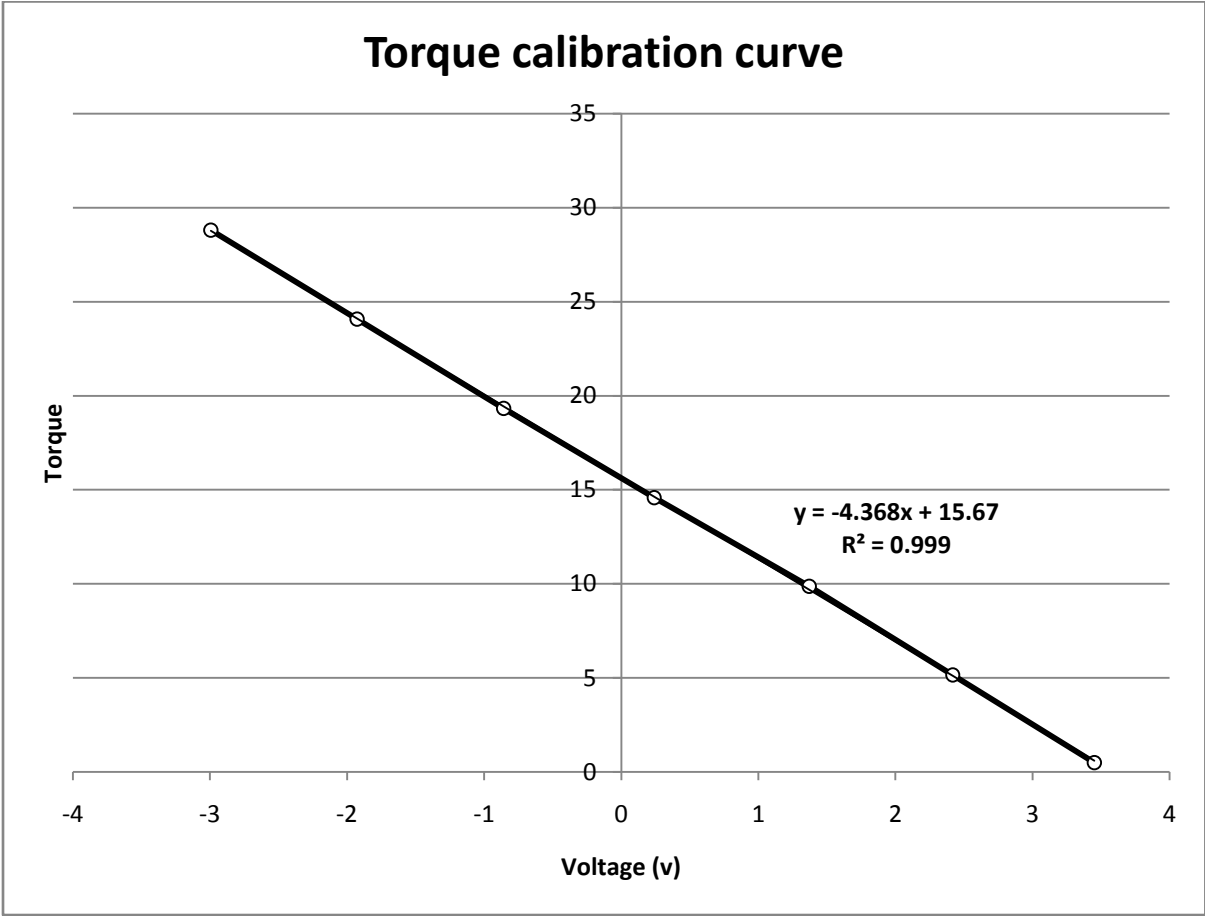


Figure 4.3: Plot of the relationship between torque and voltage generated by lifting different masses.

This linear relationship is given by Equation 4.3.

$$T(N.m) = -4.3687 * V + 15.679 \tag{4.3},$$

where T is the torque, in Newton–meters, and

V is the output voltage, in volts.

4.2.1.2 Speed calibration procedure

The speed calibration procedure is also carried out on an empty mill, without any weights suspended on the load beam. In order to calibrate for speed, the normal procedure is to activate the hardware on the wave-view programme and run the mill at different speeds, ranging between 10–90 speed settings. Using the revolutions (Rev) counter module of the Microsoft Visual Basic Applications software in the wave-view programme, we obtained the number of revolutions per minute for each speed setting. The relationship between the settings on the speed meter and the RPM are tabulated in Table 4.3 and plotted in Figure 4.4. We calculated the mill's critical speed using Equation 4.4, and applied it in Equation 4.5 to evaluate the percentage of the mill's critical speed.

$$\text{critical speed} = \frac{42.2}{\sqrt{D-d}} \quad (4.4),$$

where D is the diameter of the mill, and

d is the diameter of the grinding media used.

$$\% \text{ critical speed} = \frac{RPM}{\text{critical speed}} \times 100\% \quad (4.5)$$

Table 4.3: Relationship between the speed settings and actual speed of the mill

Speed Setting	RPM	% Critical Speed
0	0	0
10	11.38	14.57
20	22.76	29.15
30	34.14	43.72
40	45.52	58.29
50	56.90	72.87
60	68.29	87.44
70	79.67	102.01
80	91.05	116.59
90	102.43	130.63

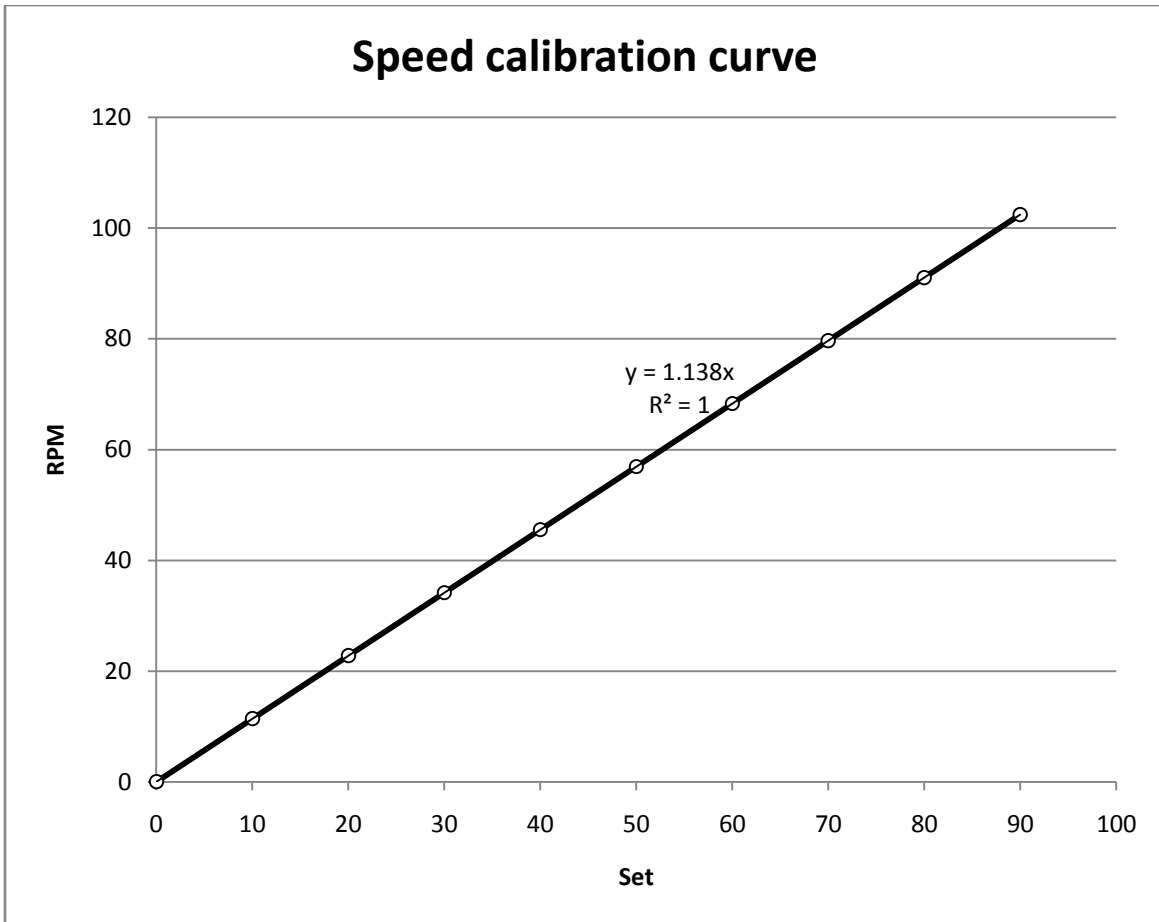


Figure 4.4: Plot of the relationship between the speed settings on the mill and the actual speed of rotation of the mill.

Figure 4.4 shows a plot of the relationship between the speed setting on the mill and the actual speed of rotation of the mill in RPMs. Speed calibration is significant in our experimental programme because it standardizes the speed specification, and it enables the researcher to evaluate the power drawn by the mill during operation by means of Equation 4.1.

4.3 Particle size analysis and classification

The next step after performing each batch test was for us to perform a particle size analysis test on the product material. A Mastersizer 2000MU wet cell was used to measure the particle size distribution.

4.3.1 Particle size analysis

An important preliminary to the particle size analysis was to homogenize the product slurry using a speed-adjustable electric mixer, after which we connected the Hydro 2000MU cell to the main unit and activated the Mastersizer software on the computer. Following the procedure in the manual supplied with the software, we specified the UG 2 ore as the material to be analyzed from the list of materials given. We placed 600ml of distilled water in the beaker, to be used as a dispersant, and circulated it around the unit at 3 000 RPM before adding the slurry. In order to prevent the larger-sized particles from settling to the bottom of the slurry, we fed the sample of material to the beaker (and hence the unit), while it was being agitated by the mixer. The Mastersizer software detects both the quantity being fed, and the point at which the quantity of material added reaches a certain pre-determined range. Figures 4.5 and 4.6 show the typical output of a Mastersizer measurement cycle. As shown on the plots, the results are volume- and not mass-based (the latter being the convention in the mineral processing field). This should not present a problem, however, because if the density of a material is constant, then the mass and the volume fractions of the material are the same.

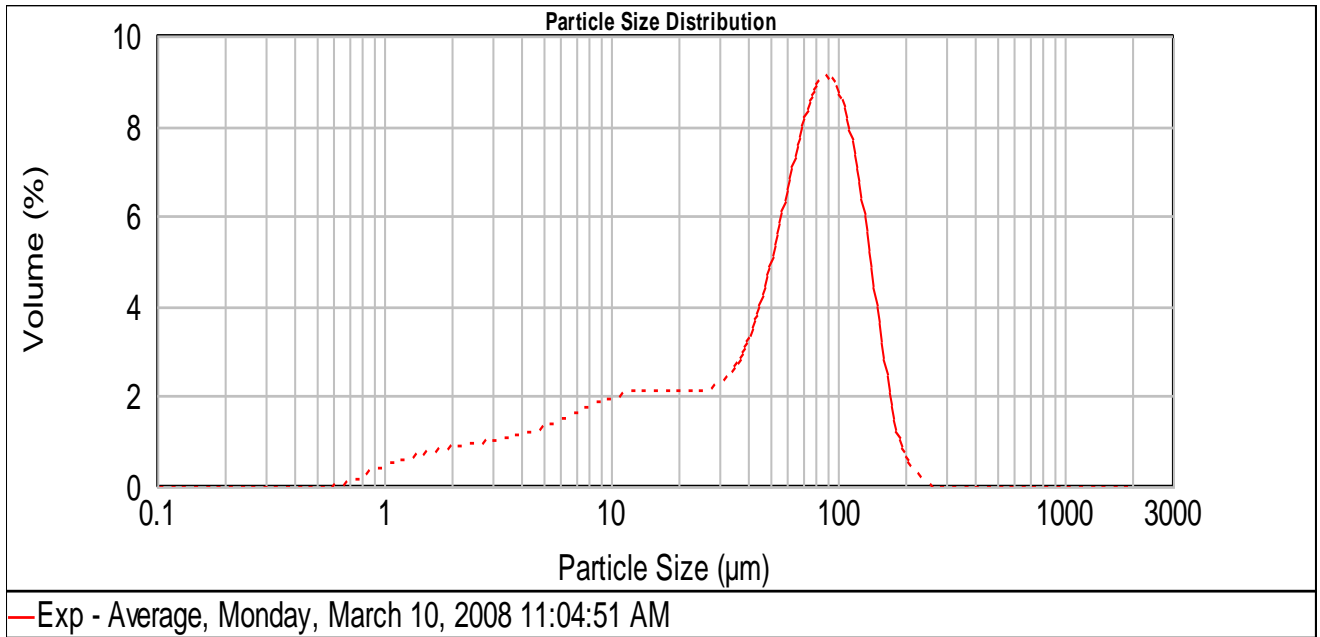


Figure 4.5: A typical frequency plot from the Mastersizer.

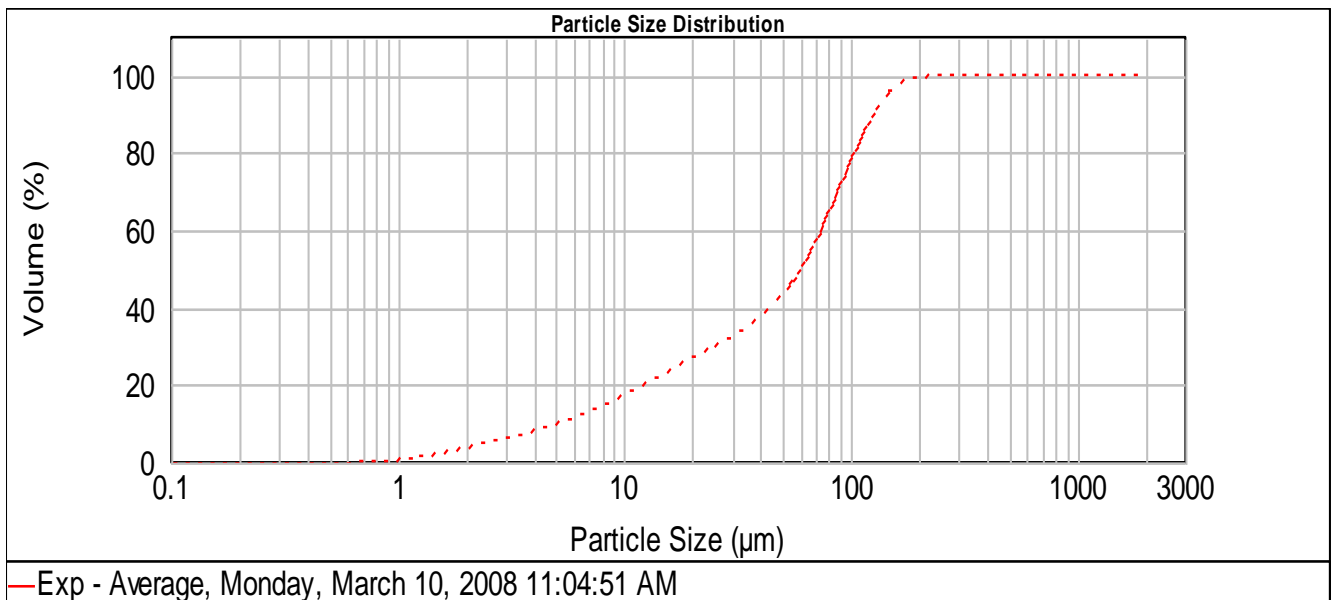


Figure 4.6: A typical cumulative plot from the Mastersizer

For data-handling purposes, the above plots make the task of analysis more difficult because they do not accommodate other graphical representations of the data. For example, it is not possible to use this interface to change the scale on the x-axis from

logarithmic to linear. Because of this inflexibility in the output style of the Mastersizer, we exported the measurement data points to Microsoft Excel, and then plotted our own frequency or cumulative graphs. This technique made it easy to manipulate the data to present it graphically in different formats.

4.3.2 Classification

After sample preparation, milling and product particle size analysis, we needed to prepare some samples of the product material to use on the Atomic Absorption Spectrometer (AAS) for chemical analysis. This involved the separation of solids into particle size ranges by means of a series of graded sieves of progressively finer mesh. We chose to work with dried samples so as to avoid the problems associated with sampling from slurry.

In performing this size classification, we first used a rotary Jones Riffle Splitter to reduce the mass of material from the mill to samples of about 100 g. Such a quantity is recommended in order to avoid blinding of the screens. After recording the empty masses of the individual sieves, we then arranged them in a stack using the square root of two series rule. The range of sieves used was 600 to 38 μm . We charged the stack of sieves with the dry sample, secured them on a mechanical shaker and sieved the samples for 20 minutes.

After this dry sieving, we took the stack of sieves to the laboratory sink and performed wet sieving, in order to break down agglomerated material on each individual sieve. This was done by gently spraying water on the top (600 μ m) sieve, and allowing it to flow down the stack, with the pan removed, and collecting the residue in a bucket. Since this water serves the purpose of removing fine material attached to the particles in each size range, wet sieving terminates when the water emerging from the bottom sieve remains clear.

We decanted the water in the bucket, took the solids from the bottom, and filtered them in a Buchner funnel. We then mixed the resultant cake from the filter and the material in the pan, weighed the mixture and transferred it to a sample holder, ready for AAS analysis.

After wet sieving, we dried the individual sieves in the laboratory oven at 30 °C for 24 hours, before re-weighing each sieve, in order to determine the mass of material retained on individual screens. The dry material was then removed from the sieves and stored in separate sample holders, ready for AAS analysis.

4.4 Atomic Absorption Spectrometer (AAS) calibration

In order to calibrate the AAS, we first prepared standard copper samples of concentrations ranging between 2–10 parts per million (ppm). We achieved this task by diluting a standard sample of known concentration with different volumes of distilled

water. We then analyzed the standard samples twice and found that they were in agreement with the calibration curves in the working manual for the AAS.

4.4.1 AAS analysis

The method given below is a standard procedure that has been used by previous researchers in the Centre (Gorimbo 2011). AAS analysis requires that the sample feed be in a liquid form. After we had separated the product material into different particle size ranges correspondent to the fineness of the sieve, we pulverized the samples in a glass crucible and weighed out about a gramme from each size range to be put into 50 ml conical flasks. We then added 30 ml of an acid mixture to each flask. This mixture was made up of three parts of 32% concentrated sulphuric acid and one part of 55% concentrated nitric acid.

The conical flasks were then placed on a hot plate set at a temperature of 60⁰C, for 30 minutes. After cooling them, we filtered the contents into 100ml volumetric flasks through filter papers in funnels. We then topped up the volume of the contents to the 100ml mark with distilled water. The now liquefied (digested) samples were then taken to the AAS and analyzed for copper.

4.5 References

Joshua Gorimbo, MSc thesis, 2011. Effect of the homoionic form of clinoptilolite on Ni²⁺ adsorption isotherms: a thermodynamic study. University of the Witwatersrand.

CHAPTER 5

5 LABORATORY SCALE APPLICATION OF BREAKAGE KINETICS DATA TO CHARACTERIZE AN UPPER GROUP (UG) 2 ORE

5.1 Introduction

We carried out the first series of wet milling batch tests in a laboratory-scale ball mill with an UG2 ore feed in which the particles were below 600 μ m in size. We obtained the feed material from Anglo Platinum Amandelbult Plant's primary cyclone underflow (feed to the secondary mill). The purpose of these experiments was to test the hypothesis that it may be possible to grind and discard selectively, that is, to mill the desired component and/or remove other components of no value, from feed material that is apparently heterogeneous. If it is shown to be possible, then one could in principle choose to grind one component only, thereby effectively reducing the feed to the subsequent processing units.

Characterization of ores is normally done using scanning electron microscopes (SEMs), X-ray Diffraction (XRD), X-ray fluorescence (XRF), and, more recently, the Mineral Liberation Analyzer (MLA) developed at the Julius Kruttschnitt Mineral Research Centre (JKMRC) at the University of Queensland in Australia. However, the above methods require not only a sophisticated level of analytical skills, but they are also time-consuming and expensive to carry out. The novelty of the work presented here lies in the simplicity of the method used to carry out the characterization, which requires only the breakage kinetics data and basic process modelling skills.

The outcome of this study could be of great benefit to scholars, mineral processors and designers of milling circuits, as it offers a new approach to how selective grinding can be achieved by simply varying the grinding period and amount of water added to the mill. Too long a grinding period wastes energy, reduces the particle size of the already liberated gangue, and may also reduce the particle size of the liberated mineral value to a size below that required for efficient separation. Too short a grinding period results in a product that is too coarse, with a low degree of liberation.

The innovation proposed in this thesis, which offers a means to increase mineral recoveries and reduce energy consumption, may be employed to change the manner in which mills are currently operated.

5.1.1 Mineral processing circuits

At present, the extraction of PGMs from ores in South Africa follows the traditional route, which involves three stages: reducing the ore to a concentrate in a minerals processing circuit; converting it to a matte in a smelter; and separating individual metals from the matte in a refinery (Bryson 2004). In this approach, the efficiency of the extraction process depends strongly on that of the first stage. The majority of PGMs produced in South Africa are obtained from the UG2 chromitite reef (Hay, Roy 2010) of the Bushveld Igneous Complex because, while the Merensky reef deposits have become depleted, those from the Plat reef are low in PGM values.

Because current mineral processing circuits are not as effective in liberating valuable minerals (values) from gangue in the UG2 ores as they could be, researchers are continually investigating ways of improving their performance. The laboratory-scale study outlined in this chapter tests our hypothesis that the UG2 ore is heterogeneous and that it may be possible to grind the desired component selectively and/or remove the component of no value. If the results prove the hypothesis true, we can derive many advantages. Selective grinding might reduce the amount of energy required by the mill, require a smaller mill size, and greatly improve overall mineral recoveries, as only material of value would be processed.

5.1.2 Process modelling

One of the tools that are commonly applied to evaluate whether comminution is being carried out effectively is process modelling (Fuerstenau, Venkataraman 1988), which in theory makes it possible to predict accurately the product particle size distribution (PSD) after a certain grinding time and under specified grinding conditions (Das, Khan & Pitchumani 1995). Process models can be used, among other things, as benchmarks that can be used by operators to set mill residence times and process conditions in order to produce particles in the size range required by a designated downstream process. The problem associated with using a less accurate model to estimate the amount of material remaining in a chosen particle size range (size class) is that one misses out on the optimum grind time to be used to produce a desired fineness of grind, and hence risks either grinding too fine (wasting energy in the process) or grinding too coarse (reducing the efficiency of downstream processes such as floatation). Using a less accurate model also

leads to over- or under-design of equipment, and following operating procedures that are neither optimal nor economic.

First order models are often valid and frequently used in the analysis of the rate of breakage of single-component (homogeneous) material in a batch laboratory scale ball mill. However, batch tests do not always fit the first order model, and there are various hypotheses as to why this happens. Austin, Shoji & Bell (1982) postulated that the non-linear breakage of material can be due to a general slowing down of all grinding rates as fines accumulate in the charge, calling this behaviour the 'mill environment' effect. However, this phenomenon is only applicable to fine dry grinding. Austin also noted that the effect also occurs when the particles are too large to be properly nipped by the balls. In this case the material behaves as if some particles are relatively weak, while others are stronger. For the latter effect, he suggests that the first order breakage model can be split into two parts, a fraction ϕ of the weak material (with a specific rate of breakage S_A) and a fraction $1 - \phi$ of strong material (with a specific rate of breakage S_B). He called this phenomenon the 'material' effect. Another possible reason why batch tests do not conform to first order kinetics could be that the material is non-homogeneous (heterogeneous). In such a case, the material would not consist of 'weak' and 'strong' but rather 'soft' and 'hard' particles.

We needed to perform further experimental tests on the material, as discussed in the next chapter, in order to eliminate the possibility of the presence of 'weak' and 'strong' as opposed to 'soft' and 'hard' particles in the ore.

Various models can be used to predict the PSD of multi-component or heterogeneous feeds, as summarized in section 5.2. These models appear to be non-first order, but can also be a simple combination of two first-order models. The models can be employed to predict the grinding of the overall mixture by fitting data obtained from simple batch tests, and this is the method we used to test our hypothesis. The model parameter estimation is arrived at via a 'force fixing' technique, which involves minimizing the numerical estimation of the sum of squares of the deviation between model prediction and experimental data. We can do this by searching in the parameter space until an acceptable fit with the experimental data is achieved.

5.1.3 Particle size classification

In this experimental work we considered three particle size ranges (size classes). These are the feed (size class 1); an intermediate or desired size class (2), and the fines (size class 3). Because the fines size class do not float easily, this result in the loss of values. The lower range of the feed size class chosen was particle sizes above 45 μm in diameter; the intermediate was particle sizes between 15–45 μm ; and the fines, particle sizes below 15 μm . Although any set of size classes and size specifications could be defined, we chose the set of sizes specified above so as to place size class 2 as the desired product within the ideal range for flotation (Maharaj, Loveday & Pocock 2011) conducive to removing the valuable material from the gangue.

5.2 Kinetic approach to grinding

In the analysis of various types of grinding mills, the concept of treating grinding as a rate process (like chemical reactor design) is well accepted (Tangsathitkulchai 2002). A batch

grinding process is commonly characterized by two main functions, selection (S_i), which gives the rates of breakage of each size class i ; and breakage (b_{ij}), which describes the size distribution of the primary product particles (Berube, Berube & Le Houillier 1979) broken from size class j and reporting to size class i . An expression of the rate for a grinding system is given by a size-mass balance equation:

$$dm_i(t)/dt = -S_i m_i(t) + \sum_{j=1}^{i-1} b_{ij} S_j m_j(t) \quad (5.1),$$

where:

i and j are size classes,

$m_i(t)$ is the mass fraction of the particles in size class i , after a grind time t ,

S_i is the specific rate of breakage of size class i

b_{ij} is the mass fraction of broken products from size class j , which appear in size class i on primary breakage, and

t is the grinding time.

Equation 5.1 makes it possible to predict the product PSD at various grinding times (Reid 1965) if the parameters b_{ij} and S_i are known for all size classes. For breakage of the feed (size class 1) material, integration of Equation 5.1 yields:

$$m_1(t) = m_1(0) \exp^{-S_1 t} \quad (5.2)$$

or

$$\ln[m_1(t)/m_1(0)] = -S_1 t \quad (5.3).$$

If the grinding process follows a first order model, then a plot of $\ln[m_1(t)/m_1(0)]$ versus t should give a straight line, the gradient of which is the selection function or first order rate of breakage (S_1) (Tangsathikulchai 2003). In many cases, breakage of material in a batch laboratory ball mill will show a reasonable approximation to what Equation 5.2 leads one to expect (Austin, Shoji & Bell 1982). Breakage does not, however, always follow a first order model (Austin, Trimarchi & Weymont 1977). There are many reasons for deviation (Rajamani, Guo 1992), including the environment inside the mill, such as slurry density (Verma, Rajamani 1995); a cushioning effect; a number of different sizes in the feed; and a range of components of varying hardness. Gardner and Rogers (1975) proposed, developed and demonstrated a two-component approach to comminution processes that exhibit heterogeneous breakage characteristics. This was based on the posit that the material is made up of two separate components, each with different breakage properties. This can be represented as two parallel first-order models, requiring a separate equation for each component, which enable the analyst to explain this discrepant behaviour (in other words, not conforming to first-order modelling) by means of similar terminology and methodology to that can be used in relation to first order modelling.

Considering a composite binary mixture of a soft and a hard material, with φ the fraction of soft material 'A' and $(1 - \varphi)$ the fraction of hard material 'B', the left-hand side of Equation 5.1 can be modified such that the total rate of breakage of size class i (as shown by Equation 5.4) results from the sum of the rates of breakage of the soft (Equation 5.5) and hard (Equation 5.6) components, taking their relative abundance in the ore into consideration.

$$d[m_i(t)]/dt = \varphi dm_{iA}(t)/dt + (1 - \varphi) dm_{iB}(t)/dt \quad (5.4),$$

in which $dm_{iA}(t)/dt = -S_{iA}m_{iA}(t),$ (5.5)

and $dm_{iB}(t)/dt = -S_{iB}m_{iB}(t).$ (5.6).

Where:

m_{iA} is the mass fraction of material of size class i *in the soft component A*, after a grind time t ,

m_{iB} is the mass fraction of material of size class i *in the hard component B*, after a grind time t ,

S_{iA} is the specific rate of breakage of the soft component in size class i , and

S_{iB} is the specific rate of breakage of the hard component in size class i .

For the feed size class (m_1), Equation 5.4 can be integrated to obtain a two-component first-order breakage model, as given by Equation 5.7. This expression is actually a modification of the single component first order model (Equation 5.2), which has been split into two parts, composed of a fraction φ of the soft component 'A' (with a specific rate of breakage S_{1A}) and a fraction $1-\varphi$ of the hard component 'B' (with a specific rate of breakage S_{1B})

$$m_1(t) = \varphi \exp^{-S_{1A}t} + (1 - \varphi) \exp^{-S_{1B}t} \quad (5.7).$$

We can also perform a similar kinetic analysis as above, for the intermediate size class (m_2) material. For this scenario, the first-order breakage model of a single component ore is given by Equation 5.8, which is Equation 5.1 applied to size class 2:

$$\frac{dm_2(t)}{dt} = -S_2m_2(t) + b_{21}S_1m_1(t) \quad (5.8),$$

where:

$m_2(t)$ is the mass fraction of material in the intermediate size class, after a certain grinding time,

$m_1(t)$ is the mass fraction of material in feed size class, after a certain grinding time,

b_{21} is the fraction of material broken from the feed size class that reports to the intermediate size class,

S_1 is the breakage rate function of feed size class material, and

S_2 is the breakage rate function of intermediate size class material.

Further integration of Equation 5.8 yields Equation 5.9:

$$m_2(t) = m_2(0)\exp^{-S_2t} + \frac{b_{21}S_1m_1(0)}{S_2-S_1}[\exp^{-S_1t} - \exp^{-S_2t}] \quad (5.9).$$

Modification of the above single component first order breakage model for the intermediate size class material, in order to incorporate a second component, results in Equation 5.10.

This expression is basically a split of the right-hand-side of Equation 5.9, into two parts,

composed of a fraction φ for the soft component 'A' and a fraction $(1-\varphi)$ for the hard component 'B', each with its own specific rates of breakage.

$$m_2(t) = \varphi \left[m_2(0) \exp^{-S_{2A}t} + \frac{b_{21A} S_{1A} m_1(0)}{S_{2A} - S_{1A}} [\exp^{-S_{1A}t} - \exp^{-S_{2A}t}] \right] + (1 - \varphi) \left[m_2(0) \exp^{-S_{2B}t} + \frac{b_{21B} S_{1B} m_1(0)}{S_{2B} - S_{1B}} [\exp^{-S_{1B}t} - \exp^{-S_{2B}t}] \right] \quad (5.10),$$

where:

$m_2(t)$ is the mass fraction of material in intermediate size class, at time t ,

$m_1(0)$ is the mass fraction of material in feed size class, at $t = 0$ minutes,

b_{21A} is the fraction of soft component broken from the feed size class that reports to the intermediate size class,

b_{21B} is the fraction of hard component broken from the feed size class that reports to the intermediate size class,

φ is the fraction of the soft component of the ore,

S_{1A} is the breakage rate function of the soft component in the feed size class,

S_{1B} is the breakage rate function of the hard component in the feed size class,

S_{2A} is the breakage rate function of the soft component in the intermediate size class, and

S_{2B} is the breakage rate function of the hard component in the intermediate size class.

5.3 Experimental procedure

The feed stock material was sampled from the primary cyclone underflow, which is the feed to the secondary mill at Anglo Platinum's (Amandelbult) mine. We started the experimental work by performing a feed sample preparation as described in Chapter 4 (section 4.1). The ball mill containing 7.8kg of graded 10mm stainless steel balls, to be used as grinding media, was charged with a prepared feed sample of 500g of pre-milled UG2 ore. We added distilled water to the mill charge, in a range of measured volumes to obtain different fractions by mass of the solids in the mixture (slurry densities), and ran the mill for grinding periods ranging from 5–120 minutes. After each specific test grind period, we emptied the contents of the mill and separated the product slurry from the grinding media on a wire mesh. We then used a Malvern Hydro 2000MU particle size analyzer to examine a sample, taking care to keep the contents moving to prevent the particles from settling. The experimental parameters used are summarized in Chapter 4 (Table 4.1).

5.4 Discussion of experimental results

The size distribution of the overall feed material used in this experimental test programme comprising typical UG2 material is presented in Figure 5.1.

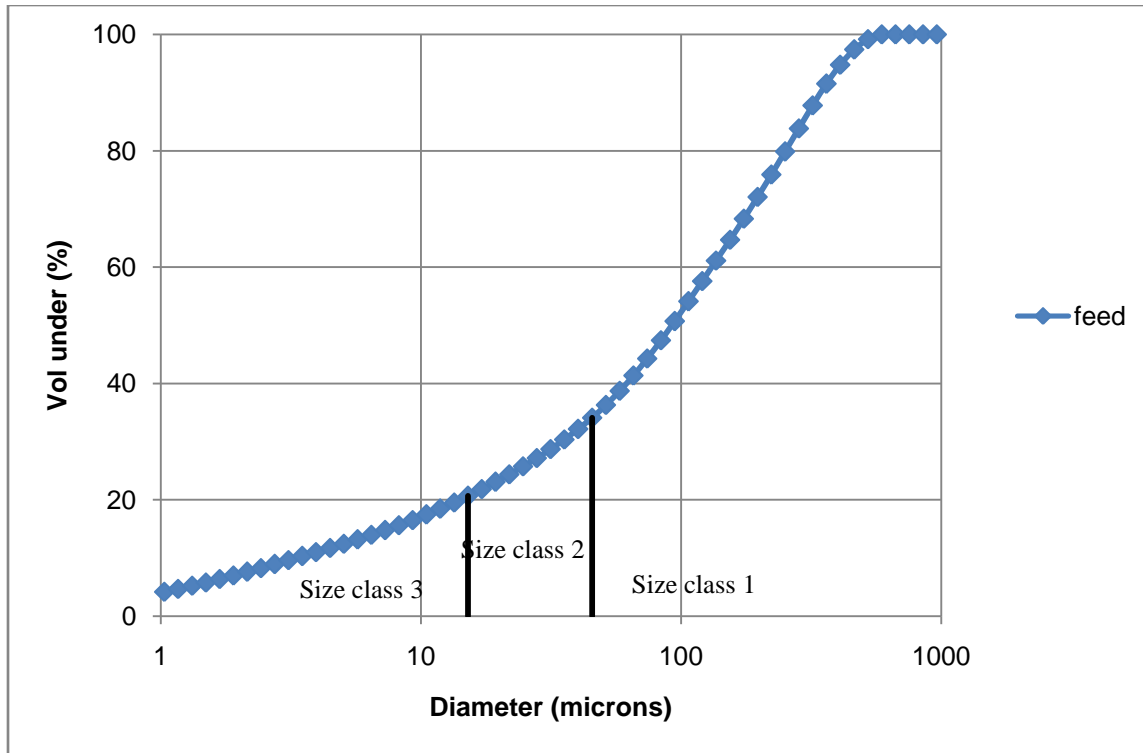


Figure 5.1: The particle size distribution (PSD) of the feed material used for the experiments. The size ranges of the feed size class (class 1), the intermediate size class (size class 2) and the fines (size class 3) are shown on the Figure.

One can see that the feed material is not mono-sized, but rather split into 67% in size class 1, 13% in size class 2, and the balance (20%) in size class 3. This PSD is summarized in Table 5.1.

Table 5.1: Size classes specification

Size class	Cut-off points (microns)	Composition (%)
1	+ 45	67
2	-45 + 15	13
3	-15	20

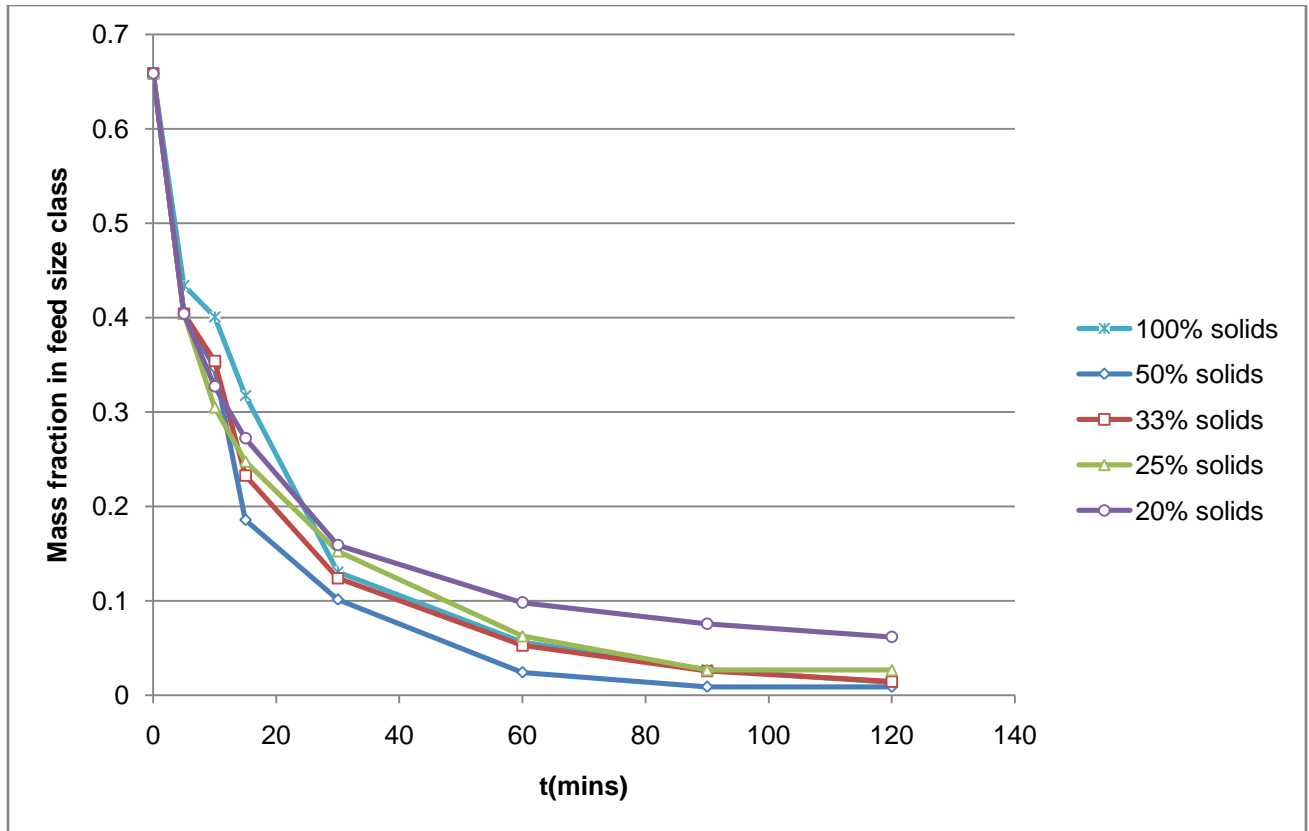


Figure 5.2: Mass fraction of feed size class material with different solid contents versus grinding time.

Figure 5.2 shows the mass fraction of material remaining in the feed size class after a grind time t , versus grind time for different percentages of solids, based on the data in Appendix A, Tables A1–A5. Straight lines are added between points to make the plot of breakage behaviour easy to follow. It can be seen in the above figure that the initial (0–10 minutes) breakage is similar for all solids concentrations and that differences occur only later, as the grinding progresses. Accordingly, we then considered the breakage kinetics of the feed size class material with different concentrations of solids, by plotting $\ln(m_1(t)/m_1(t=0))$ vs t . According to Equation 5.3, if the breakage kinetics are first order, the graphs should be linear. The results are graphically represented in Figure 5.3

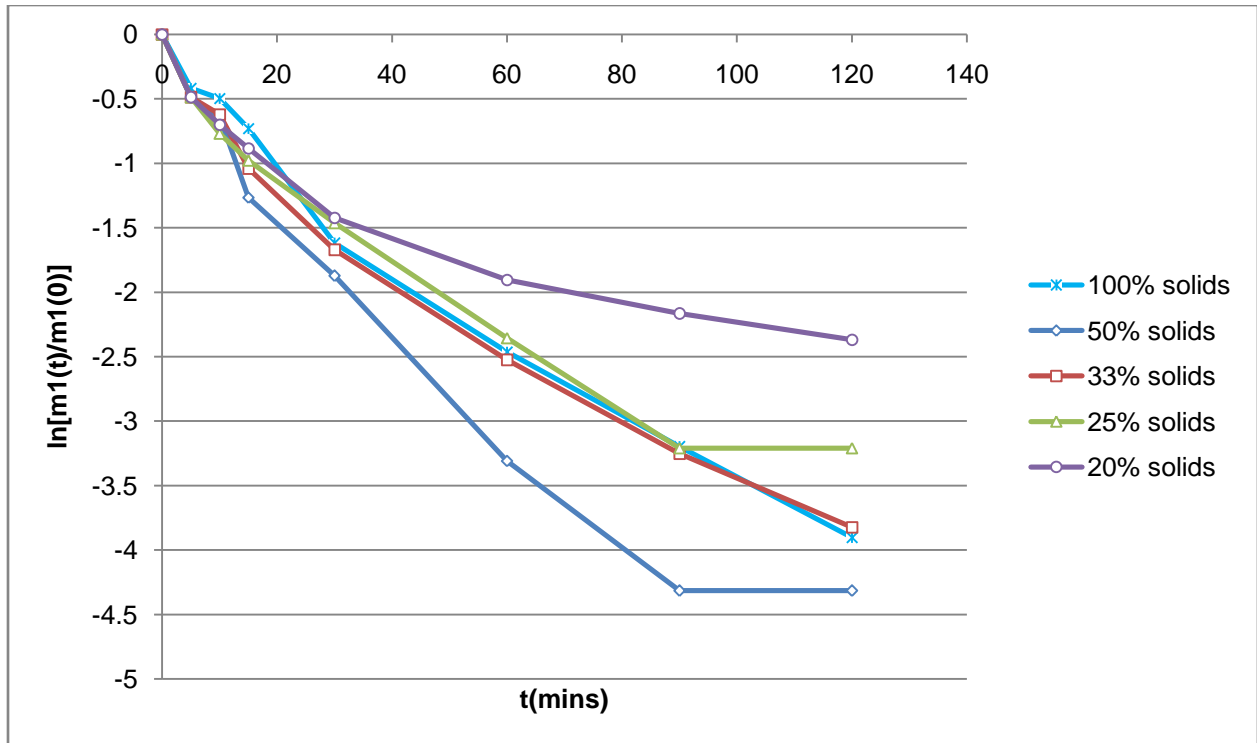


Figure 5.3: A log plot of the ratio of the mass fraction of material remaining in the feed size class after grind time, t , compared with the mass fraction of the material in the feed size class before grinding, versus grinding time, with different percentages of solids in the slurry.

Figure 5.3 is a log plot based on Equation 5.3 and experimental data from Appendix A, Table A6, which sets out the details of the mass fraction ratios of material in the feed size class after a certain grind time as a proportion to that class before grinding, versus grind time, for various slurry densities. The straight lines between points were again added on Figure 5.3 to help the reader follow the general behaviour relative to different solids content. Had the rate of breakage followed a true homogeneous first-order model, the plots would have been straight lines with the rate of breakage (S_1) being the gradient of the line, for each particular slurry density. These results clearly show that this is not the case. This indicates that the rate of breakage of the feed size class material does not follow the homogeneous first-order model.

On the basis of this dynamic behaviour we hypothesized that the material appears to contain a component (we called it 'soft') that breaks at a relatively rapid rate independent of the concentrations of the solids. The differences in breakage observed in the latter part of the plots could be accounted for by another component with different breakage characteristics (called 'hard'), which breaks at a relatively slow rate that is dependent on the solids concentrations. Another explanation of the phenomena shown in the above plots could be the presence of some weaker particles that break first in a feed that is otherwise homogeneous, under all conditions tested, and that the different pattern of breakage starts to occur after these 'weaker' particles have been milled.

We then fitted the heterogeneous (two component) model, as given by Equation 5.7 to the batch mill test data; using a least squares method to carry out the curve fitting and estimate the selection functions and the fraction of the soft component in the ore. The Table 5.2 gives the model parameter values we obtained truncated to four decimal places.

Table 5.2: Model parameter values for model described by Equation 5.7

Solids content (%)	S_{1A}	S_{1B}	ϕ
20	0.1532	0.0143	0.3983
25	0.2386	0.0286	0.5564
33	0.1962	0.0353	0.6034
50	0.1642	0.0464	0.5934
100	0.1307	0.0343	0.6587
Average			0.5620

After obtaining the above given parameters, we evaluated an average value for the fraction of the soft component in the ore (0.5620). We then fixed this parameter and used the Excel

solver again to estimate the selection functions. The results, once again abridged to four decimal places, are given in Table 5.3.

Table 5.3: Model parameter values with fixed ϕ for model described by Equation 5.7

Solids content (%)	S_{1A}	S_{1B}
20	0.1714	0.0159
25	0.1674	0.0229
33	0.1358	0.0278
50	0.1278	0.0393
100	0.0873	0.0279
average	0.1506	

We then referred back to Figure 5.2 where we observed that the initial breakage rates for all solids concentrations were the same. This prompted us to evaluate an average value (excluding the 100% solids) of the specific rate of breakage of the soft component (0.1506). The parameter was then fixed and the Excel solver used to estimate the specific rate of breakage of the harder component. The results are given in Table 5.4.

Table 5.4: Model parameter values, described by Equation 5.7

Parameter	Solids content				
	20%	25%	33%	50%	100%
$m1(0)$	0.6587	0.6587	0.6587	0.6587	0.6587
ϕ	0.5620	0.5620	0.5620	0.5620	0.5620
S_{1A}	0.1506	0.1506	0.1506	0.1506	0.0873
S_{1B}	0.0159	0.0229	0.0278	0.0393	0.0279

We then fitted the homogeneous (one component) model, as given by Equation 5.2, to the test data and compared the degree of fit obtained against that of the heterogeneous (two component) model, given by Equation 5.7. Figures 5.4–5.8, based on the experimental data Tables B1–B5 in Appendix B, show results of the degree of fit of the experimental data by application of the two models.

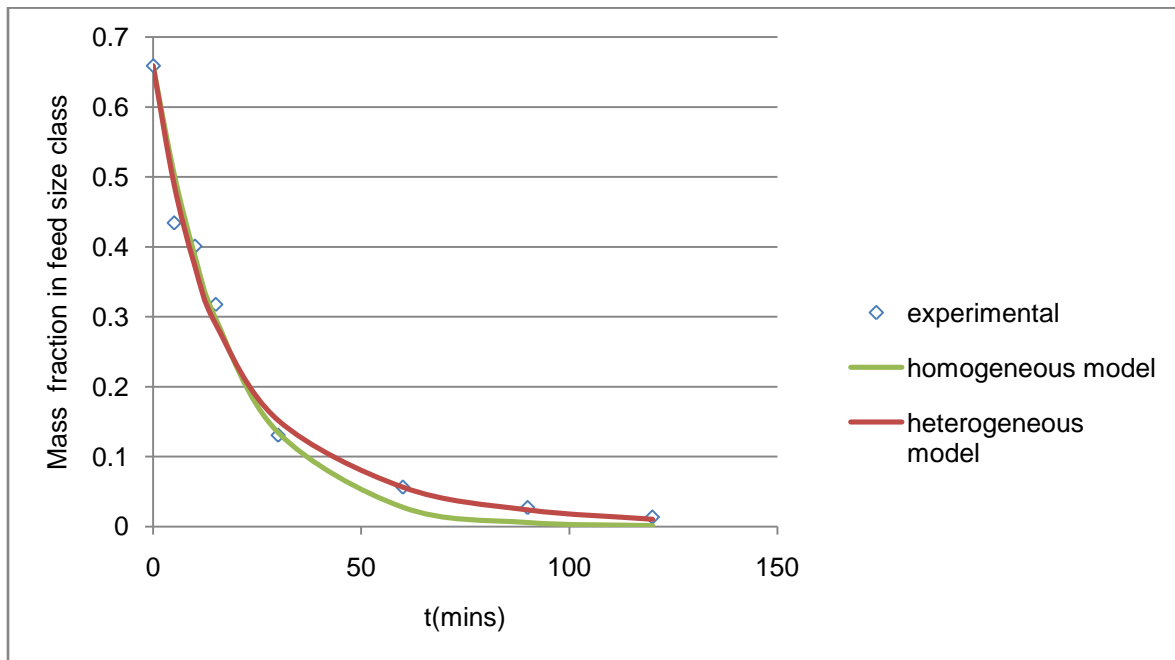


Figure 5.4: Comparison of a single–component and a two–component model, against experimental data for mass fraction of feed size class material remaining after a grind time t , under dry milling conditions.

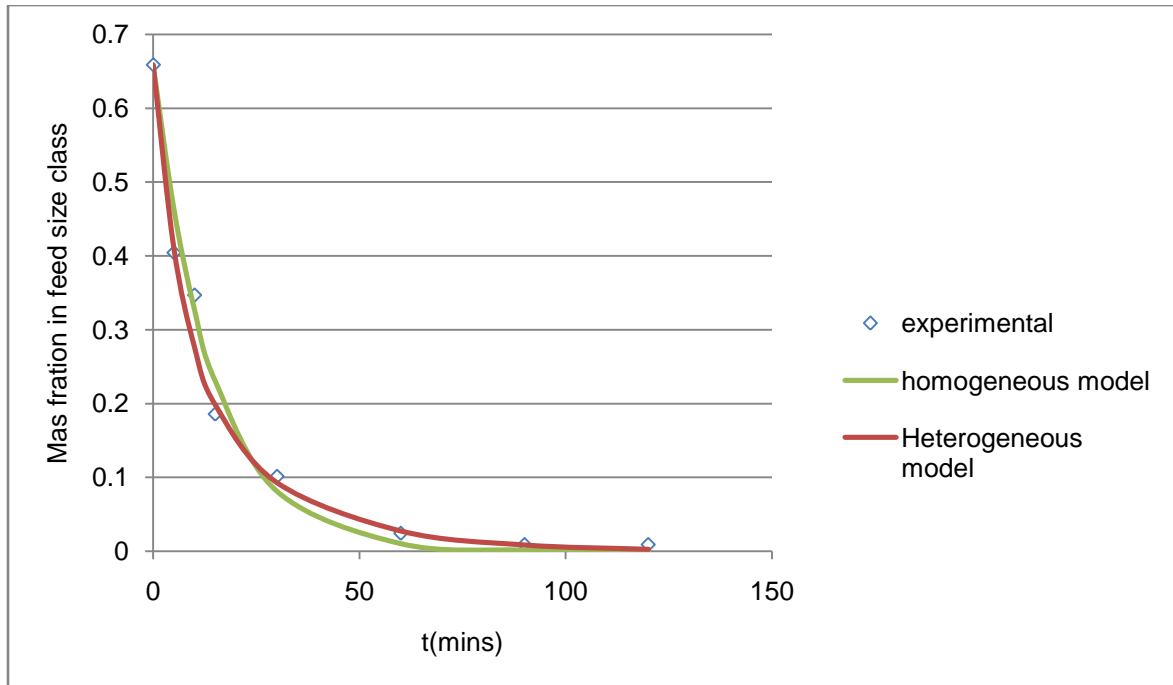


Figure 5.5: Comparison of a single-component and a two-component model, against experimental data for mass fraction of feed size class material remaining after a grind time t , with a 50% solids content.

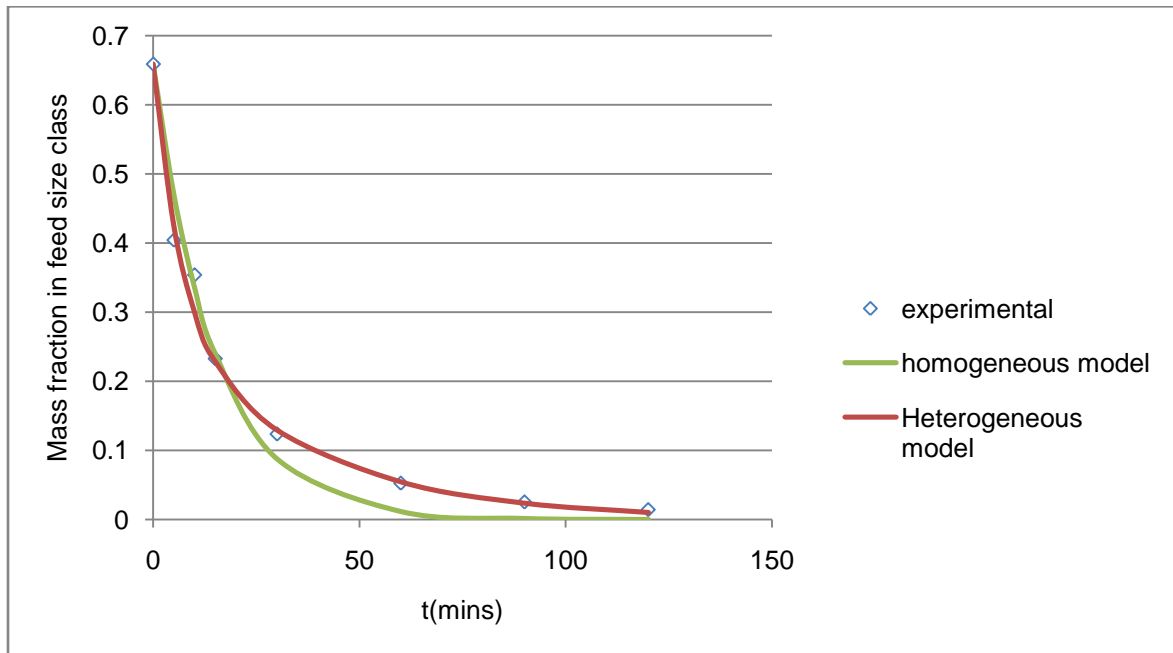


Figure 5.6: Comparison of homogeneous versus heterogeneous models, against experimental data for mass fraction of feed size class material remaining after a grind time t , with a 33% solids content.

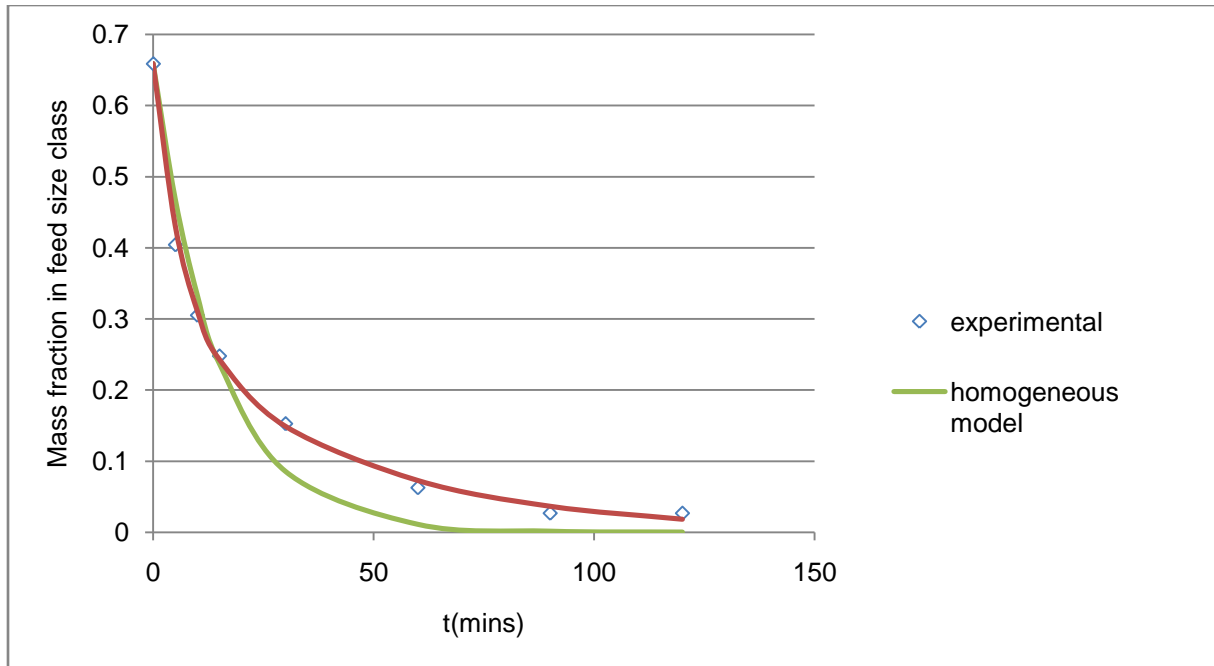


Figure 5.7: Comparison of a single-component and a two-component model against experimental data for mass fraction of feed size class material remaining after a grind time t , with a 25% solids content.

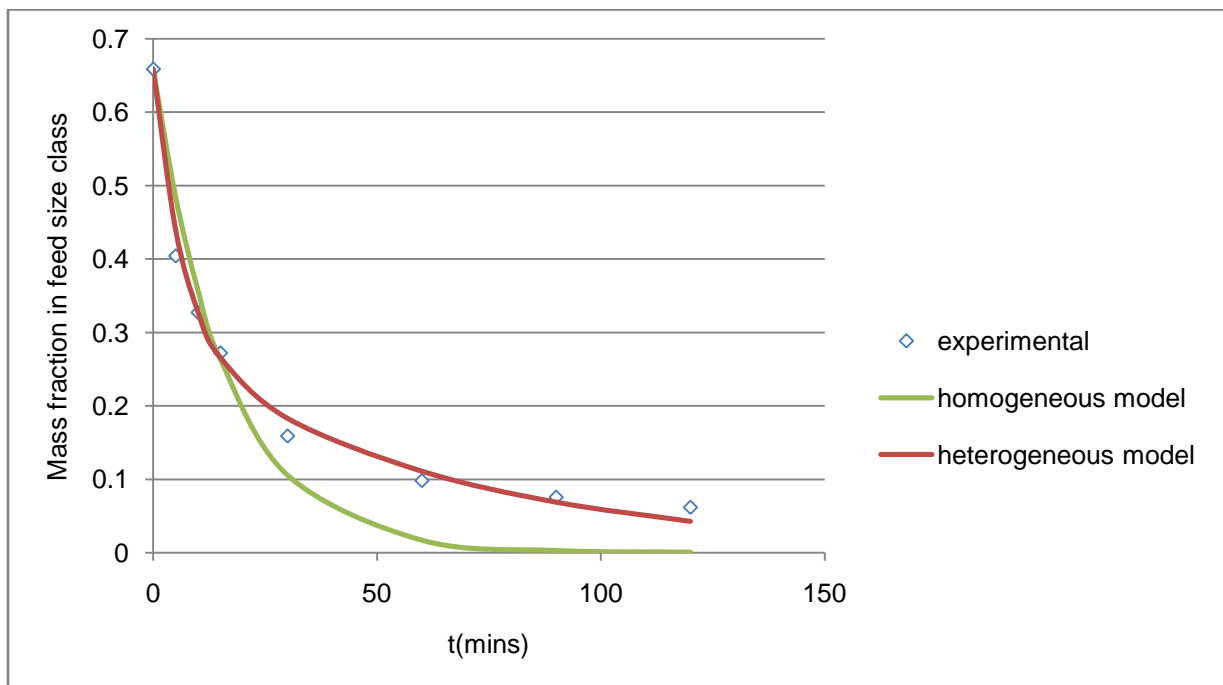


Figure 5.8: Comparison of homogeneous and heterogeneous models against experimental data for mass fraction of feed size class material remaining after a grind time t , with a 20% solids content.

Figure 5.4 is a dry milling comparison of the two models, against experimental data for mass fraction of feed size class material remaining after a grind time t . This figure shows that a heterogeneous (two-component) model approximates the experimental results more closely than the homogeneous (single-component) model, although the fit of the latter is not markedly worse at short grinding times.

Figure 5.5 is a wet milling comparison of a single-component and a two-component model, against experimental data for mass fraction of feed size class material remaining after a grind time t , with 50% solids content. This plot provides greater support for the idea that a two-component model offers a better approximation to the data.

Figure 5.6 is also a wet milling comparison of the two models, but with 33% solids content. It can be observed that in this case the two-component model is clearly a better approximation than that offered by the first-order model. This figure reveals that as the solids content in a milling process decreases, the graph appears to asymptote and the rate of grinding drops very low.

Figures 5.7 and 5.8 show the results of the comparison of the two models with 25% and 20% solids contents respectively. They too show a trend indicating that the lower the solids content, the greater the deviation predicted by the homogenous first-order model. The two-component model, on the other hand, offers a better forecast of what the experimental data show. In particular it is clear that the breakage rate for extended grinding times is very

slow. The graph of the mass fraction versus time asymptotes at long durations, and the value of the asymptotes increases with decreasing solids concentration.

The parameter values of the two-component model fitting the feed size class fraction, for all the solids contents we investigated are summarized in Table 5.4 above. The Excel solver worksheets for this data are found in Appendix B, Tables B1–B5.

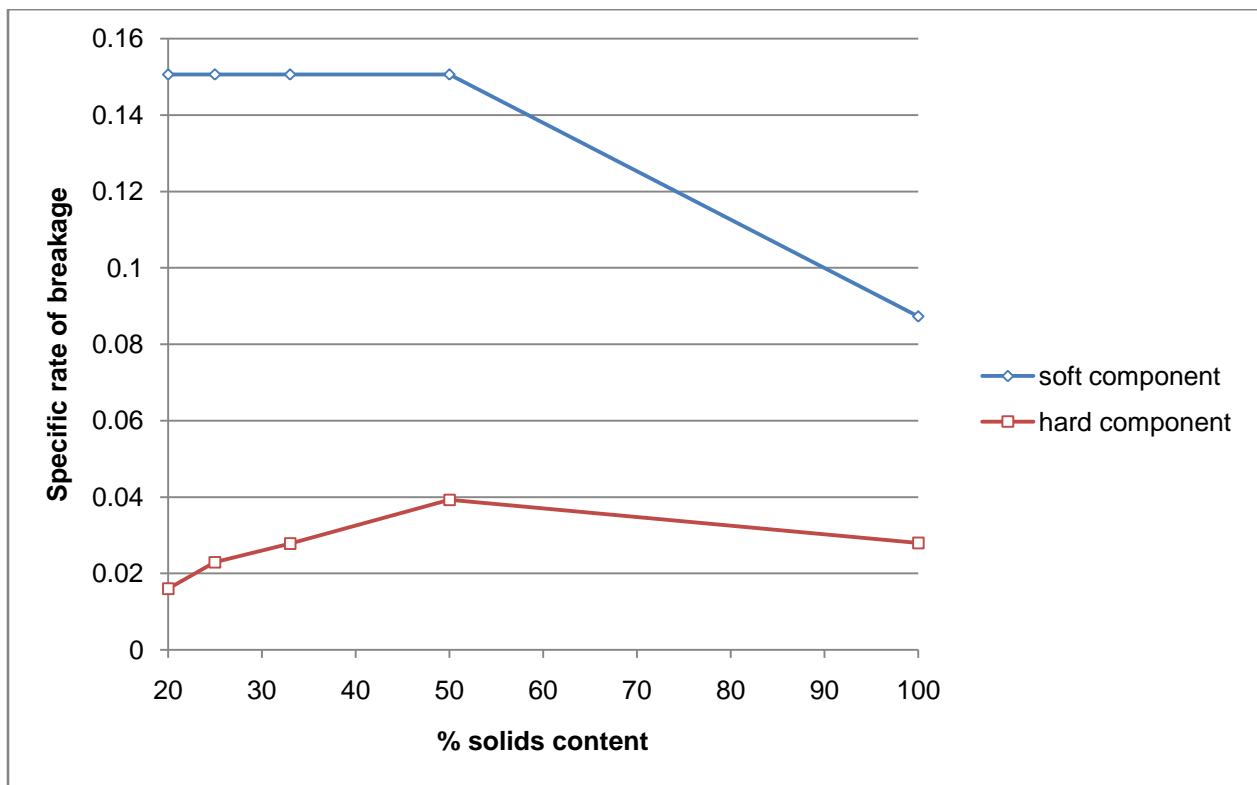


Figure 5.9: Specific rates of breakage of soft and hard components of the ore, versus percentage solids content.

Figure 5.9 is a plot of the specific rates of breakage (for the feed size class material) of soft and hard components of the ore versus the concentration of solids in the slurry feed, based on data from Table 5.4. As in Figure 5.3, Figure 5.9 demonstrates that for wet milling, the

rate of breakage of the 'soft' component is constant over different solid concentrations, and that this rate is higher than that for dry milling. A possible reason for the higher wet milling rates is that the liquid medium is placing the particles in more advantageous breakage regions. Figure 5.9 also shows that the rate of breakage of the 'hard' component varies with slurry density, and reaches a maximum at 50% solids content under the conditions tested.

In terms of mill operation, Figure 5.9 suggests that in order to promote the separation of two components of varying hardness, one should exploit the differences in the rates of breakage of the components. For all solids concentrations investigated, the rates of breakage of the soft component are much higher than for the hard component. This should make it possible for a mill operator to mill the soft material before the hard. When we take an even closer look at Figure 5.9, we notice that there is a bigger difference between the rates of breakage of the components for lower solids content than for higher solids content. For example, at 20% solids the difference between the rate of breakage of the soft component (0.15 per second) and the hard (0.0159 per second) is 0.1341 per second, while at 50% solids the difference is 0.111. This implies that it is more advantageous to run the mill at low solids content in order to promote selective grinding.

After achieving selective grinding, the hard and soft components of the ore have to be separated before the concentration process continues. If the values are concentrated in the hard component, the soft can be discarded after the separation process, leaving the hard component as the feed to the next milling stage. The block diagram in Figure 5.10 summarizes this reasoning.

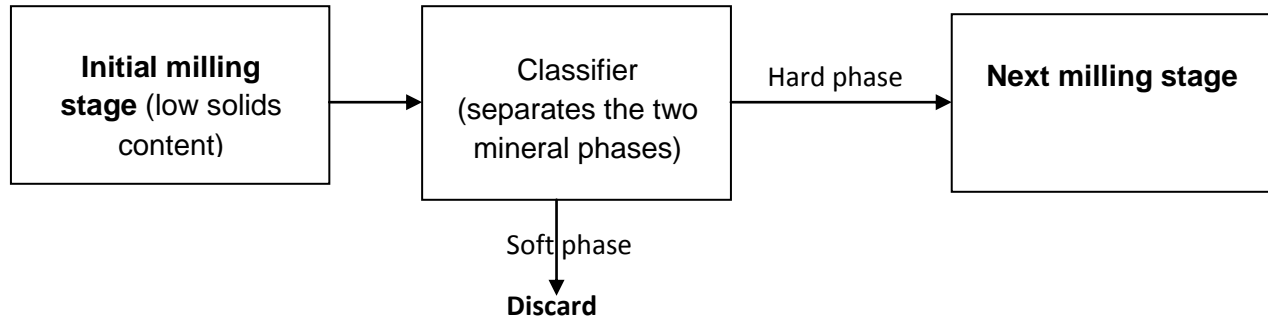


Figure 5.10: General block diagram of mill set-up used to achieve selective grinding and separation of the soft component from the harder component.

5.4.1 Results for the intermediate size class material

The graphs we obtained of the middle size class material plotted against grinding time showed a similar behaviour for all the solids concentrations investigated, in that the two-component model is a better fit to the experimental data than the single-component model. Accordingly, to avoid repetition we give only one graph of the results.

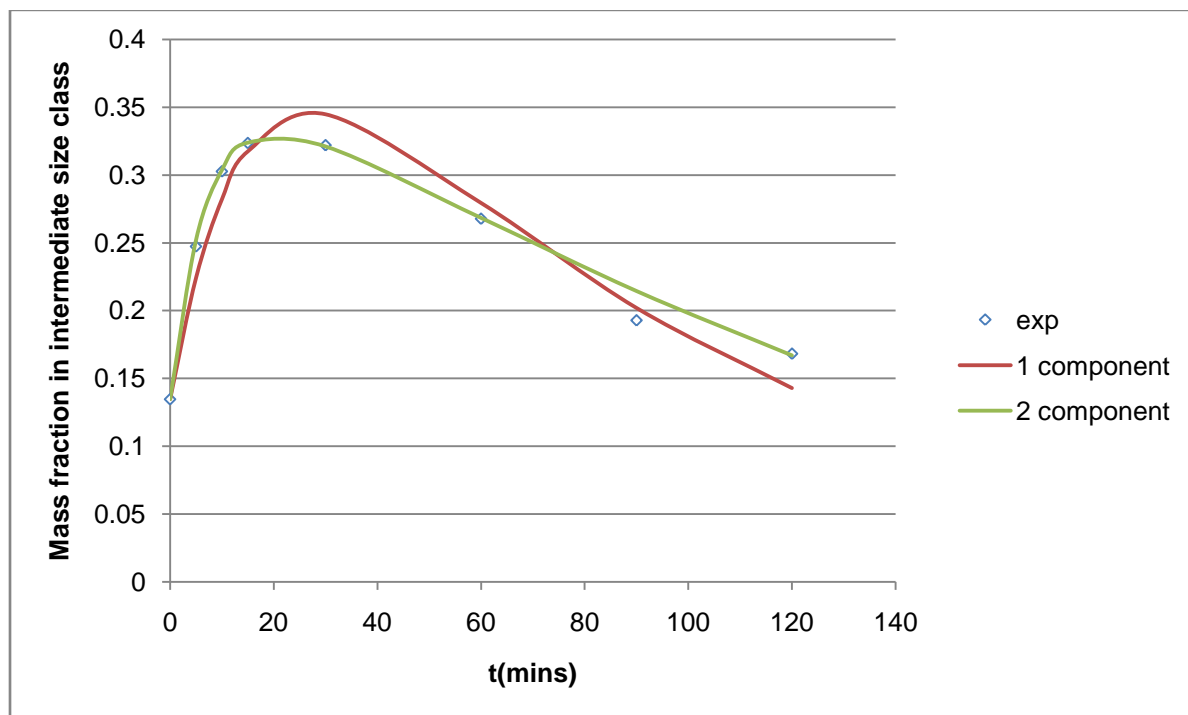


Figure 5.11: A typical comparison of homogeneous and heterogeneous models against experimental data for the mass fraction of intermediate size class material remaining after a grind time t , with 20% solids content.

The above figure shows a typical comparative degree of fit of a single-component and a two-component model based on experimental data for the breakage of material both within and outside the intermediate size class, with 20% solids content. We used Appendix B, Table B6 and Equations 5.9 and 5.10 to obtain Figure 5.11, applying a least squares method to the experimental data after having fixed some parameters (ϕ , S_{1A} , S_{1B}) obtained from the feed size class approximations and using an average value for S_{2A} , as was done with S_{1A} when considering the feed size class material. This enabled us to estimate what the remaining parameters should be. This typical plot of the mass fraction of material remaining in the intermediate size class after a certain grinding time concurs with what was observed earlier for mass fraction of material remaining in the feed size class, in that the two-component is superior to the single-component model. A more detailed analysis of the variations of the intermediate size class material with grinding period and solids content will be dealt with in chapter 7.

The parameter values, truncated to four decimal places, of the two-component model fitting the intermediate size class case for all the solids contents we considered are presented in Table 5.5.

Table 5.5: Model parameter values for model described by Equation 5.10

Parameter	Solids content (%)				100%
	20%	25%	33%	50%	
$m1(0)$	0.6587	0.6587	0.6587	0.6587	0.6587
$m2(0)$	0.1346	0.1346	0.1346	0.1346	0.1346
φ	0.5620	0.5620	0.5620	0.5620	0.5620
S_{1A}	0.1506	0.1506	0.1506	0.1506	0.0873
S_{1B}	0.0159	0.0229	0.0278	0.0392	0.0279
b_{21A}	0.5624	0.5607	0.5000	0.5751	0.5491
S_{2A}	0.0159	0.0159	0.0159	0.0159	0.0138
S_{2B}	0.0115	0.0116	0.0117	0.0140	0.0049
b_{21B}	0.9901	0.7852	0.8867	0.5013	0.9089

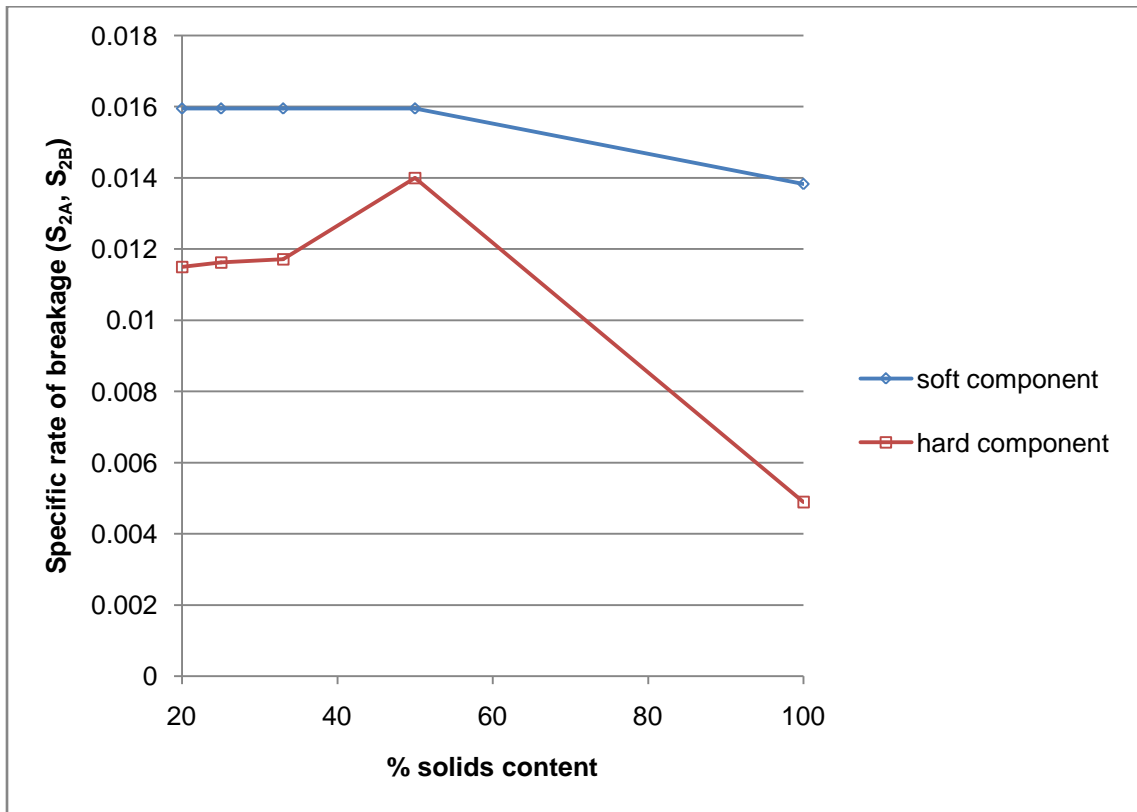


Figure 5.12: Specific rates (S_{2A} , S_{2B}) of breakage of the soft and hard components of the ore in the intermediate size class, versus percentage solids content.

Figure 5.12 is a plot of the specific rates of breakage (for the intermediate size class material) of soft and hard components of the ore versus the concentration of solids in the slurry feed, based on data from Table 5.5, which is a summary of data in Appendix B, Tables B6–B10. Figure 5.12 concurs with what we observed in Figure 5.9 in that the rates of breakage of the soft component are higher than those of the hard component. It is also clear from Figure 5.12 that there is a higher difference between the rates of breakage of the components in ore with lower solids content than with higher solids content. For example, at 20% solids the difference between the rate of breakage of the soft component (0.0159 per second) and that of the hard component (0.0115 per second) is 0.0044 per second, while at 50% solids the difference is 0.0019. This result further supports our suggestion that running the initial milling stage at low solids content will encourage the selective grinding of the soft component of the ore prior to the separation of the two constituent components and subsequent processing of the harder component.

5.5 Conclusion

The results obtained in this chapter partially validate our hypothesis that the feed material is made up of at least two components. This idea is explored in greater detail in the next chapter. The general conclusion in the case of both the feed and intermediate size classes considered here is that the two-component parallel first-order model offers a better approximation to the experimental data, possibly because of the heterogeneous mineralogical composition of the material.

In terms of mill operation, we also found that selective grinding of these components can be achieved by varying the grinding period and the slurry density or the solids content in the mill. A low solids content promotes preferential size reduction of the soft component.

A great deal of research can follow from the implications of the conclusion above. For example, a flow-sheet can be developed for the separation of the soft from the hard phase, after milling. The effects of change in the concentration of solids could also be used to adjust flow sheets.

5.6 References

- Austin, L.G., Shoji, K. & Bell, D. 1982, "Rate equations for non-linear breakage in mills due to material effects", *Powder Technology*, vol. 31, no. 1, pp. 127-133.
- Austin, L.G., Trimarchi, T. & Weymont, N.P. 1977, "An analysis of some cases of non-first-order breakage rates", *Powder Technology*, vol. 17, no. 1, pp. 109-113.
- Berube, M.A., Berube, Y. & Le Houillier, R. 1979, "A comparison of dry and wet grinding of a quartzite ground in a small batch ball mill", *Powder Technology*, vol. 23, no. 2, pp. 169-178.
- Bryson, M.A.W. 2004, "Mineralogical control of minerals processing circuit design", *Journal of The South African Institute of Mining and Metallurgy*, vol. 104, no. 6, pp. 307-309.
- Das, P.K., Khan, A.A. & Pitchumani, B. 1995, "Solution of the batch grinding equation", *Powder Technology*, vol. 85, no. 3, pp. 189-192.
- Fuerstenau, D.W. & Venkataraman, K.S. 1988, "The comminution of multicomponent feeds under batch and locked-cycle conditions: Kinetics, simulation and energy distribution", *International Journal of Mineral Processing*, vol. 22, no. 1-4, pp. 105-118.
- Gardner, R.P. & Rogers, R.S. 1975, "A two-component mechanistic approach for the comminution of material that exhibits heterogeneous breakage characteristics", *Powder Technology*, vol. 12, no. 3, pp. 247-258.

- Hay, M.P. & Roy, R. 2010, "A case study of optimising UG2 flotation performance. Part 1: Bench, pilot and plant scale factors which influence Cr₂O₃ entrainment in UG2 flotation", *Minerals Engineering*, vol. 23, no. 11-13, pp. 855-867.
- Maharaj, L., Loveday, B.K. & Pocock, J. 2011, "The effect of the design of a secondary grinding circuit on platinum flotation from a UG-2 ore", *Minerals Engineering*, vol. 24, no. 3-4, pp. 221-224.
- Rajamani, R.K. & Guo, D. 1992, "Acceleration and deceleration of breakage rates in wet ball mills", *International Journal of Mineral Processing*, vol. 34, no. 1-2, pp. 103-118.
- Reid, K.J. 1965, "A solution to the batch grinding equation", *Chemical Engineering Science*, vol. 20, no. 11, pp. 953-963.
- Tangsathitkulchai, C. 2003, "The effect of slurry rheology on fine grinding in a laboratory ball mill", *International Journal of Mineral Processing*, vol. 69, no. 1-4, pp. 29-47.
- Tangsathitkulchai, C. 2002, "Acceleration of particle breakage rates in wet batch ball milling", *Powder Technology*, vol. 124, no. 1-2, pp. 67-75.
- Verma, R. & Rajamani, R.K. 1995, "Environment-dependent breakage rates in ball milling", *Powder Technology*, vol. 84, no. 2, pp. 127-137.

CHAPTER 6

6 USE OF THE ATOMIC ABSORPTION SPECTROMETER ANALYSIS TO CHARACTERIZE THE UG2 ORE

6.1 Introduction

In the previous chapter, we used breakage kinetic theory to characterize the data we obtained from the feed material (UG2 ore) used in the experiments. Our aim was to test the hypothesis that the material was made up of at least two components and also investigate if it is possible to grind and remove the soft component before grinding the hard component. However, the results we obtained were inconclusive in that they could not eliminate the possibility of the presence of weaker particles in the feed. A heterogeneous ore and a homogeneous one that contains weaker particles have similar breakage characteristics. In the former, the 'soft' is broken down before the 'harder' component, while in the latter the weak particles break first, followed by the stronger.

In this chapter, we describe our use of an alternative and perhaps more direct approach to characterizing the feed sample, to see if we could obtain any evidence that would confirm (or disprove) the initial hypothesis that the material is heterogeneous. The anticipated benefits of determining the nature of the ore's composition, that is, whether or not it is heterogeneous, are that such knowledge:

- can be explored by designers of comminution circuits in proposing flow-charts that can concentrate the material efficiently, based on its constituents; and

- can be used by plant operators to help them adjust mill operating conditions in favour of milling only the mineral phase of interest so that grinding could be done selectively
 - if PGMs are concentrated in the soft component they could mill preferentially to break these initially, or
 - if PGMs are concentrated in the hard component, these could remain unmilled and passed over to the next milling stage.

6.1.1 The atomic absorption spectrometer (AAS) characterisation technique

There are many methods that can be used to identify and/or quantify the mineral phases in an ore. The most common include the SEM, XRD, XRF, MLA and the method we previously proposed, that is the use of breakage kinetic data. All, save for the last, of these methods are time-consuming and costly to perform. On the other hand, they have the added advantage of being more accurate than both the breakage kinetic and AAS techniques, because the method they employ involves direct measurement of the ore sample.

The AAS method gives an indirect measure of the mineralogical composition of an ore, in that what the instrument measures is the concentration of a specific element in a sample. This enables us to infer the mineralogical composition of the ore, using the element as a tracer for a mineral phase.

The PGMs in the UG2 ore are believed to be associated with the base metal sulphides (Penberthy, Oosthuizen and Merkle., 2000), so it follows that when this type of ore is processed, the copper concentration should increase as the PGM concentration rises. This was why we chose to use the AAS to analyze the concentration of one of the base metal elements (copper) in the ore before using the results to make inferences about the mineralogical nature of the sample. Another reason for our selection of copper as the tracer element rather than any of the many other base metals was that the operating procedure employed to carry out the measurement for copper on the AAS instrument is relatively simple.

6.2 Experimental procedure

The milling part of the procedure was carried out as described in Chapter 5 (section 5.3), with the single deviation that we used only dry run samples for the AAS analysis. This was intended to eliminate the difficulties associated with taking samples from the slurry. A further consideration was that the addition of water to an ore in a mill does not affect its mineralogical nature. We also elected to use the feed and only two milling durations, 10 and 30 minute runs, believing that the results would be sufficiently representative of the other grinding periods.

After milling and separation of the product material from the grinding media on a wire mesh, we used a Jones Riffle Splitter to split the mill product into about 100g samples. We dry and then wet sieved a sample, before drying it in an oven set at a temperature of 30°C for 24 hours. We then took the dried material retained on each sieve and

pulverized it into a fine powder. This we did in order to liberate any minerals locked in the samples. After pulverization, we thoroughly mixed the pulverized material and arranged it into a small cone shape before using a straw to collect and measure out masses of about one gramme each from all the sieve size classes. However, the material retained on the larger sieve sizes after milling was insufficient to make up a gramme, so instead we used all the mass that had been retained (see Figure 6.3). Each sample was placed in a conical flask and digested in an aqua regia solution for about 30 minutes. After that, we filtered the samples into volumetric flasks and topped the volume up to the 100ml mark with distilled water. We calibrated the AAS using copper standards before taking samples for the analysis.

The results for the sieve and AAS analysis of the feed samples, after 10 and 30 minutes' grinding time, are presented in the following section. For the AAS, we took two measurements for each size range and calculated an average. The results shown in the graphs are based on this average.

6.3 Analysis and discussion of results based on the AAS technique

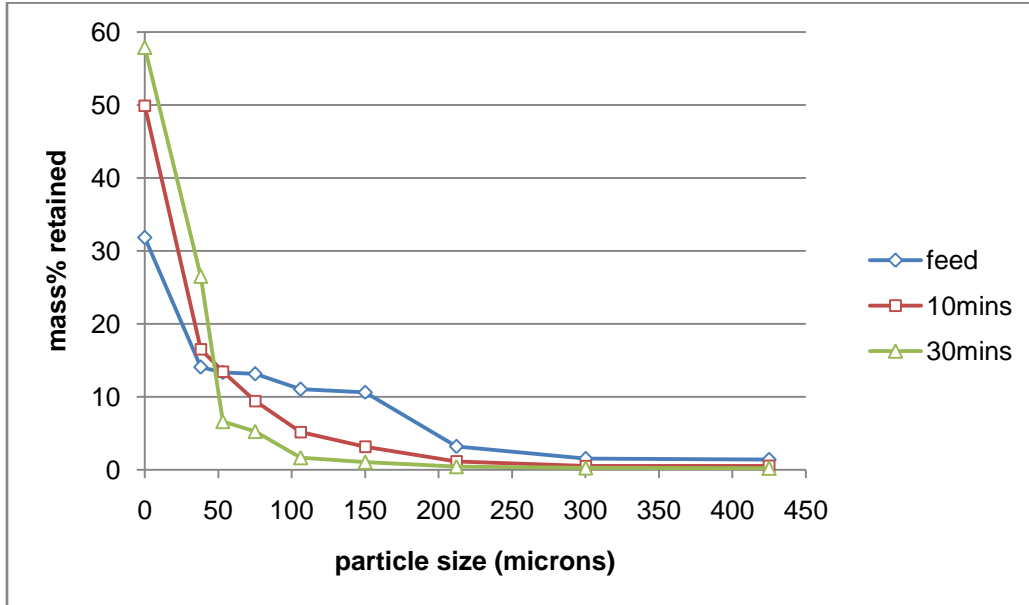


Figure 6.1: Plot of the mass percentage of material retained on each sieve against sieve size for the feed material and after 10 and 30 minutes of grinding

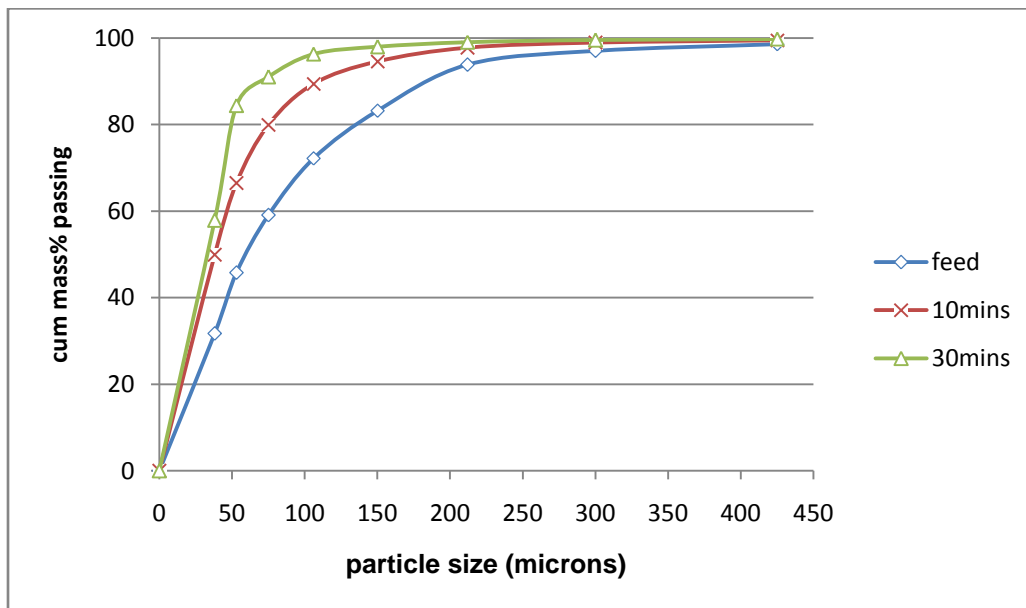


Figure 6.2: The cumulative mass percentage of material passing a sieve size against the sieve size for the feed material, after 10 and 30 minutes of grinding

Figure 6.1 shows the size distribution graph of the material in the form of the percentage of the mass of sample that remained on each sieve for the feed, after grinding periods of 10 and 30 minutes, plotted against that sieve size. This graph is based on data that can be seen in detail in Appendix B, Tables B1–B3. We denoted the size of the material on the pan as zero to enable us to draw the graphs. Samples of about 100g were used in all the three cases to perform the size analysis test. It can be seen from Figure 6.1 that very little of the material was retained on the 425 and 300 μ m sieves, but a lot more remained on the finer sieves.

Figure 6.2 also shows the size distribution graph of the same samples in a different format. The plot gives the cumulative percentage of the mass of material that passes through each sieve, against that sieve size. The data for this graph are to be found in Appendix B, Tables B1–B3. Figure 6.2 shows that the longer the grinding period, the finer the resultant material, which is as expected. This result can be elaborated on: if we compare the 80% cumulative mass passing the feed, for the 10 and 30 minute grind samples, it is found to be nearly 150, 75 and 53 μ m respectively. Hence the longer one mills, the finer the material gets.

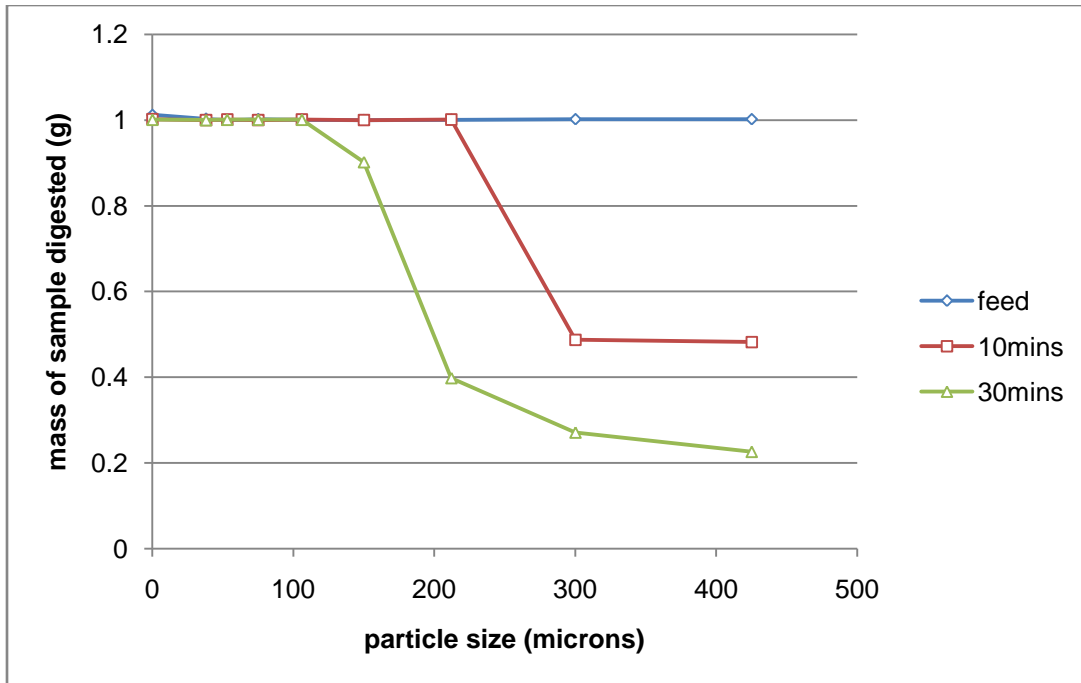


Figure 6.3: Mass of the sample digested against sieve size for the feed material and after 10 and 30 minutes of grinding. The mass is measured to the accuracy of the scale, namely 0.01g

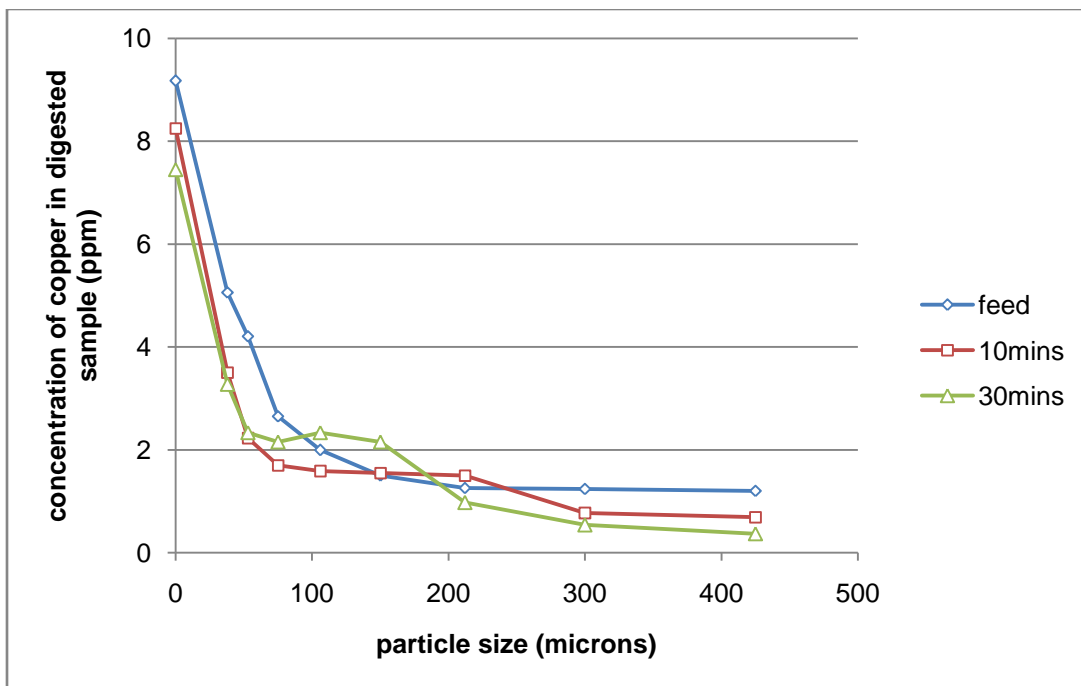


Figure 6.4: Plot of the concentration of copper in a digested sample against sieve size for the feed material and after 10 and 30 minutes of grinding

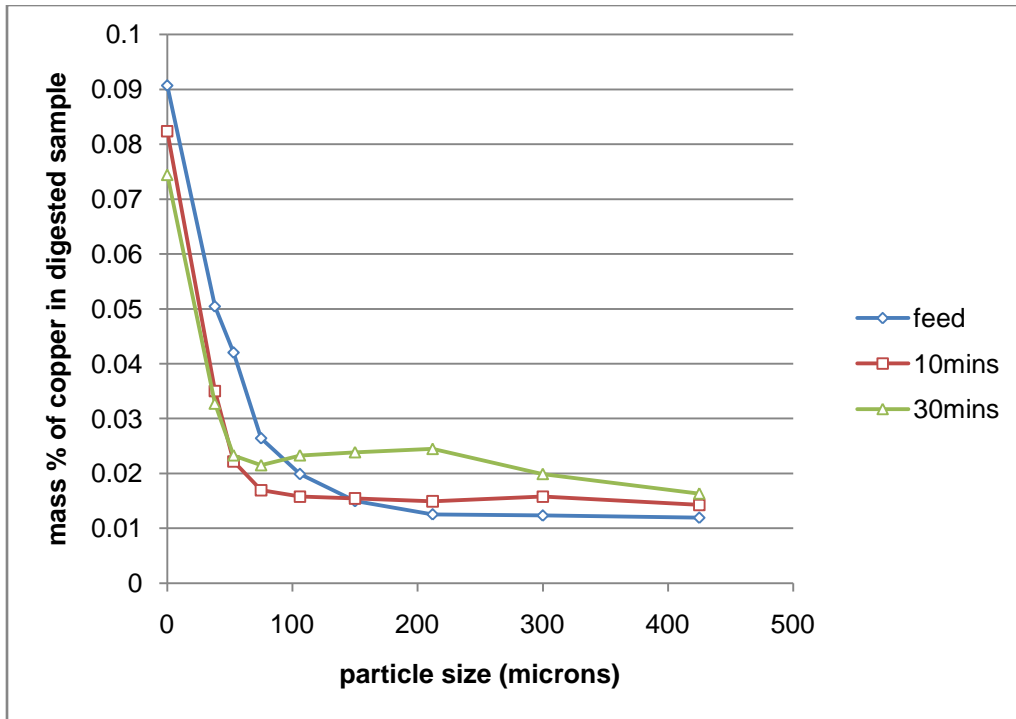


Figure 6.5: The percentage by mass of copper in a digested sample against particle size for the feed material and after 10 and 30 minutes of grinding

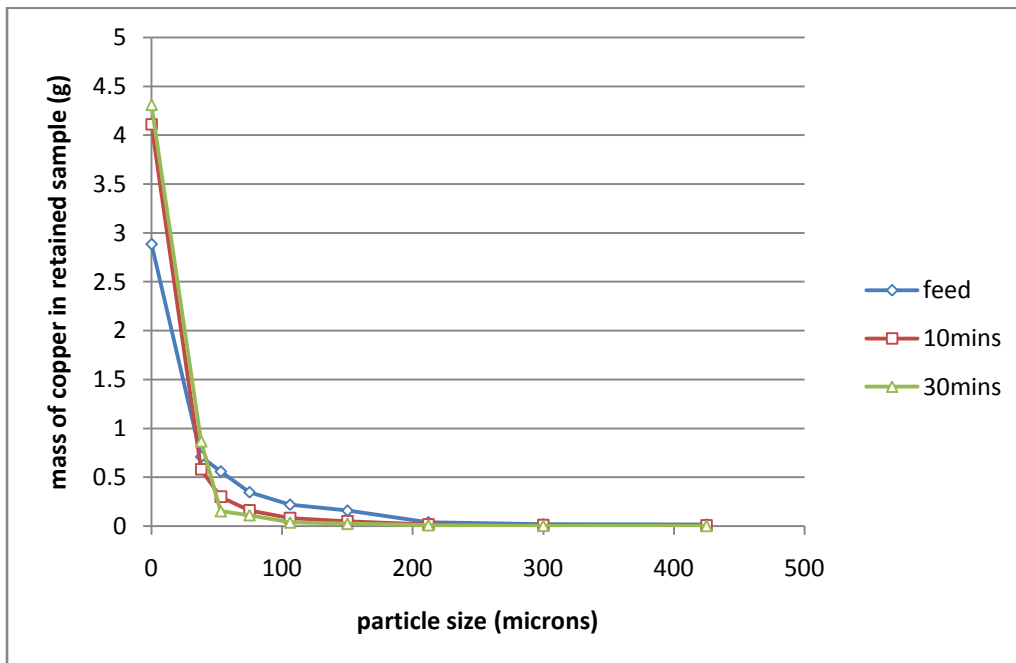


Figure 6.6: Plot of the mass of copper in a sample retained on each sieve against that sieve size for the feed material and after 10 and 30 minutes of grinding

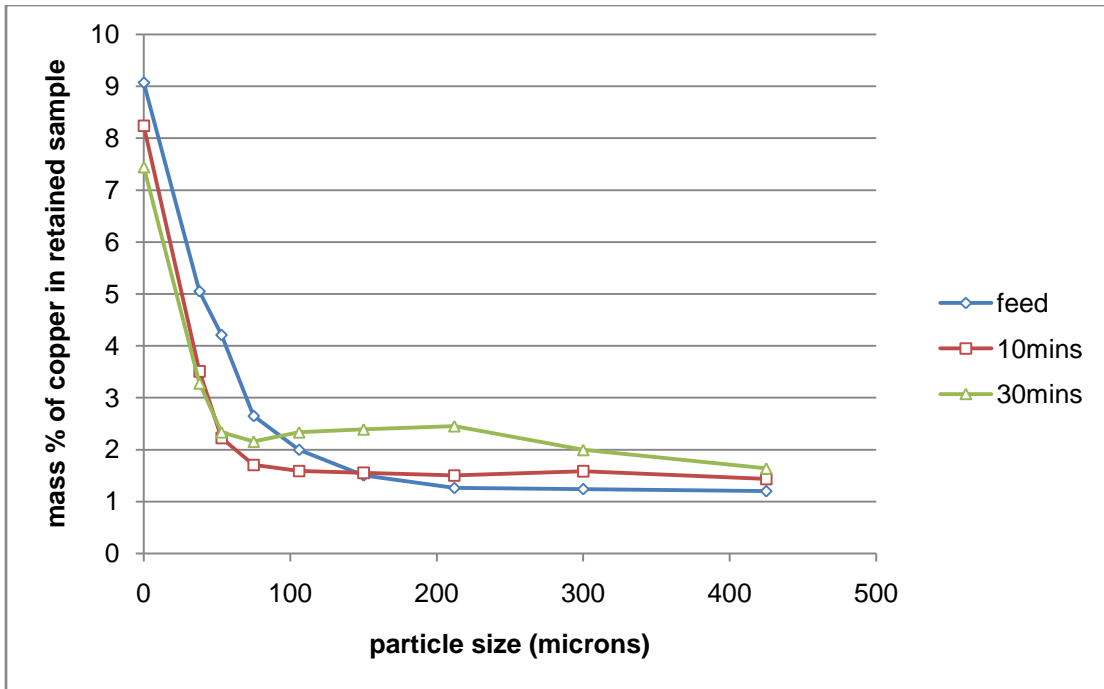


Figure 6.7: The percentage by mass of copper in a sample retained on a sieve against that sieve size for the feed material and after 10 and 30 minutes of grinding

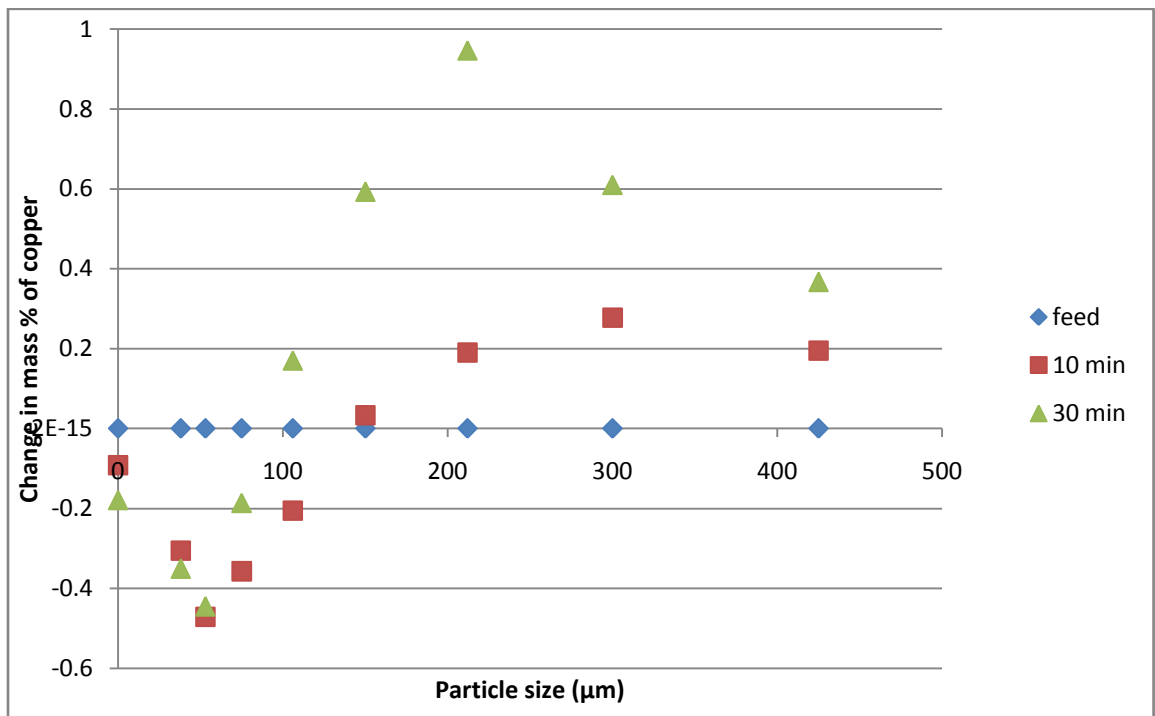


Figure 6.8: Change in mass percentage of copper against particle size for the feed material and after 10 and 30 minutes of grinding

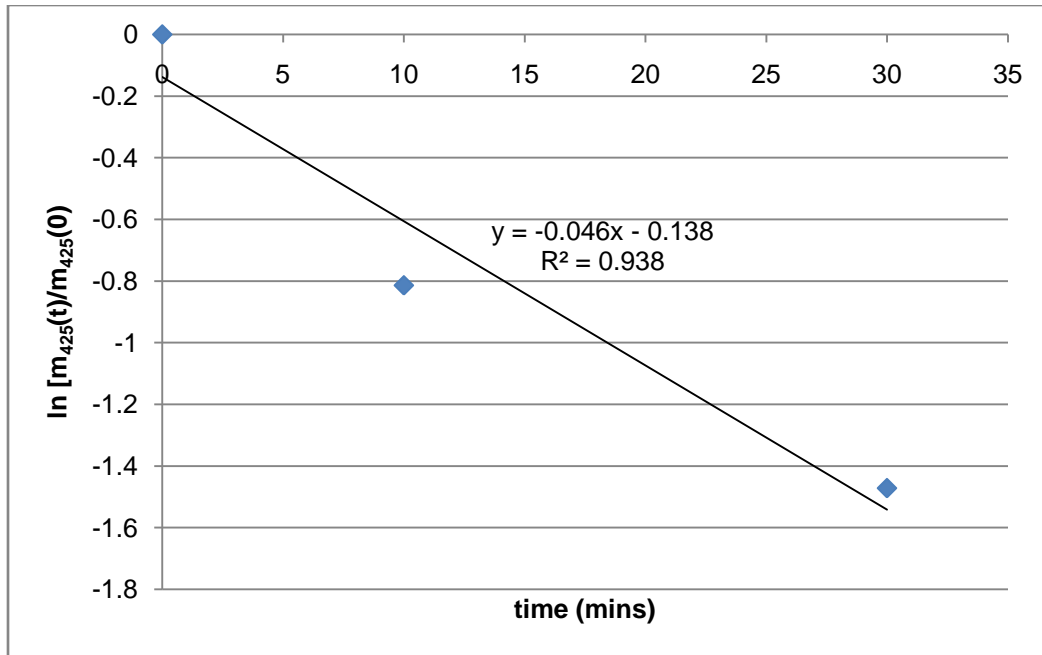


Figure 6.9: Natural logarithm of the ratio of mass of copper remaining on the largest sieve size (425µm) after a certain grinding time to that initially on that sieve against grinding time

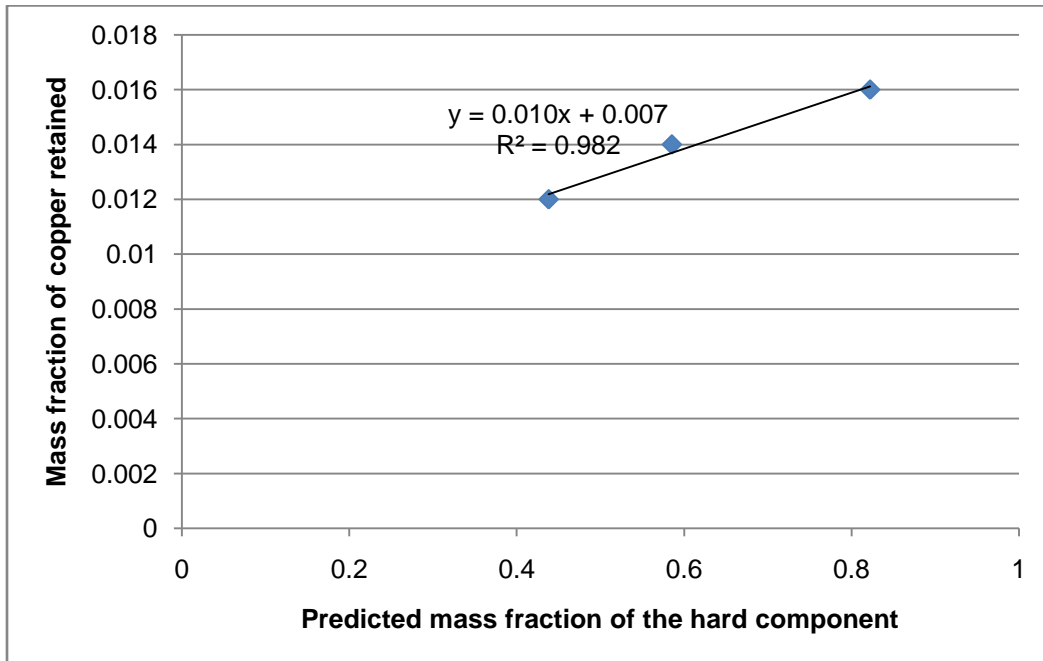


Figure 6.10: Plot of the measured mass fraction of copper on largest sieve (425µm) versus predicted mass percentage of the hard component in the largest size class

The data we used to plot Figures 6.3–6.7 were obtained from Appendix B, Tables B4–B6. Figure 6.3 represents the mass of the material that we digested for the experiment using feed material, after 10 and 30 minutes' grinding respectively. As previously mentioned, we aimed to use samples weighing about one gramme from each sieve and for each grinding period, but were frustrated by the limited quantity of material remaining on individual meshes after sieving the products of the different grinding periods. After 10 and 30 minutes of milling, very little material remained on the 425 and 300 μ m sieves.

In Figure 6.4 we see the concentration of copper in the material we digested, as obtained from individual sieves for the feed and the two different grinding scenarios considered. As we pointed out in Figure 6.3, the different masses retained by each sieve made it impossible for us to use Figure 6.4 to draw any scientific analysis or comparison of the scenarios considered directly. However this graph is important in that it enables us to obtain Figure 6.5, which makes it possible for us to carry out the comparison.

Figure 6.5 shows the percentages by mass of copper in the samples we digested, obtained from considering the masses from the individual sieves for the three cases considered. This graph seems to indicate that the concentration of copper in the larger particle sizes actually increases with grinding time. However, the presence of a high concentration of fines already present in the feed material could be contributing to the trend we observe.

The next graph, Figure 6.6, plots the actual mass of copper in a sample we obtained from each individual sieve for each of the cases we were considering. It is clear from the graph that the samples contained very little copper. The copper is more dispersed in the finer-sized than in the larger particles. Figure 6.6 makes it possible for us to progress towards Figure 6.7, which presents the results even more clearly for analytical purposes.

Figure 6.7 shows the mass percentage of copper in the material retained on each individual sieve, plotted against that sieve size. This graph has a similar profile to that in Figure 6.5, and it follows that it also has the same interpretation, that the concentration of copper in the large particle sizes increases, while that in the fine particle sizes decreases, with grinding time. To enable us to render these differences in changes of copper concentration more clearly, we 'normalised' Figure 6.7 to obtain Figure 6.8.

Figure 6.8 reveals the changes in mass percentage of copper retained on each sieve size for the three cases considered. In this figure we have removed the effect of the high percentage of fines in the feed material to emphasize the changes in concentration in the 10 and 30 minutes grind samples.

Figure 6.8 shows that *the concentration of copper in the larger particle sizes actually increases with grinding time, and the longer the grinding time, the greater the increase.* This can only mean that the copper is not associated with a mineral phase that is softer and being preferentially broken. *For the finer size classes the concentration of copper*

decreases with grinding time. This is further evidence that the material that is being preferentially broken from the larger size classes does not contain much copper, but actually ‘dilutes’ the copper that was already present in the fine size classes. From this grinding behaviour and the AAS results, it is clear that *there is a softer phase that is preferentially milled and that is poorer in copper content.* Since PGMs are associated with base metal sulphides, as mentioned earlier on, we have used copper as a tracer for the PGMs. We are therefore led to believe that the rich mineral phase of the PGMs is not being broken as quickly as the soft material, and that the PGMs are concentrated in the larger particle sizes. Evidence is provided by the increased mass of copper in the large particle sizes, and the decreased mass of copper in the fine particle sizes, by percentage.

Figure 6.9 charts the natural logarithm plot of the ratio of mass of copper remaining on the largest sieve size (425 μm) after a certain grinding time to that initially on that sieve against the grinding time. Equation 5.3 in chapter 5 as well as Appendix B, Tables B4–B6 were used to generate the data for this graph. The purpose of this plot is to compare the rate of copper breakage to that of either the ‘soft’ or ‘hard’ components. If the rate of breakage of copper is equal or close to that of the soft component, then the tracer element copper as well as the PGMs would be associated with that phase, but if this rate is close to that of the hard component then the copper and PGMs are indeed associated with that phase. Figure 6.9 reveals the rate of breakage of copper to be 0.0468s^{-1} , while Table 5.3 (chapter 5) shows that the rate of breakage of the soft component is 0.0873s^{-1} and that of the hard component is 0.0279s^{-1} . Hence, since the

kinetic of copper is closer to that of the hard component, we can infer that the PGMs are indeed more concentrated in the hard phase.

In Figure 6.10 the relationship between the predicted mass fraction of the 'hard' component of the ore and the experimentally measured mass fraction of copper retained on the biggest sieve (425µm) size, for the three cases considered, is plotted. The model we used for the prediction is a modification of the kinetic analysis Equation 5.2 (chapter 5). In developing this model, we considered the mass fraction of the hard component (B) of the ore after a certain grinding period to be given by:

$$\begin{aligned} & \text{Mass fraction of hard component}(t) \\ &= \frac{\text{Mass of hard component}(t)}{\text{Mass of hard component}(t) + \text{mass of soft component}(t)} \quad 6.1 \end{aligned}$$

If we consider B to represent the hard component and A the soft component, it follows that the mass fraction of B (m_B) at some time t is related to the masses of components A and B (M_A and M_B respectively) by:

$$m_B(t) = \frac{M_B(t)}{M_B(t) + M_A(t)} \quad 6.2$$

From application of Equation 5.2:

$$M_B(t) = M_B(0) \exp^{-S_B t} \quad 6.3.$$

Thus Equation 6.2 becomes:

$$m_B(t) = \frac{M_B(0) \exp^{-S_B t}}{M_B(0) \exp^{-S_B t} + M_A(0) \exp^{-S_A t}} \quad 6.4.$$

If we divide both the numerator and denominator of the right hand side of Equation 6.4 by $M_A(0) + M_B(0)$, the result is Equation 6.5:

$$m_B(t) = \frac{\left(\frac{M_B(0)}{M_A(0)+M_B(0)}\right) \exp^{-S_B t}}{\left(\frac{M_B(0)}{M_A(0)+M_B(0)}\right) \exp^{-S_B t} + \left(\frac{M_A(0)}{M_A(0)+M_B(0)}\right) \exp^{-S_A t}} \quad 6.5.$$

The ratio: $\frac{M_A(0)}{M_A(0)+M_B(0)}$ is the mass fraction of the soft component in the ore (φ), and

Table 5.3 (chapter 5) gives this value as 0.562. If we substitute this value into Equation 6.6, the result is Equation 6.7:

$$m_B(t) = \frac{(1 - \varphi) \times \exp^{-S_B t}}{(1 - \varphi) \times \exp^{-S_B t} + \varphi \times \exp^{-S_A t}} \quad 6.6$$

$$m_B(t) = \frac{0.438 \times \exp^{-0.0279 \times t}}{0.438 \times \exp^{-0.0873 \times t} + 0.562 \times \exp^{-0.0873 \times t}} \quad 6.7,$$

where:

S_A is the specific rate of breakage of the soft component, and

S_B is the specific rate of breakage of the hard component of the ore.

Application of Equation 6.7 to the material remaining in the largest size class (425 μ m) for the feed, and 10 and 30 minute grinding periods gave the results in Table 6.1.

Table 6.1: Relationship between the predicted mass fraction of the hard component and the measured mass fraction of copper in the largest size class

Grind time (mins)	Total mass of material retained (g)	Mass of copper retained (g)	Mass fraction of copper retained	Predicted mass fraction of the hard component
0	1.4300	0.0171	0.0120	0.4380
10	0.5300	0.0076	0.0143	0.5853
30	0.2400	0.0390	0.0163	0.8224

We can observe from Table 6.1 and Figure 6.10 that as the mass fraction of copper retained in the largest size class increases with grinding time, as does the predicted mass fraction of the hard component. This similarity in grinding behaviour and the linear relationship that exists between copper and the hard component further supports our hypothesis that the tracer element (copper) and hence the PGMs are associated with the hard phase. It is interesting that if we extrapolate this graph, which may not be a good assumption, the model predicts that the mass fraction of copper in the soft component is 0.0077 (that is, corresponding with the y intercept on Figure 6.10), while the mass fraction of copper in the hard component is predicted as 0,0179 (corresponding with the y value when the mass fraction of the hard component is 1).

Having concluded, from the AAS results shown and discussed above, that the ore is indeed heterogeneous, we asked ourselves the question: How we can convert this knowledge into good practice? One way of applying this knowledge to industrial comminution circuits is to propose a circuit (Figure 5.10) in which conditions in the

primary mill are set for preferential breakage, and thereafter for the pre-separation of the soft mineral phase that does not contain any values. This idea is discussed in greater detail in the next chapter.

6.4 Conclusion

The results described in this chapter validated the hypothesis that the feed material is heterogeneous. Applying the AAS analysis on the element copper, which we used as a tracer for the PGMs rich mineral phase, we found that there is a soft component that can be selectively milled, but this phase does not contain much of the element copper, and hence does not contain many PGMs. We also learned that the concentration of copper in the larger-sized particles increases with grinding period, which is evidence of the presence of another, 'harder' phase that contains copper and hence PGMs. Thus, using selective milling, we can concentrate the PGMs in the larger rich mineral phase particles. We can use this information to propose drawing up comminution flow-charts that promote selective grinding and separation of the soft and non-PGMs-containing phase in the initial milling stages. More detailed research should be undertaken to investigate the way in which conditions can be set to carry out this task.

6.5 References

Penberthy, C.J., Oosthuizen, E.J. & Merkle, R.K.W. 2000, "The recovery of platinum group elements from the UG 2 chromitite, Bushveld Complex – a mineralogical analysis", *Mineralogy and Petrology*, vol 68, pp 213-222.

CHAPTER 7

7 A LABORATORY SCALE APPLICATION OF THE ATTAINABLE REGION TECHNIQUE ON UG2 ORE

7.1 Introduction

In the previous chapters, we identified the milling characteristics of a typical PGM ore by studying the effects of slurry density and grinding time on the ways in which the ore in a laboratory scale batch mill was broken down. These experiments allowed us to identify ways in which grinding could be controlled in a more selective and thus cost-effective way. In the experiments described in this chapter, we extended the range of our research by using the AR method (summarized in section 7.3 below) to find ways of:

- reducing the grinding energy and durations required for a given results; and
- maximizing the mineral phase in the desired product size range when comminution is carried out on a typical industrial ore and under wet conditions.

No work on utilizing the AR to optimize the size reduction of a real ore in slurry has been reported previously, although earlier researchers Khumalo *et al.*, (2006, 2007, 2008) and Metzger *et al.*, (2008, 2009) used the AR method for comminution carried out under dry conditions. Both research efforts concerned the application of the approach to the milling of a test material, silica sand in the former and silica sand and quartzite in the latter. The behaviour of PGMs during milling of the UG2 ore is still poorly understood (Penberthy *et al.* 2000), which is the reason this study was undertaken.

From a milling point of view, good PGM recovery requires that the ore should be ground to an 80% passing 75 μ m product size (Hay, Roy 2010), which is sufficient to ensure the liberation of the valuable species. Ideally, operating parameters such as grinding times, grinding energy and slurry solid concentrations should be set in such a way that the feed particles are reduced to as close to the desired product particle size range as possible. Some size reduction operations use fine screens to achieve the desired particle size range, with recycling of over-sized material to the mill, but various difficulties are associated with screening, especially when it is carried out on fine material and under wet conditions. If the grinding could be done in such a way as to get the required size distribution in the mill without having to screen, this would obviously be preferable.

The AR technique may provide a useful tool to look at size reduction of PGMs because it allows us to examine the effect of either control variables or independent parameters on the performance of mills. In this chapter we describe our use of the AR method to investigate the effect of slurry density and grind time on the laboratory batch mill performance. This work is not intended to elicit operating parameters for industrial mills directly, but rather to show how the technique can be used to highlight some opportunities to improve mill performance.

7.1.1 Size reduction of ores

Ores are ground to an optimum size range (as determined by the laboratory and pilot scale tests) to produce the maximum degree of liberation. Normally the most effective size reduction conditions are established by carrying out milling experiments in the laboratory-

scale mill (Mori *et al.*, 2004). In wet milling, solids concentration and slurry viscosity are significant parameters in determining ideal conditions (Fuerstenau, Venkataraman & Velamakanni 1985). Slurry density also has a strong influence on the magnitude and trend of net power draw (Tangsathikulchai, Austin 1989). However, a researcher normally finds that for multi-component (that is, typical industrial) ores, the identification of an optimum slurry density is not obvious, because it depends on a number of factors such as the relative abundance of the constituent components, their hardness, and their degree of interlocking. Our research efforts in this chapter were also aimed at using the AR to specify the best slurry grinding conditions, within the limits of the experimental parameters chosen for the PGM ore.

7.1.2 The Attainable Region (AR) analysis method

The AR method was described and discussed in section 2.5.2 (chapter 2). The further implications of using an AR plot will be explained in the sections that follow.

7.2 Experimental procedure

The effects of slurry density, grinding time and grinding energy on the grindability of a UG2 ore were investigated in a laboratory scale batch tumbling ball mill. Dilute feeds, with solids contents ranging from 20–50% by mass were used. The material and equipment used for the experiments in this phase of the research were the same as those described in Chapter 5 (section 5.3). However, different techniques of analysis were applied according to the requirements of the AR method. The cumulative plots that we constructed, based on the experimental data obtained from the Mastersizer, enabled

us to classify the product PSD into three size classes, in accordance to the AR technique. Size class 1 was chosen to be the mass fraction of material for particle sizes above 45µm in diameter, size class 2 as the mass fraction of material for particle sizes between 15–45 µm and size class 3 the mass fraction for particle sizes below 15µm. We would like to point out that any set of size classes can be used, but our research was based on the above. As previously noted, these size classes were chosen to set size class two as the desired product within the ideal range for flotation (Maharaj, Loveday & Pocock 2011) to remove the valuable from the gangue material. Flotation of coarse sized particles results in losses in recovery, as some valuable minerals report to the tailings because of their not being liberated from the gangue minerals. Flotation of fine size class material is also not ideal due to the challenges associated with handling such particles. This leaves the intermediate size class as the optimum range for flotation.

7.3 Analysis and discussion of results according to the AR technique

A size distribution of the overall feed material used in this experimental test programme comprising typical UG2 material is presented in Figure 5.1 (chapter 5).

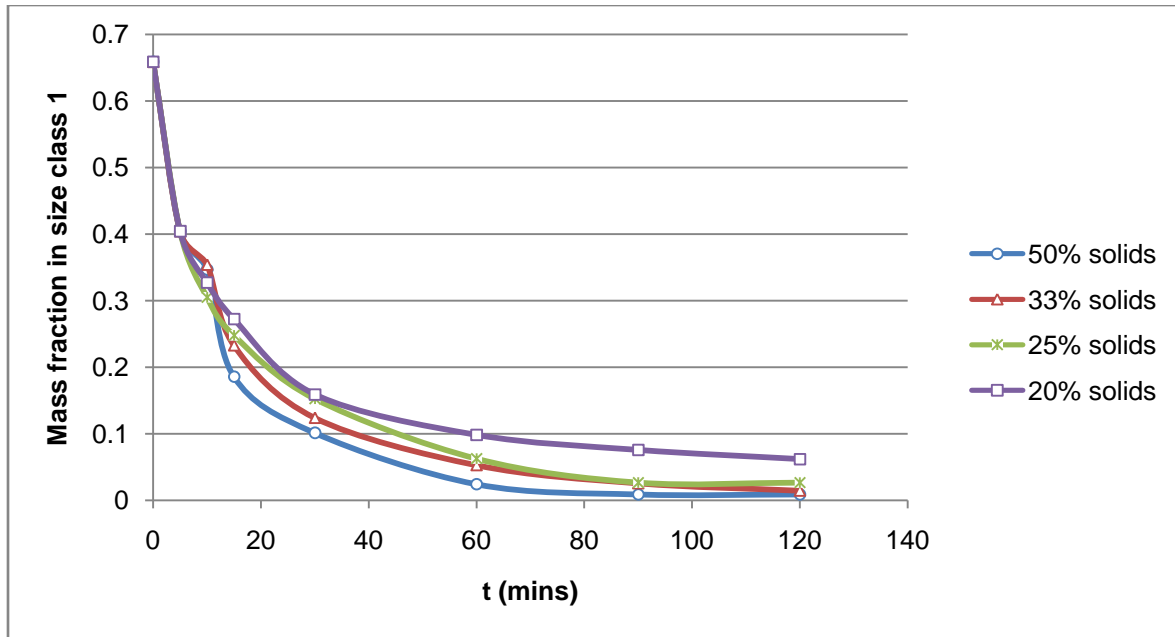


Figure 7.2: Mass fraction of material in the feed size class versus grinding time for different solid concentrations.

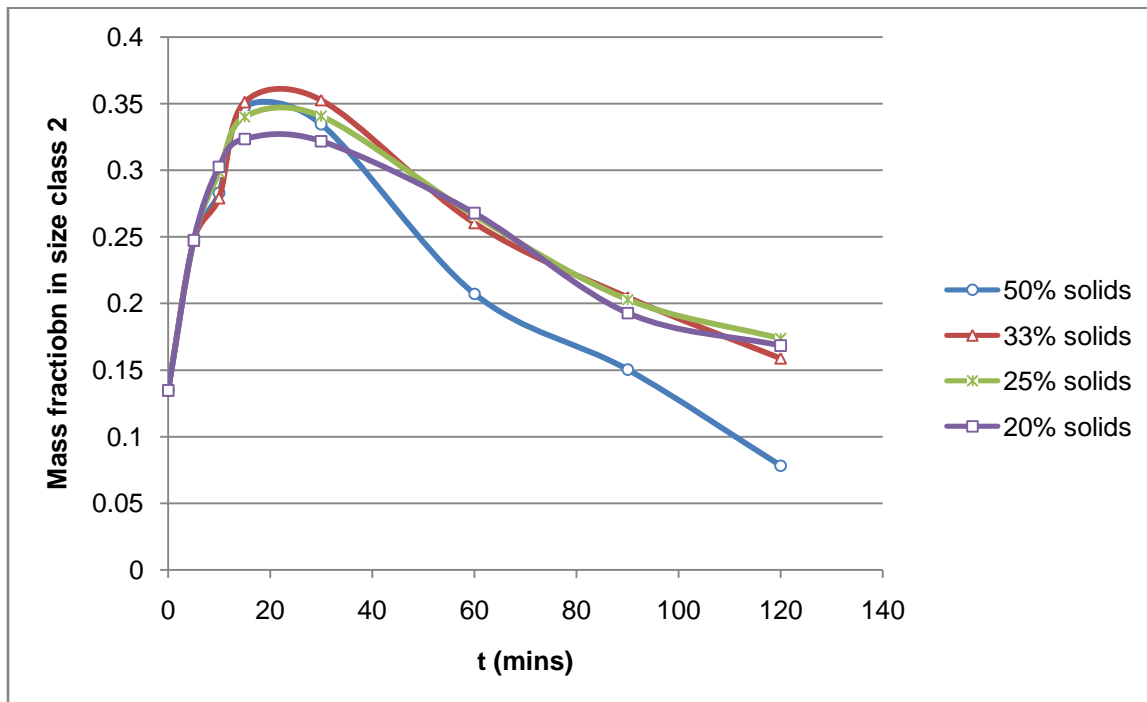


Figure 7.3: Mass fraction of material in the intermediate size class versus grinding time for different solid concentrations.

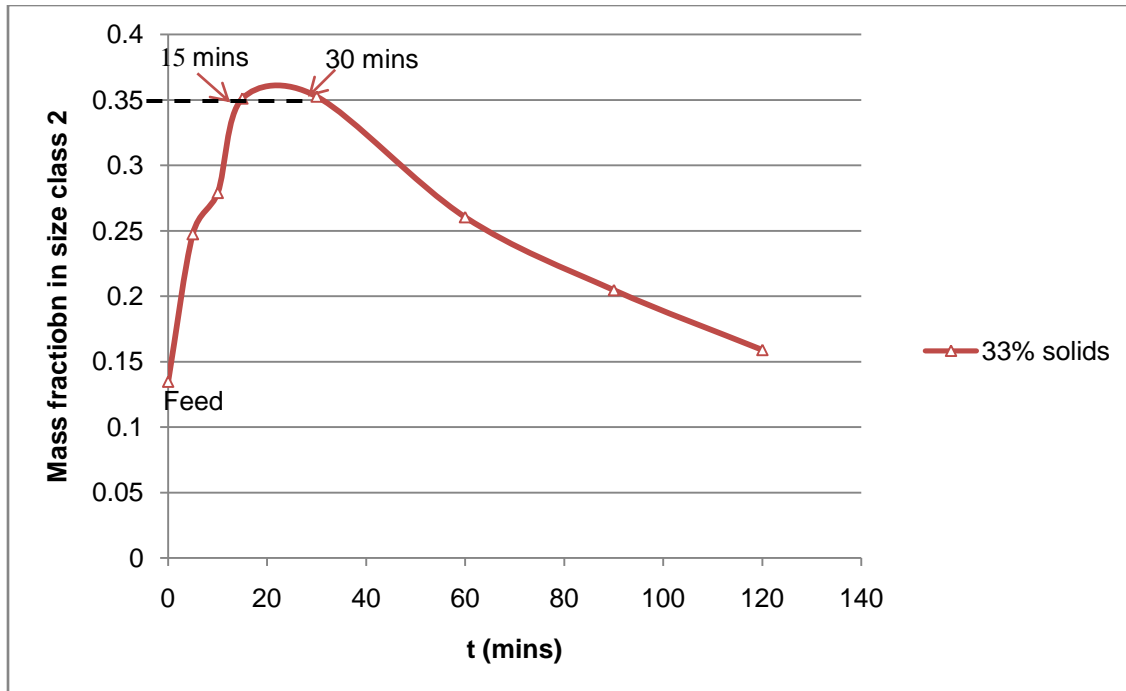


Figure 7.4: Mass fraction of material in the intermediate size class versus grinding time for 33% solids concentration.

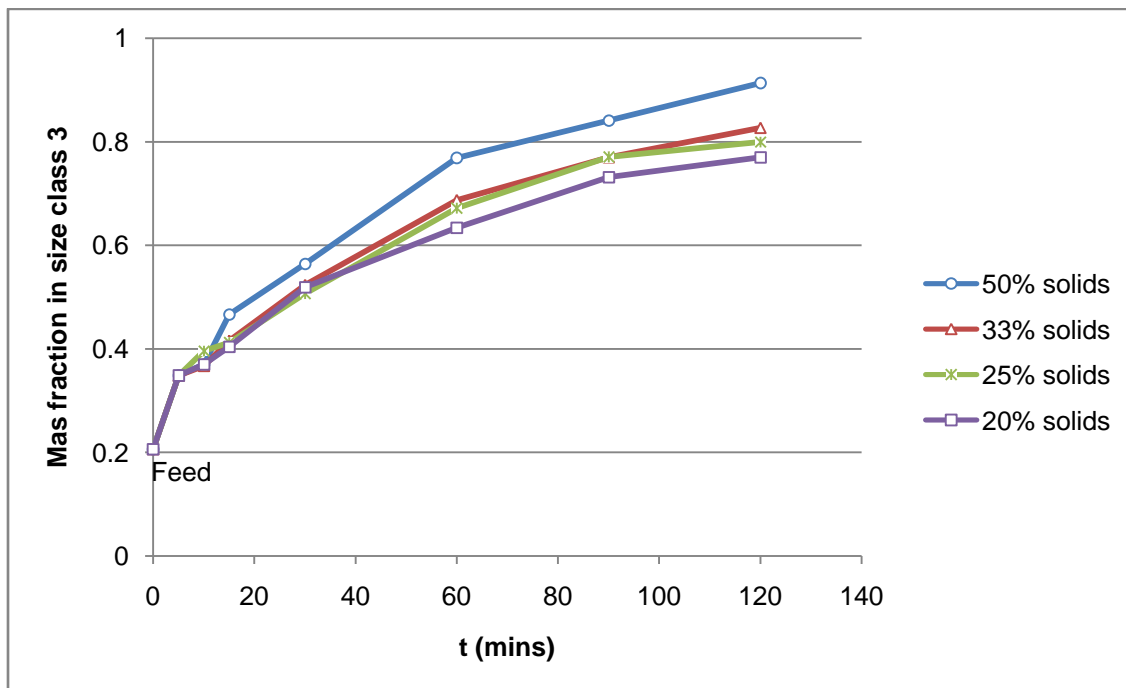


Figure 7.5: Mass fraction of material in the fines size class versus grind time for different solid concentrations

Figures 7.2, 7.3 and 7.5 show the kinetics of breakage of the feed, the intermediate and the fines size class material respectively, with various slurry densities. (These plots are derived from the experimental data set out in Appendix A, Tables A 2–A 5). We connected the experimentally determined points with lines to make the trends more easily visible.

Figure 7.2 shows that the mass fraction of material in the feed size class diminishes with an increase in grinding time, as particles leave this size class to form part of the finer size classes. The plot also reveals that as the slurry solids concentration decreases, the grinding rate falls. It is also clear from the graph that during the first 10 minutes of grinding, the grinding rate is the same, regardless of the concentration of solids. Variations occur thereafter. In the previous chapter we verified that this dynamic behaviour was caused by the heterogeneous nature of the feed material. We can therefore deduce that the material contains a component that breaks at a relatively rapid rate that is not strongly affected by the concentration of solids, and a second component with different breakage characteristics from the first, which breaks at a relatively slow rate that is dependent on the concentration of solids.

In Figure 7.3, the plot shows that as grinding proceeds, the amount of material reporting to the intermediate size class reaches a maximum and then decreases as material breaks down further, into the fines size class. If our objective is to maximize the amount in the intermediate size class, then we would need to grind for between 15–30 minutes for all slurry densities. Figure 7.3 also shows that initially the curves are superimposed.

This suggests that the influence of slurry density is not apparent at first. It is only as the particles are reduced in size that the amount of water added plays a role. This makes sense intuitively, because as the overall particle size decreases, the likelihood that the particles will be influenced by the fluid flow increases, and explains the greater influence of the slurry density on the overall breakage behaviour as milling progresses. The additional fines also increase viscosity, which means particles coat the balls more effectively, which improves their chances of being crushed. This plot implies that changes in the solids concentration can be used for developing a flow sheet that favours preferential breakage.

Figure 7.4 is obtained from Figure 7.3, showing only a single plot for the 33% solids concentration case. We can deduce from Figure 7.4 that if our objective was to have 35% of intermediate size class material in the product, we can achieve this by either grinding for 15 minutes or for 30 minutes. Since the longer we grind, the more energy we use, if we are aiming for energy efficiency, we should be choosing the shorter grinding time.

Figure 7.5 shows us, unsurprisingly, that the longer we grind the more fines we produce. It is evident that for infinite grind times all the curves would asymptote at 1, with the higher solids concentrations getting there first. We can also see from these curves that the less viscous the slurry (that is, the more water it contains), the fewer fines that are produced at a given time. This may be because the additional water is acting to absorb some of the impact energy normally directed at the particles. The effect

would be that particle breakage was impeded by the presence of large amounts of water. This information is crucial to the development of effective flow sheets.

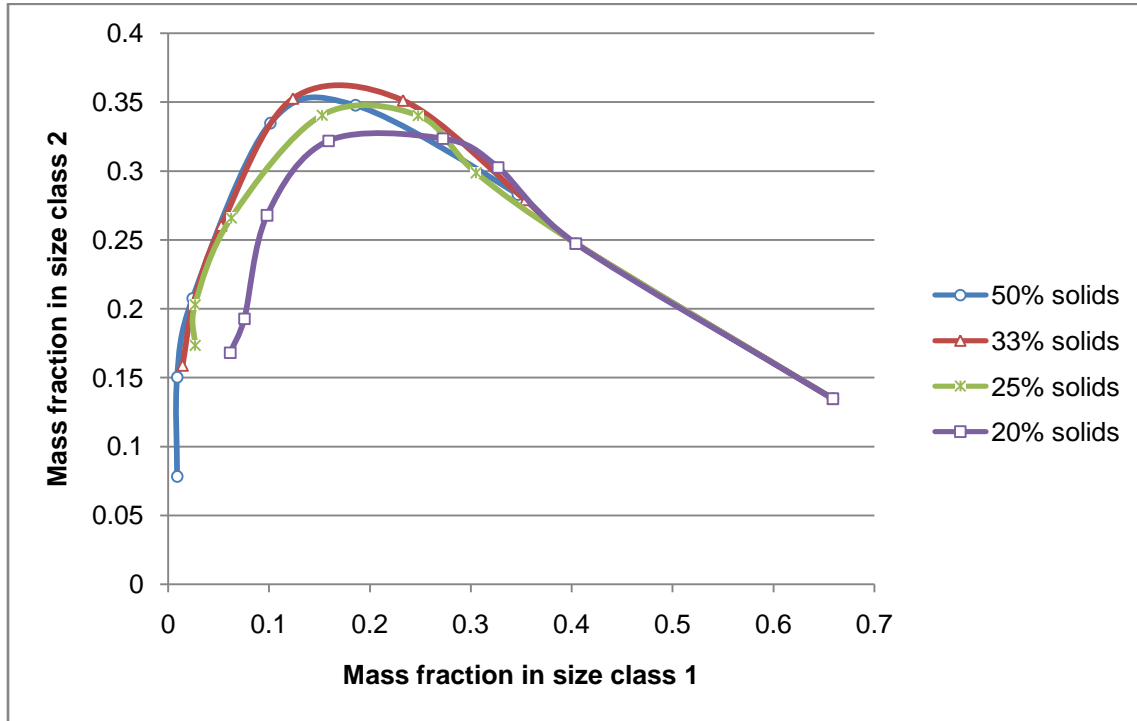


Figure 7.6: Mass fraction of material in the intermediate size class versus the mass fraction of material in the feed size class for different solids concentrations.

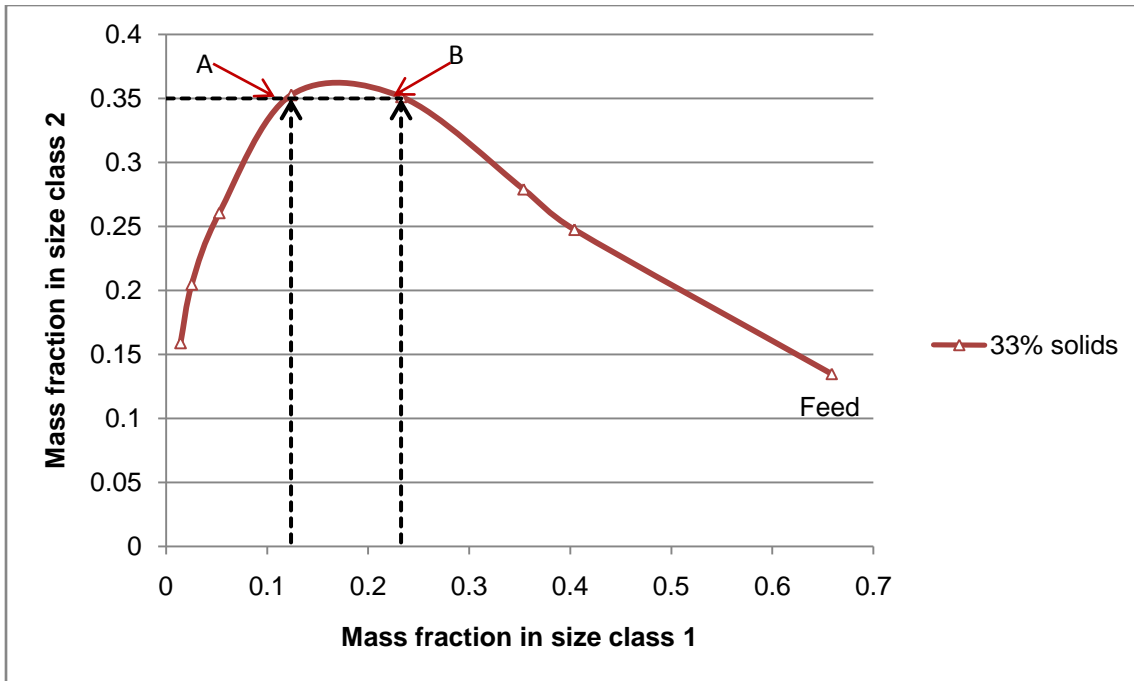


Figure 7.7: Mass fraction of material in the intermediate size class versus the mass fraction of material in the feed size class for 33% solids concentration.

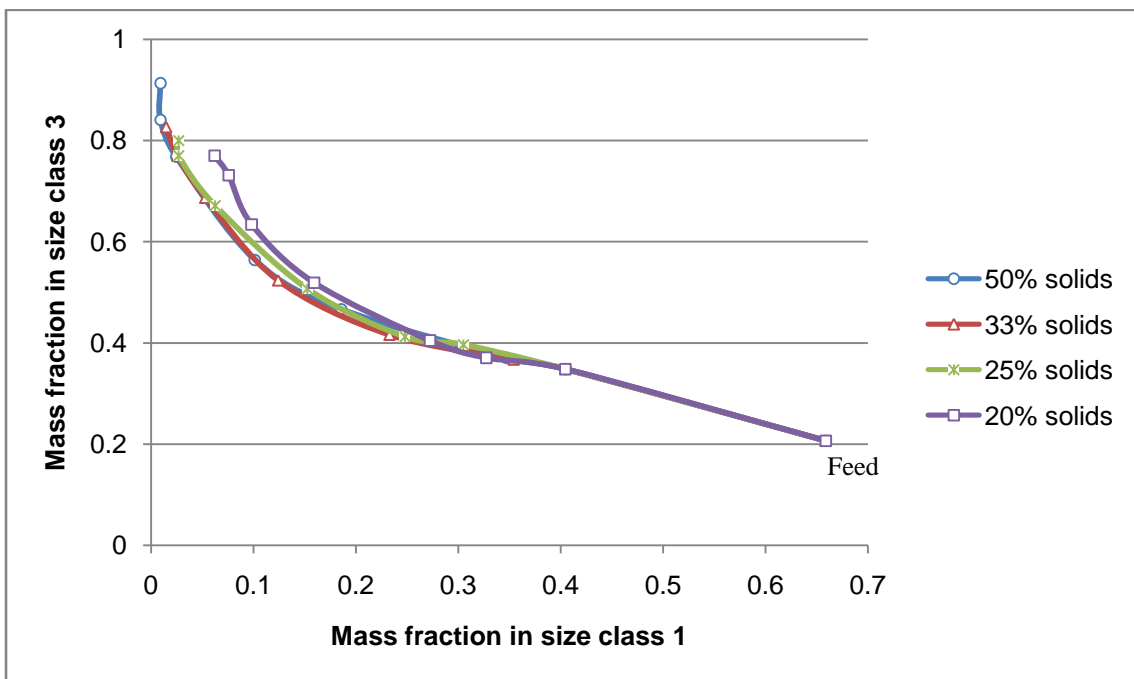


Figure 7.8: Mass fraction of material in the fines size class versus the mass fraction of material in the feed size class for different solids concentrations.

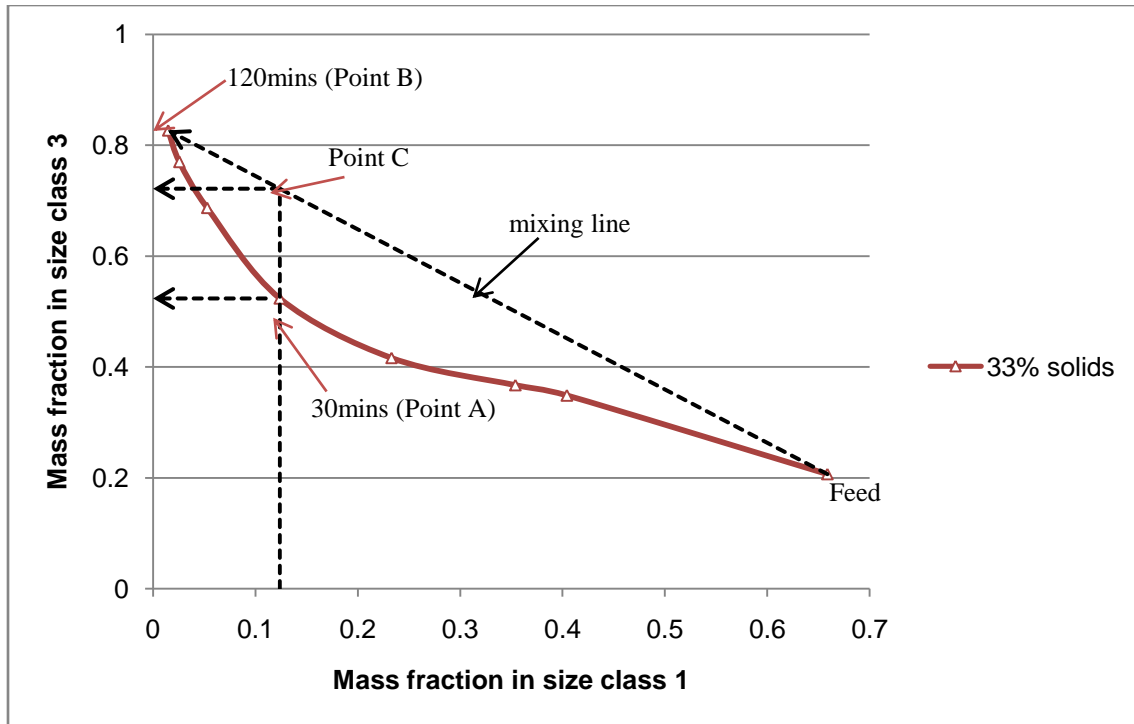


Figure 7.9a: Mass fraction of material in the fines size class versus the mass fraction of material in the feed size class for 33% solids concentration.

Using the experimental results recorded in detail in Tables A 2–A 5, Appendix A, we mapped Figures 7.6 and 7.8.

Figure 7.6 is a special plot, in that we omitted the time dimension in order to show the conversion of the feed size class to the intermediate.

The power of the AR tool lies in its capacity to represent only the variables of interest in a process. The AR is the region bounded by the curves, with the optimum parameters found on their boundaries. The region inside the curve represents the possible product mass fraction distributions. This enables us to make a number of deductions. Figure 7.6 shows that different slurry densities result in different grinding profiles, which signifies

that water has an influence on the product PSD. This in turn implies that there is a slurry density that will produce an optimum amount of material in a particular size class for any given grinding time. For instance, if we are interested in maximizing the production of intermediate size class material, then a 33% solids concentration and a grind time of between 15–30 minutes should be used.

Figure 7.7 is obtained from Figure 7.6, and shows only the 33% solids concentration case. What we can see in Figure 7.7 is that if our objective is to have 35% of the product mass in the intermediate size class, we can associate it with either 12% of product material in the feed size class and 53% of material in the fines size class (point A), or with 23% of mass in the feed size class and 42% of material in the fines size class (point B), with the aid of mass balances.

For Figure 7.8 we plotted an AR which considers the amount of material in the fines size class compared with the amount in the feed size class as grinding proceeds. This amount reduces while that in the fines size class grows, as some mass broken from the former reports directly to the latter.

PGM grains are very small (less than 10 μm) and sometimes tightly interlocked with the harder (silicate) phase (Penberthy et al 2010). In processing PGM ores, it is sometimes desirable to grind the feed to ultrafine size (that is, to produce the greatest possible amount of fines) in order to liberate and subsequently recover valuable minerals. However, because the smaller particles often cause difficulties in flow and handling, it

may be considered necessary to retain a small percentage of the original feed material in the product.

Using the 33% solids curve as an example, Figure 7.9a shows that if our objective is to have not more than 12% of un-milled material (Point A) in the product while optimizing the amount of fines, we can achieve this by milling for 30 minutes (Point A) to get the fines to constitute 52% of the product. The alternative is to take the feed and split it into two parts, after which one part can be milled for 120 minutes (Point B) and then mixed with the un-milled portion, increasing the yield of fines from 52% (Point A) to about 72% (Point C) through this mixing technique. The amount of feed material in the product is maintained to assist flow and handling. This is another demonstration of the ability of the AR approach to identify solutions to problems that are not easily realized. Different solids concentrations exhibit very similar trends to those shown by the 33% solids case. Figure 7.9a's results can be practically used in the development of flow sheets. The by-pass stream (as shown in Figure 7.9b) is a consequence of the mixing technique.

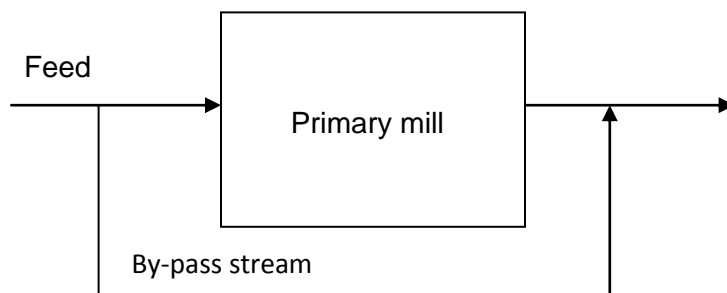


Figure 7.9b: Flow sheet development including a by-pass stream in order to maximize fines production or minimize production of intermediate sized particles for a given mass% feed material in the product.

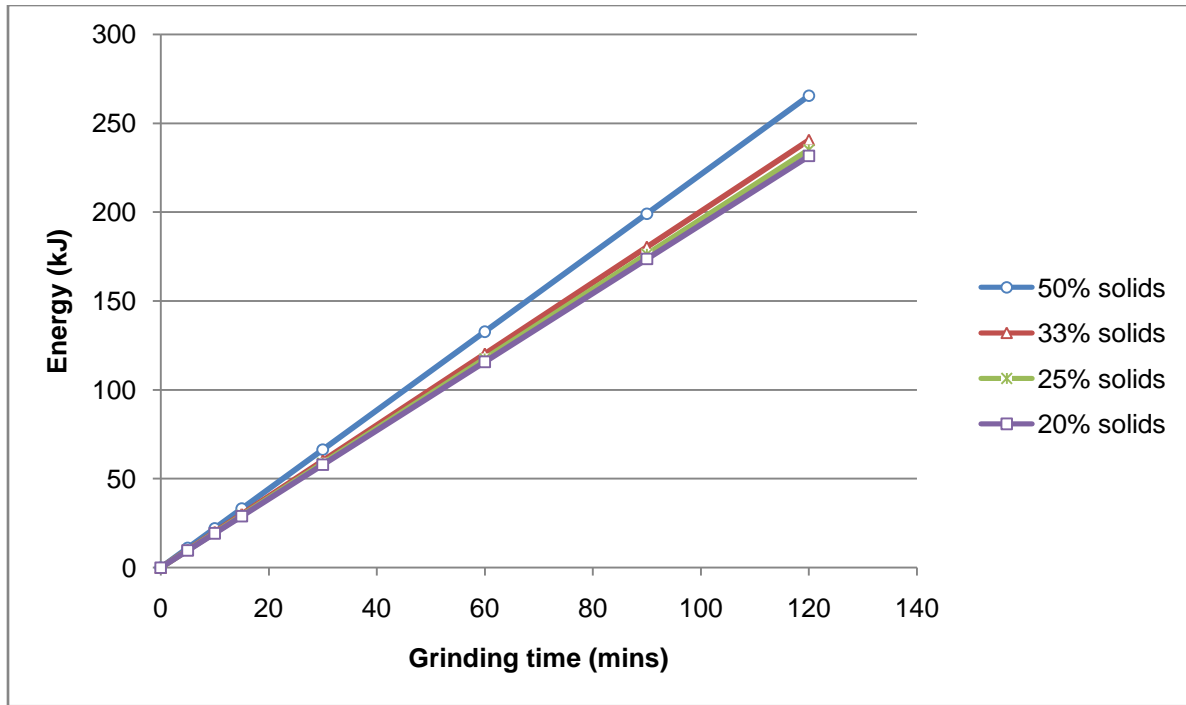


Figure 7.10: Grinding energy versus grinding time for different concentrations of solids

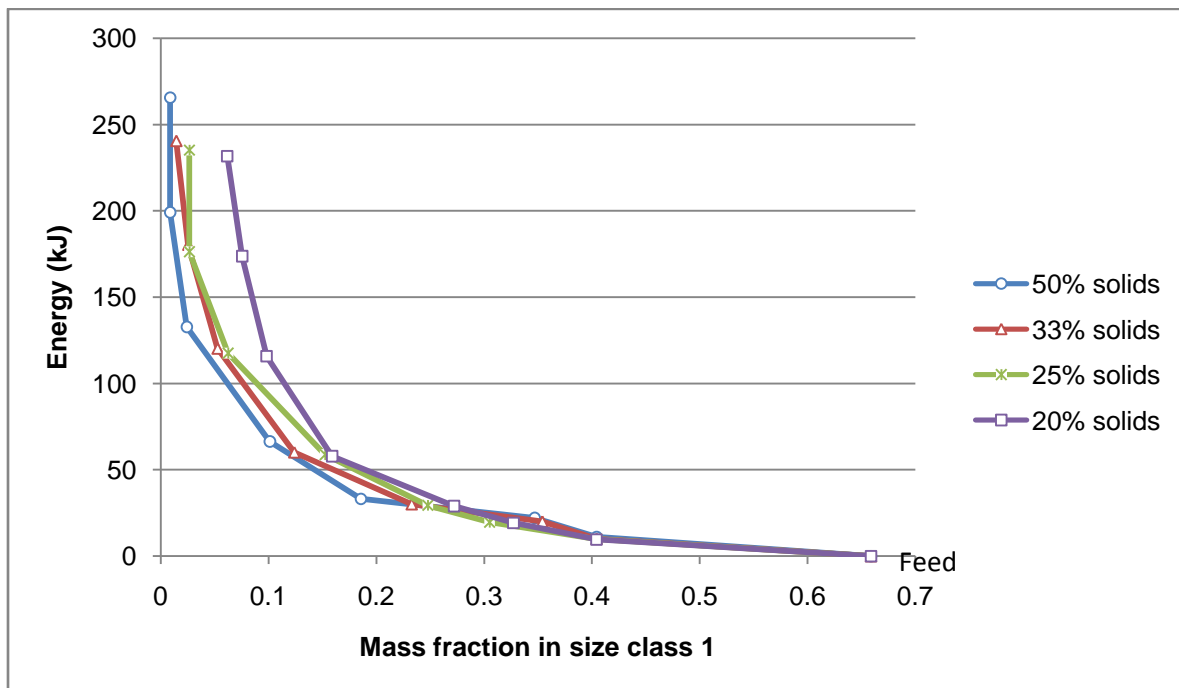


Figure 7.11: Grinding energy versus mass fraction of material in feed size class for different concentrations of solids.

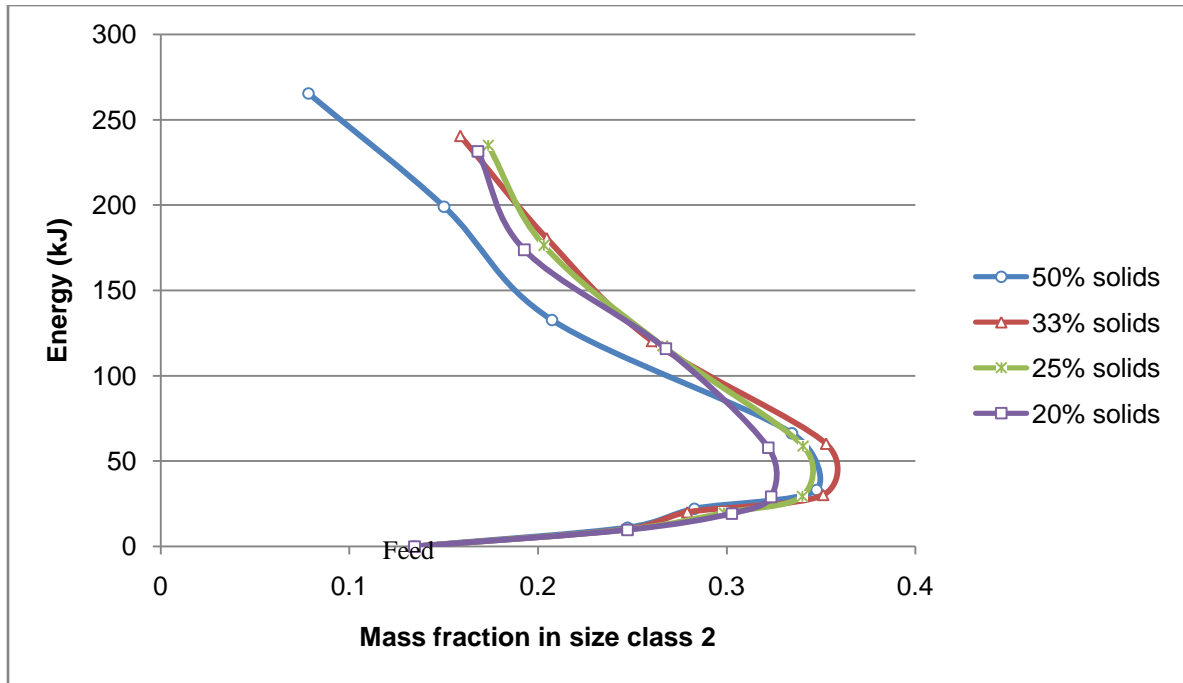


Figure 7.12: Grinding energy versus mass of material in intermediate size class for different concentrations of solids.

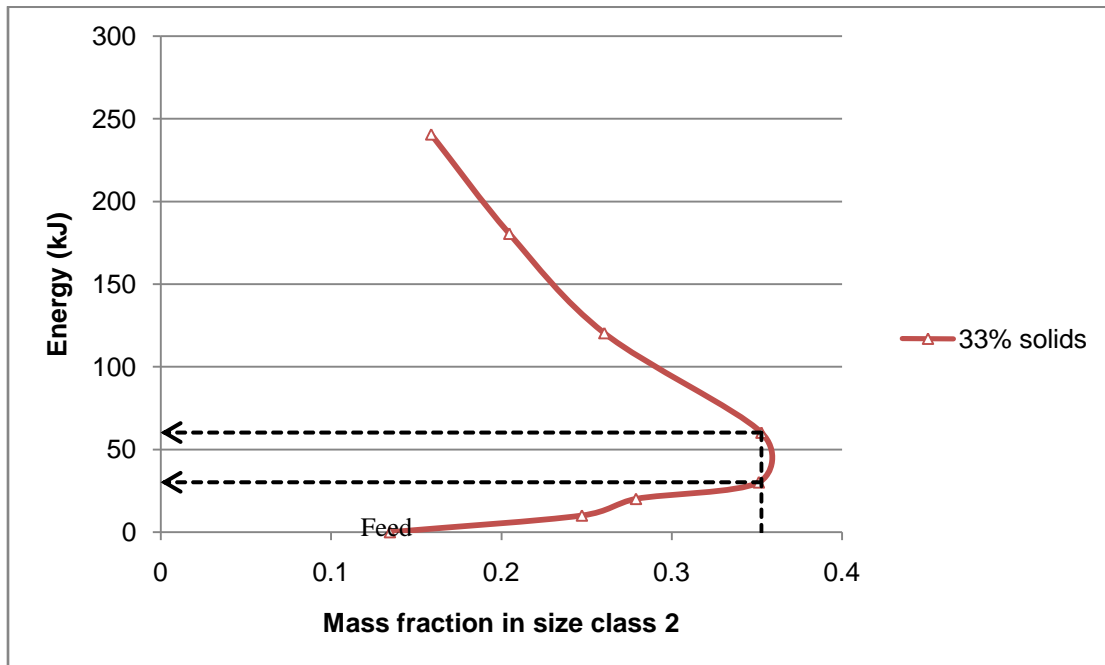


Figure 7.13: Grinding energy versus mass of material in intermediate size class for 33% solids concentration.

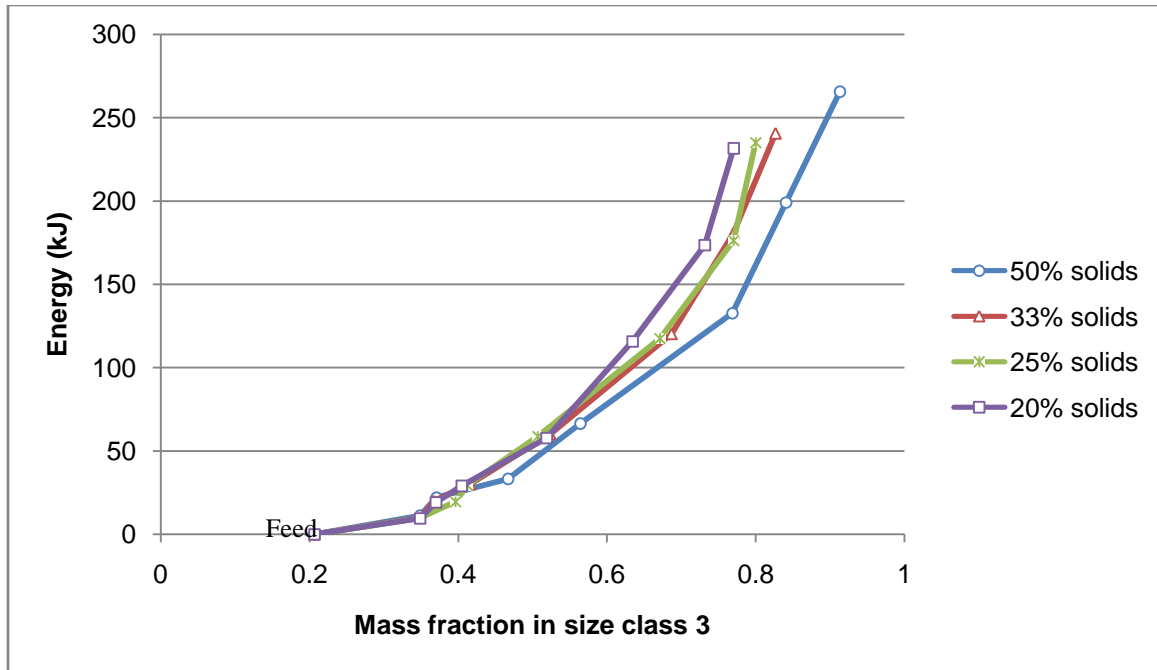


Figure 7.14: Grinding energy versus mass fraction of material in fines size class for different concentrations of solids.

Data Tables A2–A5 in Appendix A, and Tables E1–E4 in Appendix E provided the results we used to plot Figures 7.10–7.14.

Figure 7.10 shows the energy profiles associated with different slurry densities. The standard unit of energy ubiquitously used around the world is kilowatt-hour (kwh) and the conversion factor between the unit of energy (kJ) we used and the standard is that: 1 kwh = 3600kJ. Figures 7.11, 7.12 and 7.14 show the energy changes that take place when mass breaks out of the feed size class, into and out of the intermediate size class, and into the fines size class respectively. There is a linear relationship between grinding energy and grinding time. Figure 7.10 also shows that generally there is a small variation in energy consumption with an alteration in slurry density. This is probably because the pool of water developed in the mill for less viscous slurries has a moment

of rotation that follows the same direction as the mill, and therefore actually aids its rotation. The greater the pool volume, the more the contribution made by the water to the mill rotation and the lower the amount of energy drawn from the power supply. The reverse also applies: the lower the pool volume, the less contribution the water makes to mill rotation, which then requires additional energy. The main advantage of a (small) slurry pool is that it ensures the mill is fully charged with material, which allows for more effective coating of the particles and consequently greater grinding efficiency. For energy efficiency purposes it seems reasonable to operate mills under low solids concentrations, maintaining the same mill throughput. There are other advantages associated with low solids concentrations (as supported by Figure 7.8): the lower the concentrations of solids, the fewer the fines produced, and the greater the reduction in problems associated with slimes.

To plot Figure 7.11, we changed the essential variables from energy versus grinding time to energy versus mass fraction in size class 1. In this figure, we see that the mass fraction of material remaining in the feed size class diminishes as the amount of grinding energy is increased. The solids concentration affects the rate of mass decrease with energy input. Figure 7.11 concurs with Figure 7.10 in showing that the less viscous the slurry, the smaller the amount of energy used for grinding, and vice versa. This is an important characteristic that can be explored to optimize the concentration of PGM ores. We therefore hypothesize that if the amount of energy used can be controlled by varying the slurry density, it might be possible to grind the constituent components in the ore selectively on the basis of their relative hardness. Selective grinding is desirable,

since if only relevant phases are milled, energy usage will be greatly reduced. This is an important factor to consider when developing comminution flow sheets (Figure 5.10, Chapter 5).

Figure 7.12 illustrates the variations in grinding energy versus mass fraction of material in the intermediate size class for different slurry densities. What we can learn from this graph is that if the aim is to raise the mass fraction of the intermediate size class, then the same amount of energy (50kJ) can give rise to different optimums, depending on the concentration of the solids.

Figure 7.13 is obtained from figure 7.12, and plots only the 33% solids concentration scenario. It shows that if we intend to have 35% of the intermediate size class in the product, we can achieve this by using either 30 kJ of energy and grinding for about 15 minutes, or 60 kJ of energy and grinding for about 30 minutes. Once again, we have the choice of using less energy to fulfil a given objective.

In Figure 7.14 we track the changes in the mass fraction of material in size class 3 that occur in response to the amount of grinding energy. Not surprisingly, we can see in both Figures 7.12 and 7.14 that a higher concentration of solids results in a higher rate of conversion from the coarser size classes to the finer class.

7.4 Conclusion

The AR method has proved to be successful in identifying opportunities for increasing efficiency in milling a typical industrial ore. The experimental results outlined in this

chapter have indicated that less energy can be used to fulfil a desired objective, like a given amount of breakage. If the aim is to raise the mass fraction of the intermediate size class, then the same amount of energy can be used to arrive at different solutions, depending on the concentration of solids. A solids concentration of 33%, milled for between 15–30 minutes, gave us the maximum amount of material in the intermediate size class. We also found that in general, slurry density does not affect the breakage rates of the ‘soft’ components, but that breakage rates fall with decreasing slurry density for the ‘hard’ components. The results also show that we can control the amount of energy used by varying the slurry density. It should then be possible to grind the constituent components in the ore selectively, on the basis of their relative hardness. This in turn will save energy, because only relevant phases will be milled. The AR method, through the mixing technique, can be used to develop flow sheets. The AR technique also makes it possible to specify operational parameters such as the slurry density and grinding time, to obtain the most efficient comminution results.

7.5 References

- Bazin, C. & Obiang, P. 2007, "Should the slurry density in a grinding mill be adjusted as a function of grinding media size?", *Minerals Engineering*, vol. 20, no. 8, pp. 810-815.
- Fuerstenau, D.W., Venkataraman, K.S. & Velamakanni, B.V. 1985, "Effect of chemical additives on the dynamics of grinding media in wet ball mill grinding", *International Journal of Mineral Processing*, vol. 15, no. 4, pp. 251-267.
- Glasser, D., Hildebrandt, D. & Crowe, C. 1987, "A geometric approach to steady flow reactors: The attainable region and optimization in concentration space", *Industrial and Engineering Chemistry Research*, vol. 26, no. 9, pp. 1803-1810.
- Hay, M.P. & Roy, R. 2010, "A case study of optimising UG2 flotation performance. Part 1: Bench, pilot and plant scale factors which influence Cr₂O₃ entrainment in UG2 flotation", *Minerals Engineering*, vol. 23, no. 11-13, pp. 855-867.
- Khumalo, N., Glasser, D., Hildebrandt, D. & Hausberger, B. 2008, "Improving comminution efficiency using classification: An attainable region approach", *Powder Technology*, vol. 187, no. 3, pp. 252-259.
- Khumalo, N., Glasser, D., Hildebrandt, D. & Hausberger, B. 2007, "An experimental validation of a specific energy-based approach for comminution", *Chemical Engineering Science*, vol. 62, no. 10, pp. 2765-2776.
- Khumalo, N., Glasser, D., Hildebrandt, D., Hausberger, B. & Kauchali, S. 2006, "The application of the attainable region analysis to comminution", *Chemical Engineering Science*, vol. 61, no. 18, pp. 5969-5980.
- Maharaj, L., Loveday, B.K. & Pocock, J. 2011, "The effect of the design of a secondary grinding circuit on platinum flotation from a UG-2 ore", *Minerals Engineering*, vol. 24, no. 3-4, pp. 221-224.

- Matijašić, G., Žižek, K., Sofilić, U., Mandić, V. & Skopal, H. 2009, "Wet comminution kinetics of dolomite at laboratory scale", *Chemical Engineering and Processing: Process Intensification*, vol. 48, no. 4, pp. 846-851.
- Metzger, M.J., Glasser, B.J., Glasser, D., Hausberger, B., Hildebrandt, D. & Khumalo, N. 2008, "Use of the attainable region (AR) analysis to optimize particle agglomeration and breakage operations", *AIChE Annual Meeting, Conference Proceedings*.
- Metzger, M.J., Glasser, D., Hausberger, B., Hildebrandt, D. & Glasser, B.J. 2009, "Use of the attainable region analysis to optimize particle breakage in a ball mill", *Chemical Engineering Science*, vol. 64, no. 17, pp. 3766-3777.
- Mori, H., Mio, H., Kano, J. & Saito, F. 2004, "Ball mill simulation in wet grinding using a tumbling mill and its correlation to grinding rate", *Powder Technology*, vol. 143-144, pp. 230-239.
- Rule, C.M. 2009, "Energy considerations in the current PGM processing flowsheet utilizing new technologies", *SAIMM - Journal of The South African Institute of Mining and Metallurgy*, vol. 109, no. 1, pp. 39-46.
- Tangsathikulchai, C. & Austin, L.G. 1989, "Slurry density effects on ball milling in a laboratory ball mill", *Powder Technology*, vol. 59, no. 4, pp. 285-293.
- Tangsathikulchai, C. & Austin, L.G. 1985, "The effect of slurry density on breakage parameters of quartz, coal and copper ore in a laboratory ball mill", *Powder Technology*, vol. 42, no. 3, pp. 287-296.

CHAPTER 8

8 DEVELOPMENT AND DEMONSTRATION OF A PROPOSED ATTAINABLE REGION PROGRAMME

8.1 Introduction

The Attainable Region (AR) is an analytical approach that has been applied successfully in the field of chemical reactor engineering as a means of choosing optimal reactor configurations (Glasser, Hildebrandt & Crowe 1987). Since milling can also be considered a rate process in which the various particle sizes are broken from larger sizes to smaller ones in a manner analogous to reactor systems, the AR approach has been extended to apply to comminution (Khumalo *et al.*, 2006, 2007, 2008). The research carried out in the study described in this chapter concerns an aspect of using AR in comminution in a more flexible manner — by introducing a software programme that extends the capabilities of AR analysis.

A complete AR analysis requires a description of the set of all possible outputs for a system. In this case the system includes the mass fraction of material in three broad particle size ranges (size classes) and the amount of energy consumed in grinding. The procedure employed for defining the AR in comminution for the fundamental processes of breakage and mixing has been described by Khumalo *et al.* (2006) and Metzger *et al.* (2009). This procedure is based only on sieve analysis data, with set target size ranges of the material of interest. An AR plot is dependent on the set cut-off points, so if the set points change, a cumbersome manual process has to be undertaken to come up with a

new AR plot. For this reason, we have developed a user- friendly software programme that allows changes to be made by simply re-entering new product set points. In this chapter, we review the AR approach, discuss the software we propose, and demonstrate what it is capable of.

8.2 Particle population grouping

Comminution involves a large number of ore particles. If the aim is to characterize these, it is neither practical nor useful to consider their sizes on an individual basis. Instead, we employ statistical principles. At the heart of this approach is the grouping of particles into classes on the basis of their size. This has already been discussed at length in Chapter 7 section 7.1.2. The brief summary below is relevant to the construction of an AR plot. Although the sizes of the particles can be classified into any number of groups, typically three broad size classes are used:

- (i) the feed size class, which is taken as the largest size class, also called size class 1 (m_1);
- (ii) the middle-sized class, which is the result of a moderate extent of breakage, and is termed size class 2 (m_2); and
- (iii) the fines size class, which is the result of a relatively large breakage extent and is termed size class 3 (m_3).

The reason for dividing the classes into three is that it is often the case that the desired product lies in an intermediate particle size range. Although it is desirable to reduce the size of the feed material, excessive comminution into the fines size class presents

many difficulties, including increased cohesion between the smaller particles and handling concerns (the danger of inhalation) as a result of the entrainment of smaller particles. Consequently, an intermediate size is considered best for many downstream operations. In addition, grinding beyond the point at which the desired size class has been reached results in over-grinding, which is a waste of time and energy. This is one of the reasons for the poor efficiency (and unnecessary cost) of many grinding operations.

8.3 Describing grinding as a reaction process

Grinding involves the application of mechanical force to cause fracturing and breakage of particles into smaller fragments. Although each particle breaks differently, it has been found that statistically the breakage process is consistent, which has made it possible for engineers to formulate equations that describe the rate of breakage (selection function) and distribution of particles resulting from fragments (breakage function). It is therefore quite acceptable to treat grinding as a reaction that involves the conversion of material 'A' of a particular size distribution to a product 'B' of a specified size distribution (more products can be specified if required). It should be evident that the rate of conversion from feed material 'A' to product 'B' is dependent on the size distribution of 'A' and the specified size distribution of 'B'. In terms of the terminology thus far presented, the 'reactions' are the milling stages from m_1 to m_2 , from m_2 to m_3 and from m_1 to m_3 , following the particle size classes given in the previous section.

8.4 Demonstration of the current AR procedure

In this section we demonstrate how the AR curves change with alterations in the cut-off points specification. The data we used was obtained from Appendix A, Figure A1.

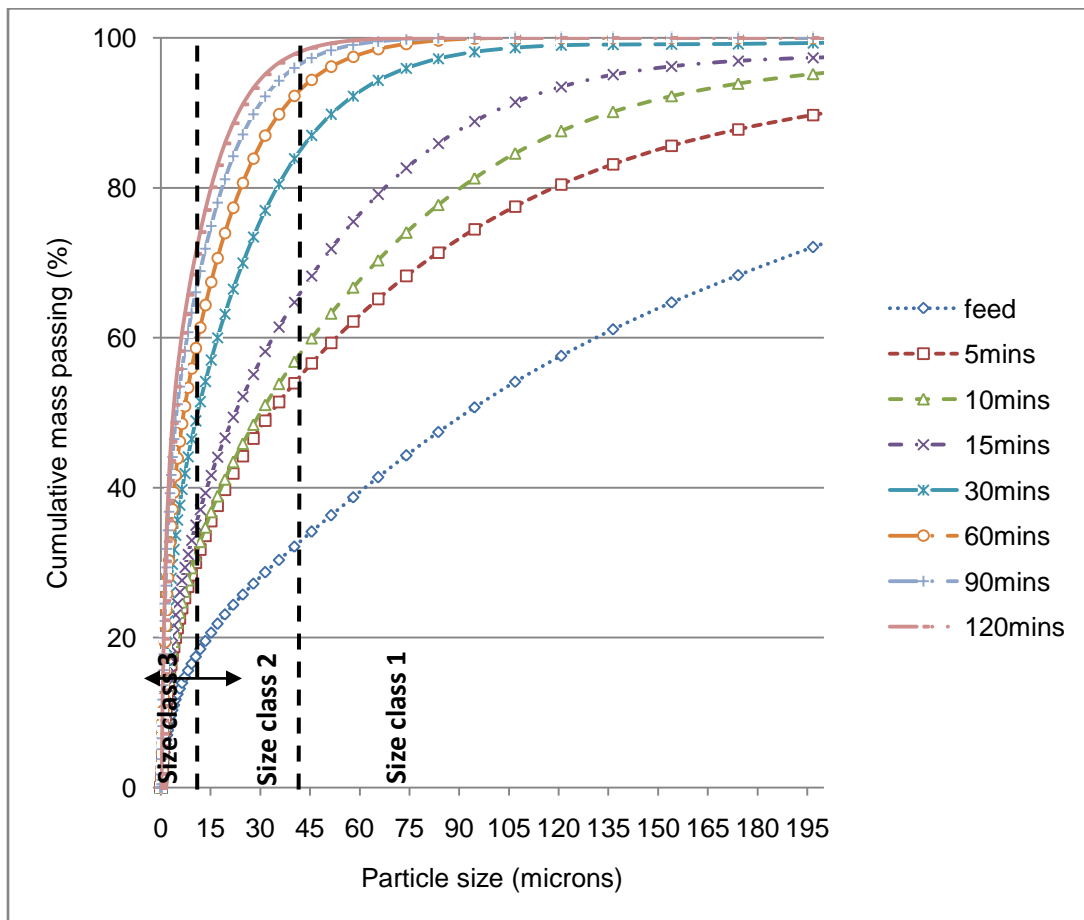


Figure 8.1: A cumulative mass % of material passing a particle size versus particle size for different dry grinding periods (this graph is obtained from Appendix A, Figure A1).

Figure 8.1 is a typical cumulative plot of the mass percentage of material passing a particle size versus particle size for different milling durations. In this figure, we chose to set the intermediate size class between 15–45 μm , the feed size class above 45 μm , and the fines size class below 15 μm .

Table 8.1: Attainable Region data

Grinding Time (mins)	Size Class 1 (m1)	Size Class 2 (m2)	Size Class 3 (m3)
0	0.6587	0.1346	0.2067
5	0.4340	0.2205	0.3455
10	0.4007	0.2318	0.3675
15	0.3174	0.2661	0.4165
30	0.1304	0.2996	0.5700
60	0.0561	0.2695	0.6744
90	0.0269	0.2240	0.7491
120	0.0133	0.1862	0.8005

Table 8.1 shows the AR data generated by Figure 8.1, showing the mass fraction of material in each of the three chosen size classes after specific grinding times. The procedure we followed to generate data in Table 8.1 is as follows: Taking the feed (0mins grinding time) as an example, in order for us to obtain the mass fraction of material in the size class 1, we find the difference between total mass fraction (which is 1) and the cumulative mass fraction of material passing the 45 μ m particle size (0.3413). In order for us to evaluate the mass fraction of material in size class 2, we calculated the difference between the cumulative mass fraction of material passing the 45 μ m particle size (0.3413) and that passing the 15 μ m particle size (0.2067). To again calculate the mass fraction of material in size class 3, we found the difference between the cumulative mass fraction of material passing the 15 μ m particle size (0.2067) and that passing the pan (which is 0). We repeated this procedure for the 5, 10, 15, 30, 60, 90 and 120 minutes grinding periods to generate the data in Table 8.1. This is the data required in plotting the AR curves.

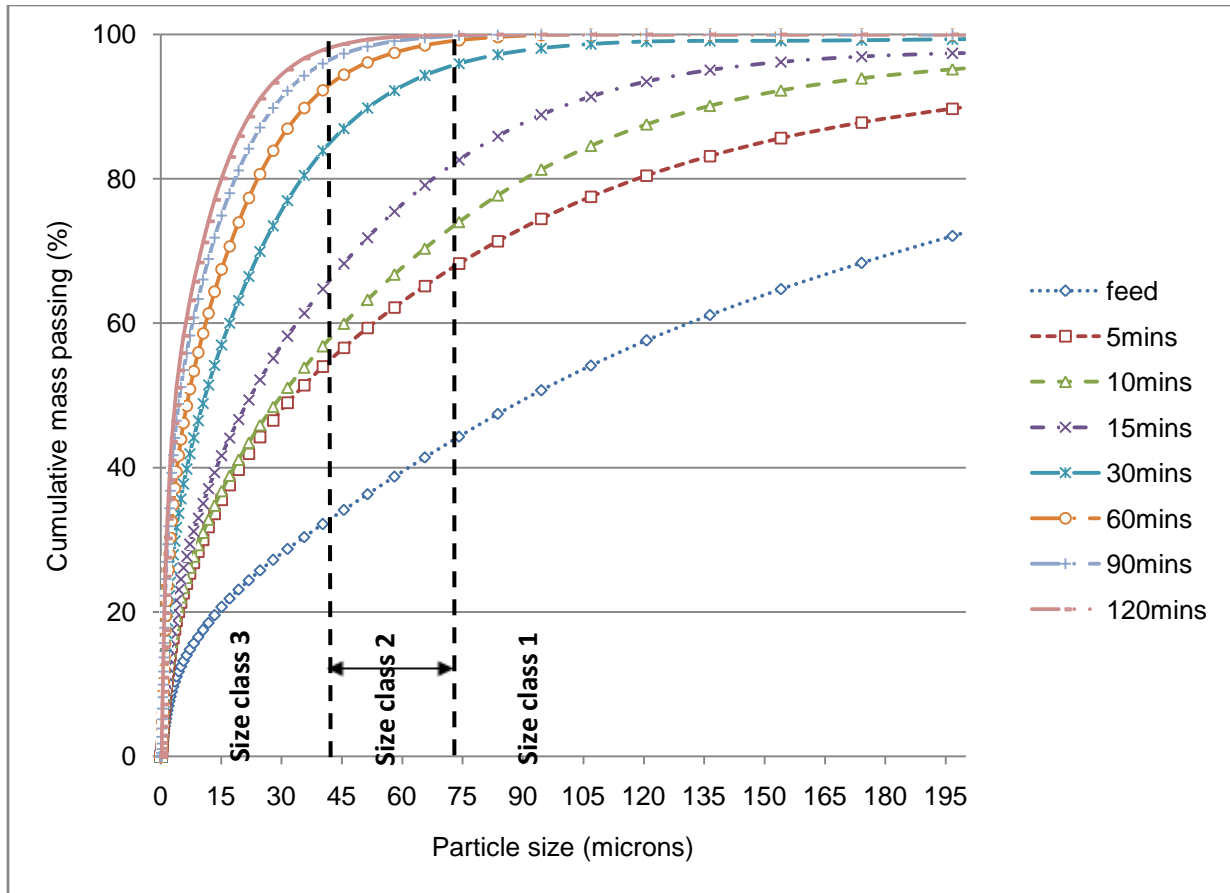


Figure 8.2: Cumulative mass % of material passing a particle size versus particle size. We redefined the size classes to make size class 1 above 75 μm , size class 2 to be between 45-75 μm and size class 3 below 45 μm .

Figure 8.2 is also a cumulative plot of the mass percentage of material passing a particle size versus particle size for different milling periods. The cut-off point specifications are changed in this figure so that the intermediate size class lies between 45–75 μm , the feed size class above 75 μm and the fines size class below 45 μm . This can be called the first scenario.

Table 8.2: AR data

Grinding Time (mins)	Size Class 1 (m1)	Size Class 2 (m2)	Size Class 3 (m3)
0	0.5571	0.1016	0.3413
5	0.2977	0.1363	0.5660
10	0.2597	0.141	0.5993
15	0.1739	0.1435	0.6826
30	0.0405	0.0899	0.8696
60	0.0082	0.0479	0.9439
90	0.0021	0.0248	0.9731
120	0.0005	0.0128	0.9867

Table 8.2, like the previous table, shows the AR data generated from the relevant plot, which sets out the mass fraction of material in each of the three chosen size classes after specific grinding times. What can be seen below is an example of an AR plot that uses the data contained in Tables 8.1 and 8.2.

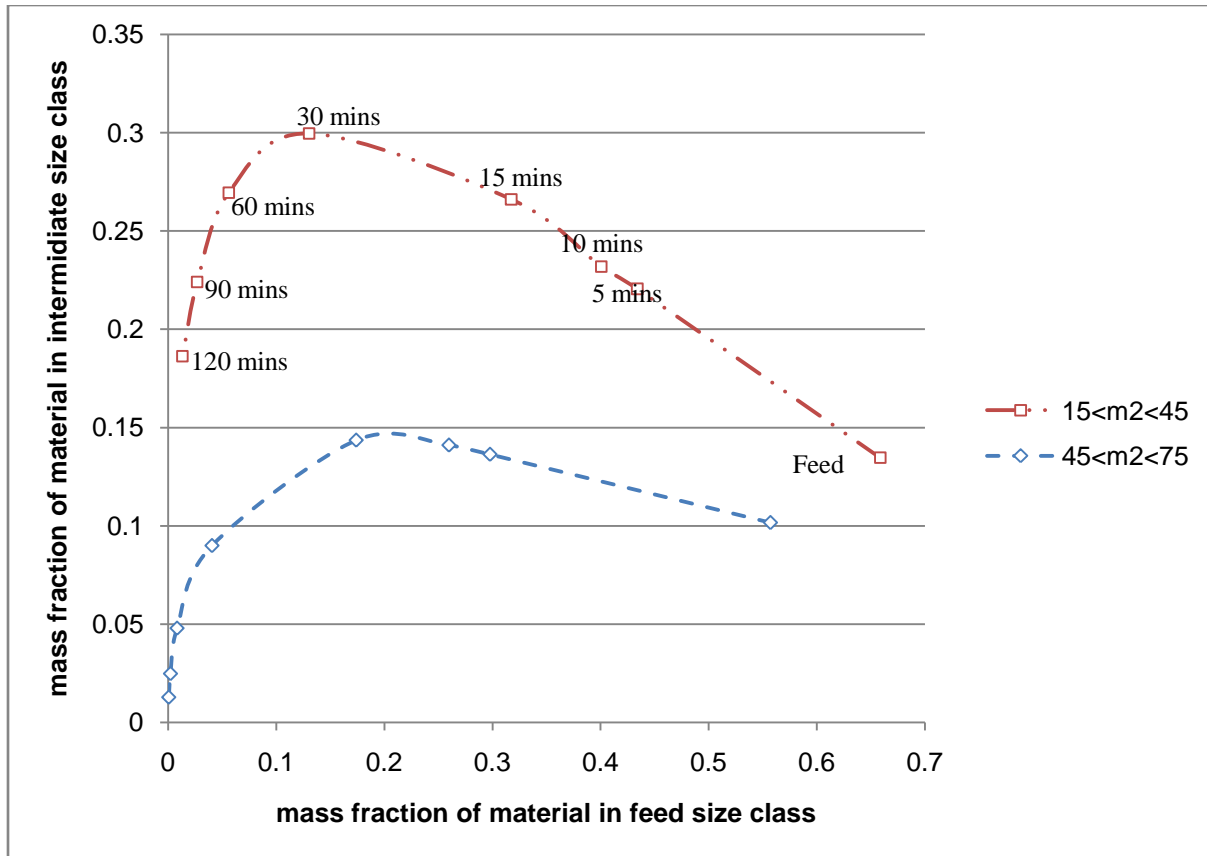


Figure 8.3: Example of an AR plot of the mass fraction of material in the intermediate size class versus the mass fraction of material in the feed size class. In the red curve size class 2 lies between 15-45 μm while in the blue curve size class 2 is between 45-75 μm .

We constructed the AR plot shown in Figure 8.3 by following the procedure outlined by Khumalo *et al.* (2007) and Metzger *et al.* (2009). Each point corresponds to a different duration of mill operation, starting from a single feed point. This simple plot provides some very important information on the process. Two salient features are that:

1. the boundary curve describes the processes used, and can be interpreted as referring to the pieces of equipment used for the operation, which implicitly identifies the equipment required for greatest efficiency. It can be seen that in

both cases the shape of the curves are similar, which means that as they are convex, mixing would reduce the amount of intermediate product produced. Thus to maximise the amount of intermediate product for a given amount of breakage of the feed, one would try to run the mill as close to plug flow conditions as possible in the case of a continuous mill.

2. Secondly, the turning point of the curve indicates an optimum solution for the case of when the objective is to maximize the mass in the intermediate size class. In both situations, the optimal grinding time to maximize the mass of intermediate produced is around 30 minute, but for the different definitions of the intermediate product, different amounts of intermediate product are produced.

The second point offers both the solution to the problem of creating optimal grinding conditions and of finding the process control policy most suited to achieving that objective (that is, identifying the run time required to achieve that optimum).

The above example demonstrates how rapidly the AR tool can be used to show whether a particular cut-off specification is worth pursuing, as the relative difficulty of achieving the grinding target is shown in the plot. The AR plot may even assist in the selection of the optimum cut-off points for the product desired.

8.5 Preparation of data for AR analysis

The prerequisite for analysis by the AR method is that the material has to have been ground, whatever the grinding equipment used for comminution. It may even be preferable to use more than one method of comminution, and then use the AR approach to assess the effectiveness of each by comparison. 'Different comminution routes' may refer to using multiple types of reduction equipment, whether in a series or in parallel, or simply varying the grinding conditions in a particular mill. The product can then be analyzed using the appropriate sizing method. In the case of our investigation, we used the Malvern Mastersizer equipped with a Hydro 2000MU wet cell.

Since energy input is an important aspect of comminution, we included in our AR software a theoretical power model that calculates mill power draw and thus is able to predict the total energy input for a given data set, provided that the user enters the mill dimensions and operational conditions. Where power readings are available, a user can simply enter the power measurement (which overrides the theoretical calculation).

The theoretical power model is discussed in the following section.

8.5.1 Mill power

The AR software can calculate a mill's power need theoretically by making an estimate of the net and gross power demand (kW) of a conventional ball mill as a function of its known dimensions and basic operating conditions. The net power demand of a

conventional tumbling mill can be estimated with accuracy by means of the Hogg and Fuerstenau (1972) model. We expanded the original formulation to represent the independent contribution of each component of the mill charge (balls and slurry) to the total net power of the mill as follows:

$$P_{\text{net}} = \eta P_{\text{gross}} = 0.238D^{3.5}(L/D)N_c \rho_{\text{ap}} (J - 1.065J^2)\sin\alpha \quad (8.1),$$

where:

$$P_{\text{gross}} = \text{gross power draw of the mill (kW)} = P_{\text{net}} / \eta$$

η = electrical and power transmission efficiency

D = effective mill diameter

L = effective mill length

N_c = tumbling speed, expressed as a fraction of the critical centrifugation speed:

$$N_{\text{critical}} = 76.6/D^{0.5}$$

J = apparent volumetric fractional mill filling, (including the balls and the interstitial voids in between such balls)

α = charge lifting angle (defines the dynamic positioning of the centre of gravity of the mill load with respect to the vertical direction. Typically in the range of 35 to 40°)

ρ_{ap} = the apparent density of the charge (kg/m³), which may be evaluated on the basis of the indicated charge components (balls, interstitial slurry and overfilling slurry).

This leads to the extended equation:

$$\rho_{\text{ap}} = \{(1 - f_v)\rho_b J_b + \rho_b J_p f_v J_b + \rho_p (J - J_b)\} / J \quad (8.2),$$

with:

f_v = the volume fraction of interstitial voids in between the balls (typically assumed to be 40% of the volume apparently occupied by the balls)

J_b = apparent balls filing (including balls and slurry and the interstitial voids in between the balls)

J_p = interstitial slurry filling, corresponding to the fraction of the available interstitial voids (in between the ball charge) actually occupied by the slurry of finer particles

ρ_b = density of the balls (kg/m^3)

ρ_p = slurry density (kg/m^3) directly related to the weight % solids of the slurry (f_s) by: $1/[(f_s/\rho_m) + (1 - f_s)]$, and

ρ_m = mineral particle density (kg/m^3).

In this formulation, the contribution to the net mill power by the balls in the charge becomes:

$$\rho_b = [(1 - f_v)\rho_b J_b / \rho_{ap} J] \cdot (\eta P_{gross}) \quad (8.3).$$

Similarly, the contribution to the net mill power by the interstitial slurry in the charge becomes:

$$\rho_s = [\rho_b J_p f_v J_b / \rho_{ap} J] \cdot (\eta P_{gross}) \quad (8.4),$$

and the normally negligible contribution of the overfilling slurry on top of the charge becomes:

$$\rho_o = [\rho_p (J - J_b) / \rho_{ap} J] \cdot (\eta P_{gross}) \quad (8.5).$$

We used the power model in Equation 8.1 to compare the degree of correlation between the energy as predicted by the model against experimentally collected data. As shown by Figure 8.4, there is a good correlation between the two.

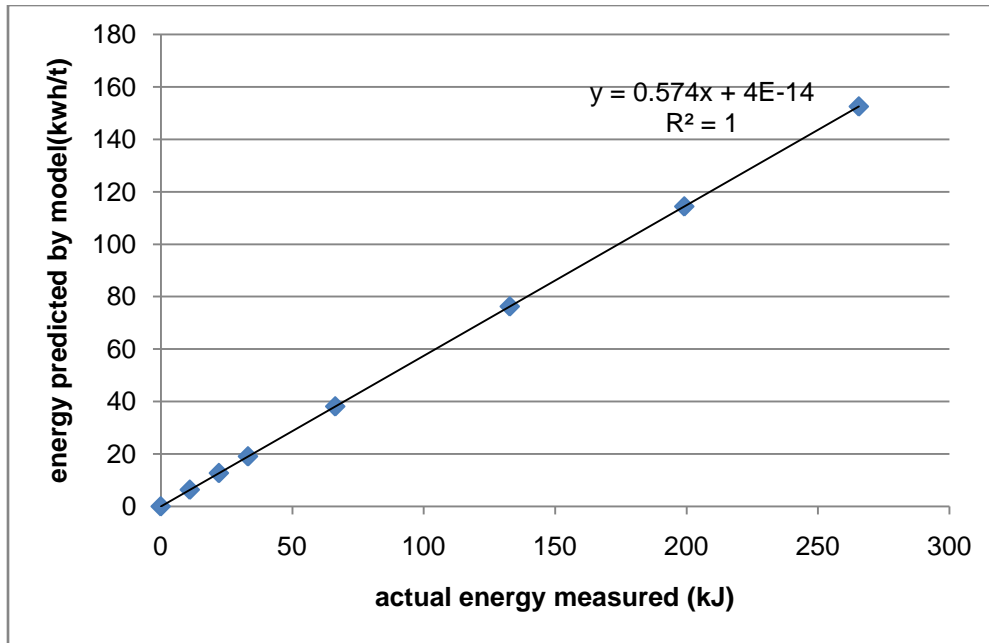


Figure 8.4: Comparison of actual energy measured against model prediction, for a 50% by mass solids concentration.

8.6 Demonstration of the proposed AR programme

The software we developed has been coded to simplify and speed up the process of analyzing size data. Appendix E gives the procedure and an illustration of how to operate the AR programme. The required input is the entire worksheet containing the size analysis data, as shown in Appendix F. The head of each column should be the appropriate grind time, as this is used to compute energy input. As seen in Figure 8.4 below, the user interface is very simple. All that is required is to create blank output worksheets, enter the source data on the spread sheet, and specify the cut-off points. The user can then select which data to include in the AR analysis by clicking the relevant item in the selection list box. An item can be deselected by clicking the highlighted item again. A further click on the process button completes the process. The results are posted to the output file.

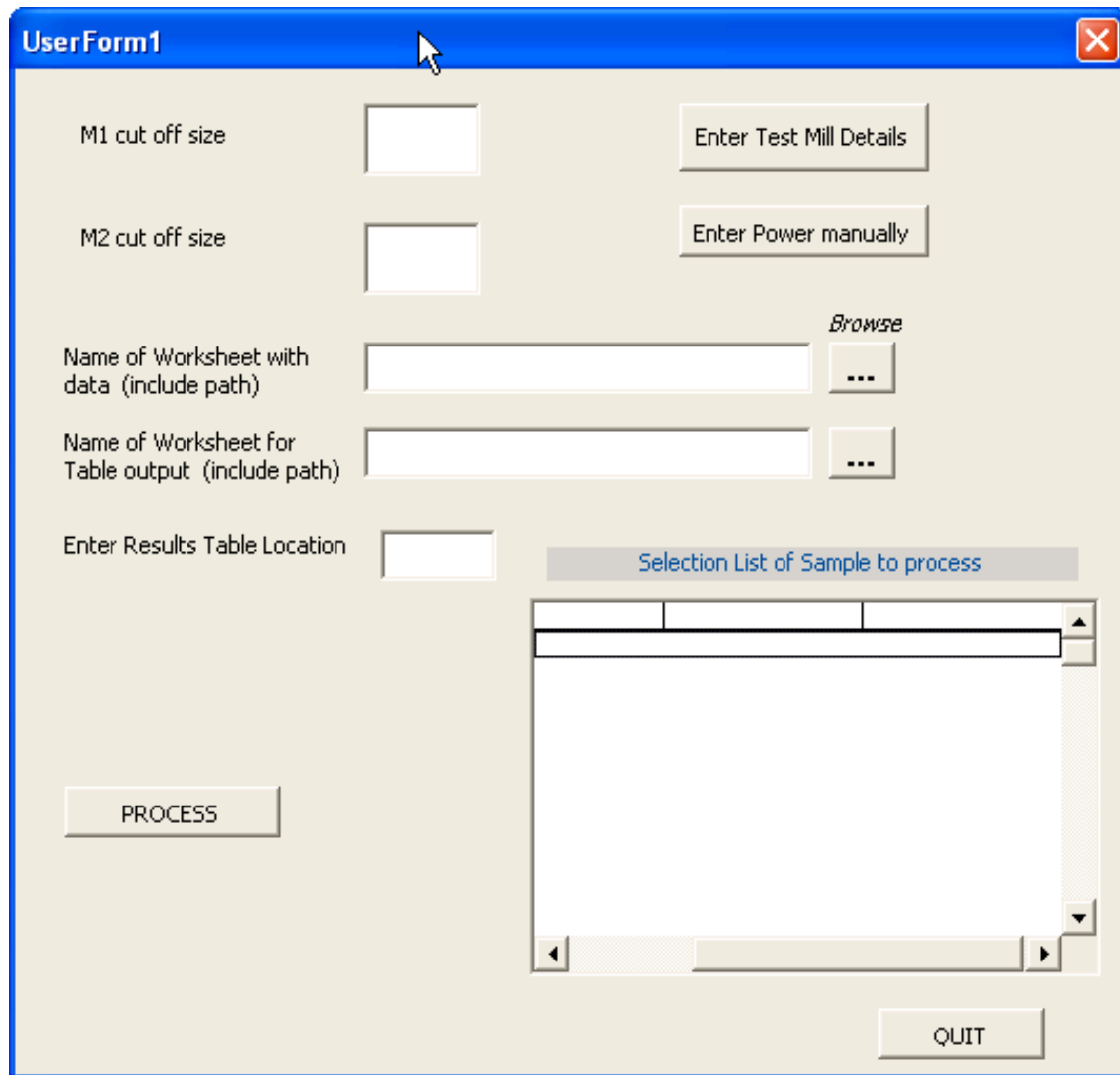


Figure 8.5: The user interface of the AR programme

8.7 Conclusions

In this chapter, we developed and demonstrated the AR software that saves the purpose of speeding up milling data processing. We also discussed the power model that was used to theoretically evaluate the power drawn by the mill during operation. Power can either be calculated by the programme or recorded directly from the milling set up. The software is a user friendly programme that can save the user about 90% of the time it takes when following a manual procedure.

8.8 References

Hogg and Fuerstenau, 1972, "*Power Relations for Tumbling Mills*", *Trans. SME-AIME*, Vol. 252, pp. 418-432.

CHAPTER 9

9 CONCLUSIONS

In summary, the aim of this thesis was to identify opportunities of increasing the milling efficiency of a UG2 ore. In order to achieve this task, we first tested the hypothesis that the feed material was heterogeneous (contained at least two components). XRD, SEM, XRF and MLA are well known techniques of characterizing mineral samples, but these sophisticated methods are time consuming, expensive and require some level of technical expertise to analyze the results. We then presented and used a simple method that relies only on the breakage kinetic data and knowledge of basic process modeling skills to carry out the hypothesis testing. The initial results obtained from our test work only partially validated the hypothesis that the material was heterogeneous, as the results could not eliminate the possibility of the presence of weaker particles in the feed. A heterogeneous and a homogeneous (one component) ore containing weaker particles exhibit similar breakage behaviour. In the former, the 'soft' is broken down before the 'harder' component, while in the latter the weak particles break first, followed by the stronger.

We then employed a more direct method of characterization in which we used the Atomic Absorption Spectrometer (AAS) to analyze the concentration of the element copper. Copper was used as a tracer element for the PGMs' rich mineral phase, because the mode of occurrence of PGMs' is such that they are associated with base metals. The results we got justified the presence of a 'soft' mineral phase that does not contain much of copper. We also found that the concentration of copper in the larger-

sized particles increases with grinding time, which is evidence of the presence of another, 'harder' mineral phase that contains copper and hence PGMs'. This method validated our hypothesis that the feed material was heterogeneous. The anticipated benefits of determining the nature of the ore's composition, that is, whether or not it is heterogeneous, are that such knowledge:

- can be explored by designers of comminution circuits in proposing flow-charts that can concentrate the material efficiently, based on its constituents,
- can be used by plant operators to help them adjust mill operating conditions in favour of milling only the mineral phase of interest.
 - If PGMs are concentrated in the soft component—could preferentially mill to break these initially,
 - If PGMs are concentrated in the hard component, thus grinding could be done selectively.

After establishing the nature of the ore's composition, we again tested the hypothesis that it may be possible to selectively mill and discard the desired or the undesired mineral phase. The anticipated benefits of achieving selective grinding are that it reduces the amount of energy required by the mill, requires a smaller mill size, and greatly improves overall mineral recoveries, as only material of value would be processed. Our experimental results validated the hypothesis that it is possible to achieve selective grinding by varying the slurry density and the grinding period in a mill.

We then used the Attainable Region (AR) method to find ways of reducing the grinding period and grinding energy required to achieve a desired result, as well as maximize the material in the desired size range. No work on utilizing the AR to optimize the size reduction of a real industrial ore in slurry has been reported previously, although earlier researchers have used the method for comminution carried under dry conditions and on test material. The experimental results we obtained proved that the AR method was successful in identifying opportunities for increasing the efficiency in milling a typical industrial ore. A solids concentration of 33% by mass, milled for between 15–30 minutes, gave us the maximum amount of material in the intermediate size class.

An AR plot is dependent on the set cut-off points, so if the set points change, a cumbersome manual process has to be undertaken to come up with a new AR plot. For this reason, we then proposed, developed and demonstrated an AR programme that allows changes to be made by simply re-entering new product set points. The results show that the software does save the user a lot of time and extends the capabilities of AR analysis.

CHAPTER 10

10 RECOMMENDATIONS

The fundamental objective of comminution in the mineral processing industry is not merely to reduce the particle size but to 'liberate' the constituent mineral phases that make up an ore so that valuable minerals can be separated from the gangue. The current trend in mineral processing is towards the exploitation of low grade ores as the high grade ones get depleted, and the effective liberation of values from these low grade ores remains one of the major challenges for mineral processors. It is our recommendation that efficient size reduction and liberation from low grade ores, like the UG2, be achieved by designing/retrofitting and operating comminution circuits in a way that will convert the maximum of energy input into selective grinding in order to produce an optimum amount of the desired sizes of fragments.

Future work should focus on establishing a mill-set up and flow-sheet that can achieve selective grinding of any heterogeneous ore. Other mill conditions such as ball size, mill speed and powder fillings should also be investigated in order to determine the optimal mill parameters to use in the mill-set up. Separation units such as floatation cells should also be investigated and included in the flow-sheet, as their efficiency is critical in achieving preferential milling and separation. The AR software is still in its infancy and more work needs to be done so that it can be fully automated and commercialized.

APPENDIX A: CLASSIFICATION OF PRODUCT MATERIAL INTO THREE SIZE CLASSES

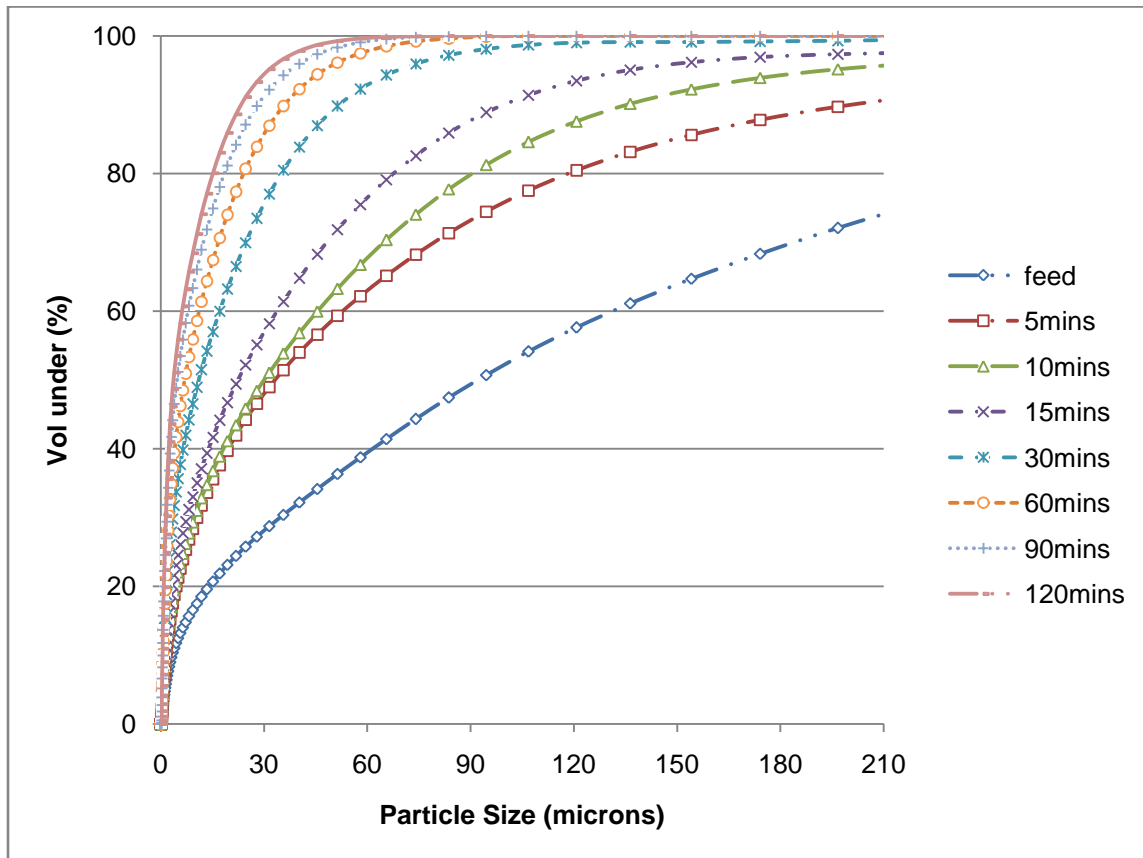


Figure A 1: A plot of volume percentage of material below a particle size vs particle size for different dry grinding times.

Table A 1: Size classification based on Figure A1

Grinding Time	Feed Size Class	Intermediate Size Class	Fines Size Class
0	0.6587	0.1346	0.2067
5	0.4340	0.2205	0.3455
10	0.4007	0.2318	0.3675
15	0.3174	0.2661	0.4165
30	0.1304	0.2996	0.5700
60	0.0561	0.2695	0.6744
90	0.0269	0.2240	0.7491
120	0.0133	0.1862	0.8005

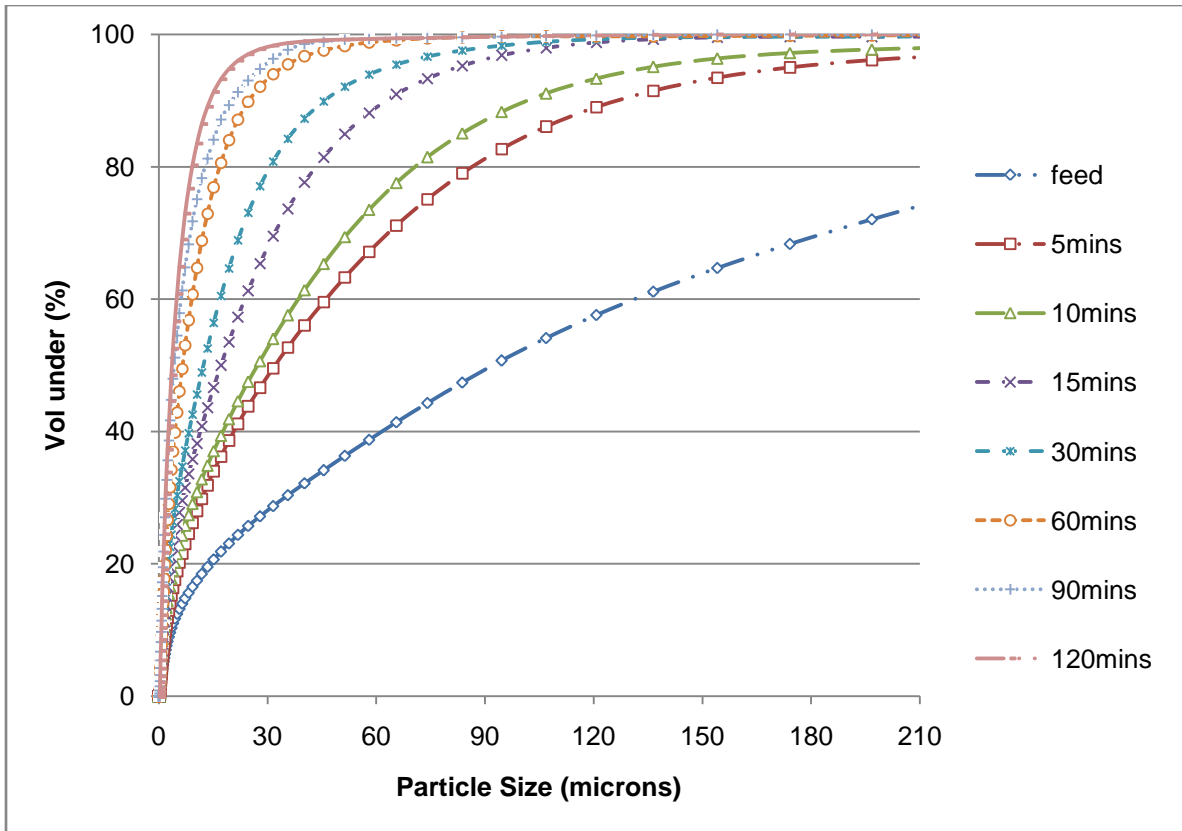


Figure A 2: A plot of volume percentage of material below particle size vs particle size for different grinding times with 50% solids content.

Table A 2: Size classification based on Figure A2

Grinding Time	Feed Size Class	Intermediate Size Class	Fines Size Class
0	0.6587	0.1346	0.2067
5	0.4042	0.2473	0.3485
10	0.3468	0.2828	0.3704
15	0.1856	0.3476	0.4668
30	0.1012	0.3346	0.5642
60	0.0241	0.2073	0.7686
90	0.0088	0.1502	0.8410
120	0.0088	0.0782	0.9130

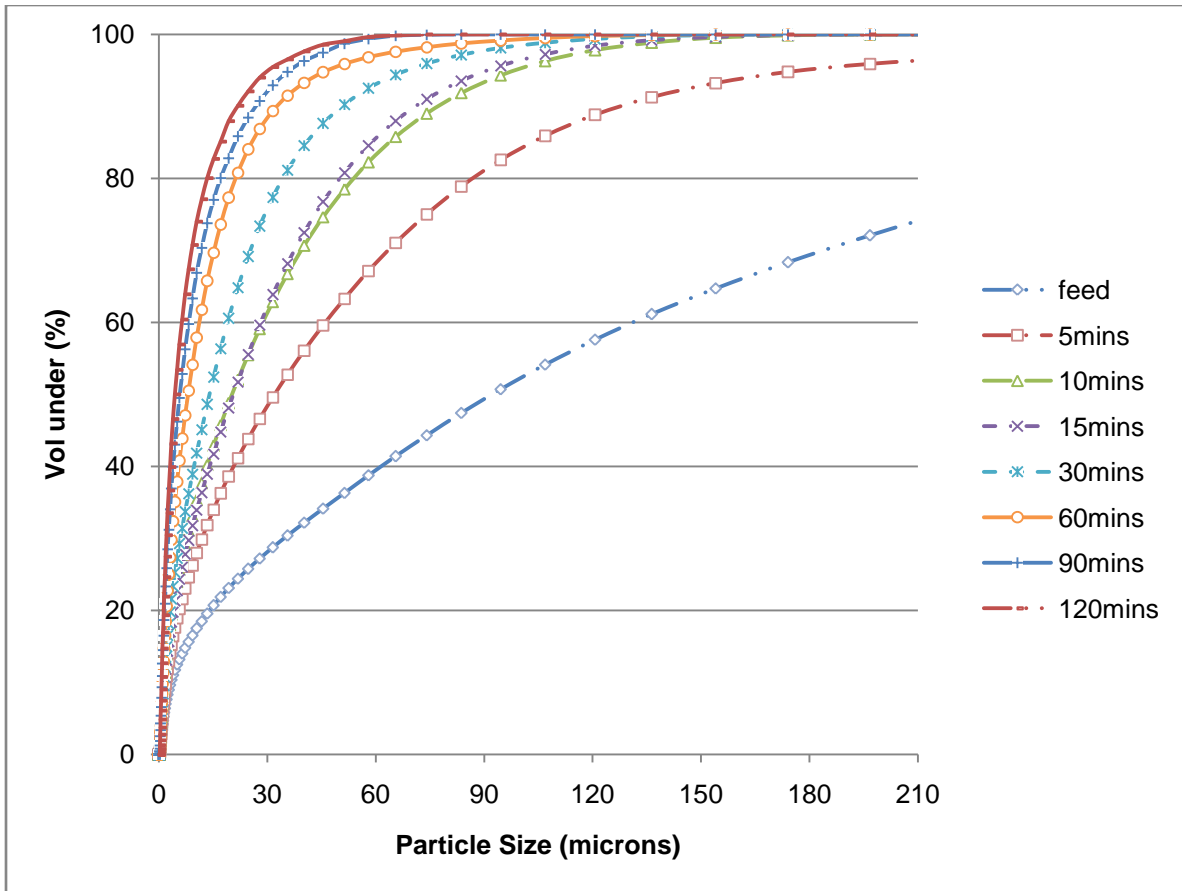


Figure A 3: A plot of volume percentage of material below particle size vs particle size for different grinding times with 33% solids content.

Table A 3: Size classification based on Figure A3

Grinding	Feed	Intermediate	Fines
Time	Size Class	Size Class	Size Class
0	0.6587	0.1346	0.2067
5	0.4042	0.2473	0.3485
10	0.3539	0.2790	0.3671
15	0.2327	0.3511	0.4162
30	0.1238	0.3526	0.5236
60	0.0527	0.2504	0.6969
90	0.0255	0.2046	0.7699
120	0.0144	0.1588	0.8268

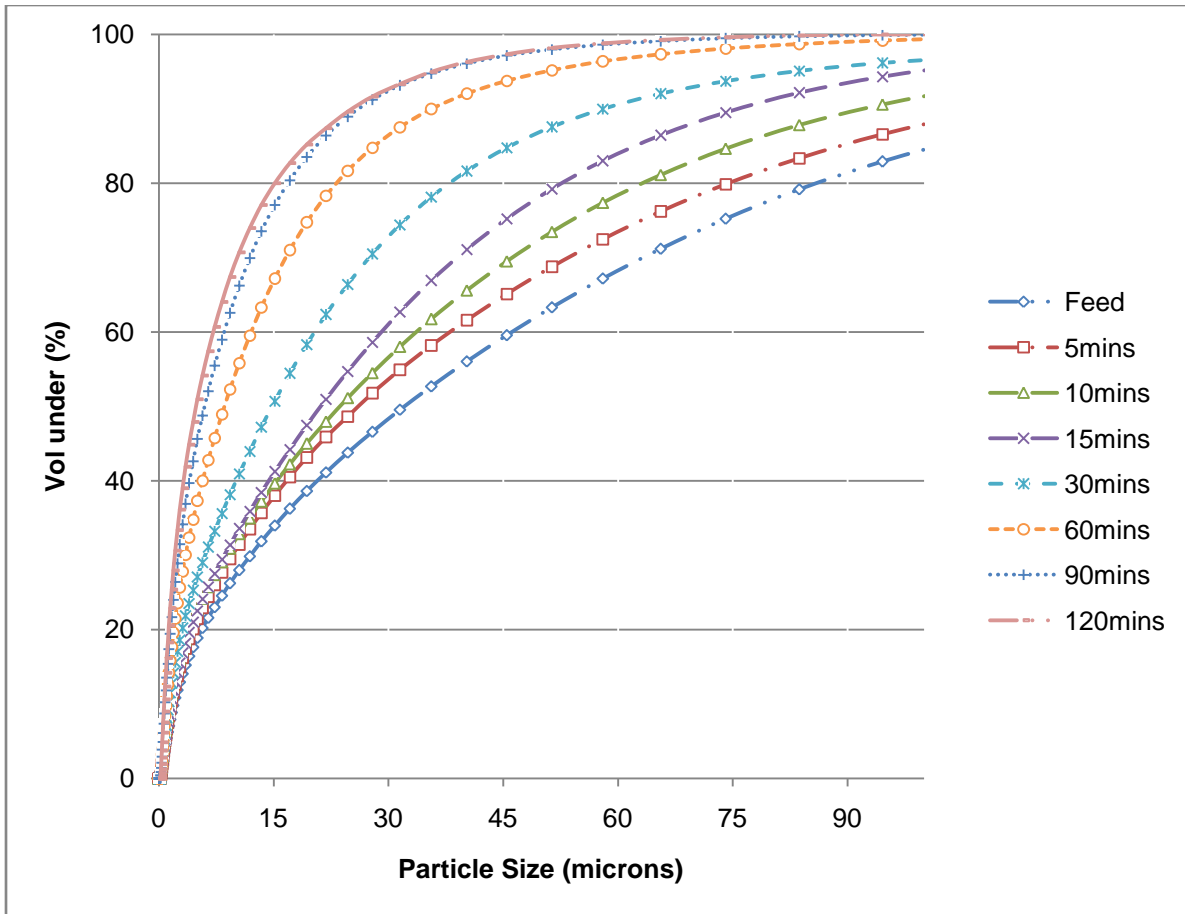


Figure A 4: A plot of volume percentage of material below particle size vs particle size for different grinding times with 25% solids content.

Table A 4: Size classification based on Figure A4

Grinding	Feed	Intermediate	Fines
Time	Size Class	Size Class	Size Class
0	0.6587	0.1346	0.2067
5	0.4042	0.2473	0.3485
10	0.3050	0.2986	0.3964
15	0.2477	0.3402	0.4121
30	0.1525	0.3405	0.5070
60	0.0625	0.2660	0.6715
90	0.0266	0.2030	0.7704
120	0.0266	0.1735	0.7999

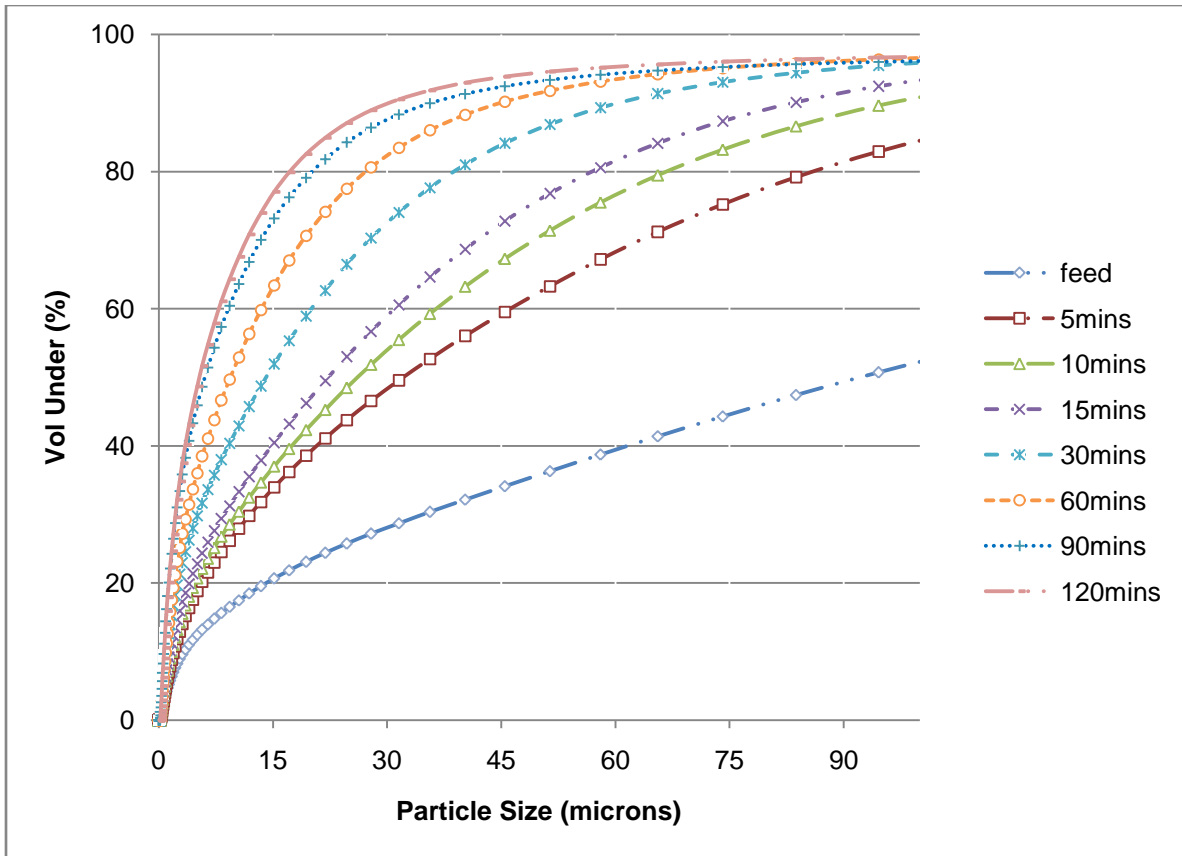


Figure A 5: A plot of volume percentage of material below particle size vs particle size for different grinding times with 20% solids content.

Table A 5: Size classification based on Figure A5

Grinding Time	Feed Size Class	Intermediate Size Class	Fines Size Class
0	0.6587	0.1346	0.2067
5	0.4042	0.2473	0.3485
10	0.3271	0.3026	0.3703
15	0.2721	0.3235	0.4044
30	0.1589	0.3219	0.5192
60	0.0981	0.2677	0.6342
90	0.0755	0.1928	0.7317
120	0.0617	0.1682	0.7701

Table A 6: Ratio of the natural logarithm of the mass fraction of material remaining in the feed size class after grinding time t, to the initial, with different solids content

t (mins)	100% Solids		50% Solids		33% Solids		25% Solids		20% Solids	
	m1	ln[m1(t)/m1(0)]	m1	ln[m1(t)/m1(0)]	m1	ln[m1(t)/m1(0)]	m1	ln[m1(t)/m1(0)]	m1	ln[m1(t)/m1(0)]
0	0.6587	0.0000	0.6587	0.0000	0.6587	0.0000	0.6587	0.0000	0.6587	0.0000
5	0.4340	-0.4172	0.4042	-0.4884	0.4042	-0.4884	0.4042	-0.4884	0.4042	-0.4884
10	0.4007	-0.4971	0.3468	-0.6415	0.3539	-0.6213	0.305	-0.7700	0.3271	-0.7000
15	0.3174	-0.7301	0.1856	-1.2667	0.2327	-1.0405	0.2477	-0.9780	0.2721	-0.8841
30	0.1304	-1.6197	0.1012	-1.8732	0.1238	-1.6716	0.1525	-1.4631	0.1589	-1.4220
60	0.0561	-2.4631	0.0241	-3.3081	0.0527	-2.5257	0.0625	-2.3551	0.0981	-1.9043
90	0.0269	-3.1981	0.0088	-4.3155	0.0255	-3.2516	0.0266	-3.2094	0.0755	-2.1661
120	0.0133	-3.9025	0.0088	-4.3155	0.0144	-3.8230	0.0266	-3.2094	0.0617	-2.3680

APPENDIX B: COMPARISON OF HETEROGENEOUS AND HOMOGENEOUS MODEL PARAMETERS

Table B 1: Excel solver estimated parameters for heterogeneous and homogeneous models for the feed size class with 100% solids content

φ	0.5620	φ	0.5620
S_{1A}	0.0873	S_1	0.0530
S_{1B}	0.0279	$m_1(0)$	0.6587
$m_1(0)$	0.6587		

Heterogeneous Model			Homogeneous Model		
t	$m_1(t)$	$m_1(t)^*$	diff	$m_1(t)^*$	diff
0	0.6587	0.6587	0.0000	0.6587	0.0000
5	0.4340	0.4902	-0.0562	0.5055	0.0715
10	0.4007	0.3729	0.0278	0.3880	-0.0128
15	0.3174	0.2897	0.0277	0.2977	-0.0197
30	0.1304	0.1518	-0.0214	0.1345	0.0041
60	0.0561	0.0560	0.0001	0.0275	-0.0286
90	0.0269	0.0235	0.0034	0.0056	-0.0213
120	0.0133	0.0101	0.0032	0.0011	-0.0122
SUMQ			0.0052		0.0071

Table B 2: Excel solver estimated parameters for heterogeneous and homogeneous models for 50% solids content

φ	0.5620	φ	0.5620
S_{1A}	0.1506	S_1	0.0699
S_{1B}	0.0393	$m_1(0)$	0.6587
$m_1(0)$	0.6587		

t (mins)	Heterogeneous Model			Homogeneous Model	
	$m_1(t)$	$m_1(t)^*$	diff	$m_1(t)^*$	diff
0	0.6587	0.6587	0.0000	0.6587	0.0000
5	0.4042	0.4114	-0.0072	0.4644	0.0602
10	0.3468	0.2769	0.0699	0.3275	-0.0193
15	0.1856	0.1988	-0.0132	0.2309	0.0453
30	0.1012	0.0929	0.0083	0.0809	-0.0203
60	0.0241	0.0274	-0.0033	0.0099	-0.0142
90	0.0088	0.0084	0.0004	0.0012	-0.0076
120	0.0088	0.0026	0.0062	0.0002	-0.0086
SUMSQ			0.0052		7.4821E-05

Table B 3: Excel solver estimated parameters for heterogeneous and homogeneous models for 33% solids content

φ	0.5620	φ	0.562021
S_{1A}	0.1506	S_1	0.06714
S_{1B}	0.0278	$m_1(0)$	0.6587
$m_1(0)$	0.6587		

Heterogeneous Model			Homogeneous Model		
t (mins)	$m_1(t)$	$m_1(t)^*$	diff	$m_1(t)^*$	diff
0	0.6587	0.6587	0.0000	0.6587	0.0000
5	0.4042	0.4255	-0.0213	0.4709	-0.0667
10	0.3539	0.3007	0.0532	0.3366	0.0173
15	0.2327	0.2289	0.0038	0.2406	-0.0080
30	0.1238	0.1295	-0.0057	0.0879	0.0359
60	0.0527	0.0546	-0.0019	0.0117	0.0410
90	0.0255	0.0237	0.0018	0.0016	0.0239
120	0.0144	0.0103	0.0041	0.0002	0.0142
SUMSQ			0.0034		0.0085

Table B 4: Excel solver estimated parameters for heterogeneous and homogeneous models for 25% solids content.

φ	0.5620	φ	0.5620
S_{1A}	0.1506	S_1	0.0680
S_{1B}	0.0229	$m_1(0)$	0.6587
$m_1(0)$	0.6587		

Heterogeneous Model			Homogeneous Model		
t (mins)	$m_1(t)$	$m_1(t)^*$	diff	$m_1(t)^*$	diff
0	0.6587	0.6587	0.0000	0.6587	0.0000
5	0.4042	0.4316	-0.0274	0.4688	0.0646
10	0.3050	0.3114	-0.0064	0.3336	0.0286
15	0.2477	0.2432	0.0045	0.2374	-0.0103
30	0.1525	0.1490	0.0035	0.0856	-0.0670
60	0.0625	0.0729	-0.0104	0.0111	-0.0514
90	0.0266	0.0366	-0.0100	0.0014	-0.0252
120	0.0266	0.0184	0.0082	0.0002	-0.0264
SUMSQ			0.0011		0.0135

Table B 5: Excel solver estimated parameters for heterogeneous and homogeneous models for 20% solids content.

ϕ	0.5620	ϕ	0.5620
S_{1A}	0.1506	S_1	0.0611
S_{1B}	0.0159	$m_1(0)$	0.6587
$m_1(0)$	0.6587		

Heterogeneous Model			Homogeneous Model		
t	$m_1(t)$	$m_1(t)^*$	diff	$m_1(t)^*$	diff
0	0.6587	0.6587	0.0000	0.6587	0.0000
5	0.4042	0.4408	-0.0366	0.4854	0.0812
10	0.3271	0.3281	-0.0010	0.3576	0.0305
15	0.2721	0.2659	0.0062	0.2635	-0.0086
30	0.1589	0.1830	-0.0241	0.1054	-0.0535
60	0.0981	0.1110	-0.0129	0.0169	-0.0812
90	0.0755	0.0688	0.0067	0.0027	-0.0728
120	0.0617	0.0427	0.0190	0.0004	-0.0613
SUMSQ			0.0025		0.0261

Table B 6: Excel solver estimated parameters for heterogeneous and homogeneous models for the intermediate size class with 20% solids content

m1(0)	0.6587	m1(0)	0.6587
m2(0)	0.1346	m2(0)	0.1346
ϕ	0.5620	S ₁	0.0638
S _{1A}	0.1506	b ₂₁	0.55768
S _{1B}	0.0159	S ₂	0.0118
b _{21A}	0.5624		
S _{2A}	0.0159		
S _{2B}	0.0115		
b _{21B}	0.9901		

Heterogeneous model				Homogeneous model	
Grinding	m2(t)	m2(t)*	Diff	m2(t)*	Diff
Time					
0	0.1346	0.1346	0.0000	0.1346	0.0000
5	0.2473	0.2521	-0.0048	0.2242	0.0231
10	0.3026	0.3036	-0.0010	0.2821	0.0205
15	0.3235	0.3237	-0.0002	0.3174	0.0061
30	0.3219	0.3209	0.0010	0.3448	-0.0229
60	0.2677	0.2683	-0.0006	0.2794	-0.0117
90	0.1928	0.2143	-0.0215	0.2019	-0.0091
120	0.1682	0.1669	0.0013	0.1428	0.0254
SUMSQ			0.0005		0.0024

Table B 7: Excel solver estimated parameters for heterogeneous and homogeneous models for the intermediate size class with 25% solids content

m1(0)	0.6587	m1(0)	0.6587
m2(0)	0.1346	m2(0)	0.1346
φ	0.5620	S ₁	0.097545
S _{1A}	0.1506	b ₂₁	0.460715
S _{1B}	0.0229	S ₂	0.00889
b _{21A}	0.5607		
S _{2A}	0.0159		
S _{2B}	0.0116		
b _{21B}	0.7852		

Heterogeneous model				Homogeneous model	
Grinding	m2(t)	m2(t)*	Diff	m2(t)*	Diff
Time					
0	0.1346	0.1346	0.0000	0.1346	0.0000
5	0.2473	0.2544	-0.0071	0.2431	0.0042
10	0.2986	0.3072	-0.0086	0.3028	-0.0042
15	0.3402	0.3278	0.0124	0.3327	0.0075
30	0.3405	0.3231	0.0174	0.3409	-0.0004
60	0.2660	0.2602	0.0058	0.2739	-0.0079
90	0.2030	0.1970	0.0060	0.2104	-0.0074
120	0.1735	0.1446	0.0289	0.1612	0.0123
SUMSQ			0.0015		0.0004

Table B 8: Excel solver estimated parameters for heterogeneous and homogeneous models for the intermediate size class with 33% solids content

m1(0)	0.6587	m1(0)	0.6587
m2(0)	0.1346	m2(0)	0.1346
φ	0.5620	S ₁	0.1002
S _{1A}	0.1506	b ₂₁	0.4620
S _{1B}	0.0278	S ₂	0.0093
b _{21A}	0.5000		
S _{2A}	0.0159		
S _{2B}	0.0117		
b _{21B}	0.8867		

Heterogeneous model				Homogeneous model	
Grinding	m2(t)	m2(t)*	Diff	m2(t)*	Diff
Time					
0	0.1346	0.1346	0.0000	0.1346	0.0000
5	0.2473	0.2513	-0.0040	0.2454	0.0019
10	0.2790	0.3059	-0.0269	0.3051	-0.0261
15	0.3511	0.3298	0.0213	0.3341	0.0170
30	0.3526	0.3334	0.0192	0.3387	0.0139
60	0.2504	0.2732	-0.0228	0.2677	-0.0173
90	0.2046	0.2056	-0.0010	0.2028	0.0018
120	0.1588	0.1488	0.0100	0.1533	0.0055
SUMSQ			0.0022		0.0015

Table B 9: Excel solver estimated parameters for heterogeneous and homogeneous models for the intermediate size class with 50% solids content

m1(0)	0.6587	m1(0)	0.6587
m2(0)	0.1346	m2(0)	0.1346
φ	0.5620	S ₁	0.1067
S _{1A}	0.1506	b ₂₁	0.4884
S _{1B}	0.0393	S ₂	0.0142
b _{21A}	0.5751		
S _{2A}	0.0159		
S _{2B}	0.0140		
b _{21B}	0.5013		

Heterogeneous model				Homogeneous model	
Grinding	m2(t)	m2(t)*	Diff	m2(t)*	Diff
Time					
0	0.1346	0.1346	0.0000	0.1346	0.0000
5	0.2473	0.2574	-0.0101	0.2534	-0.0061
10	0.2828	0.3096	-0.0268	0.3111	-0.02830
15	0.3476	0.3274	0.0202	0.3338	0.0138
30	0.3346	0.3090	0.0256	0.3152	0.0194
60	0.2073	0.2216	-0.0143	0.2152	-0.0079
90	0.1502	0.1486	0.0016	0.1409	0.0093
120	0.0782	0.0971	-0.0189	0.0921	-0.0139
SUMSQ			0.0024		0.0017

Table B 10: Excel solver estimated parameters for heterogeneous and homogeneous models for the intermediate size class with 100% solids content

m1(0)	0.6587	m1(0)	0.6587
m2(0)	0.1346	m2(0)	0.1346
φ	0.562021	S ₁	0.071586
S _{1A}	0.087287	b ₂₁	0.360179
S _{1B}	0.02792	S ₂	0.006233
b _{21A}	0.474529		
S _{2A}	0.004887		
S _{2B}	0.013827		
b _{21B}	0.335803		

Heterogeneous model			Homogeneous model		
Grinding	m2	m2(t)*	diff	m2(t)*	diff
Time					
0	0.1346	0.1346	0	0.1346	0
5	0.2205	0.202344	-0.01816	0.200687	-0.01981
10	0.2318	0.244826	0.013026	0.243619	0.011819
15	0.2661	0.270624	0.004524	0.270464	0.004364
30	0.2996	0.295121	-0.00448	0.296854	-0.00275
60	0.2695	0.267728	-0.00177	0.26785	-0.00165
90	0.224	0.225254	0.001254	0.224693	0.000693
120	0.1862	0.186611	0.000411	0.186666	0.000466
			0.000545		0.000562

APPENDIX C: PARTICLE SIZE DISTRIBUTION (PSD) AND ATOMIC ABSORPTION SPECTROMETER (AAS) RESULTS

Table C 1: PSD data for the feed sample

screen size (μm)	mass retained (g)	mass % retained	cum mass passing (g)	cum mass% passing
0	31.84	31.74	0.00	0.00
38	14.09	14.04	31.84	31.74
53	13.33	13.29	45.93	45.78
75	13.16	13.12	59.26	59.07
106	11.07	11.03	72.42	72.18
150	10.65	10.61	83.49	83.22
212	3.22	3.21	94.14	93.83
300	1.54	1.53	97.36	97.04
425	1.43	1.43	98.90	98.57
Total	100.33	100		

Table C 2: PSD data for the sample after 10mins of grinding

screen size (μm)	mass retained (g)	mass % retained	cum mass passing (g)	cum mass% passing
0	49.92	49.92	0.00	0.00
38	16.54	16.54	49.92	49.92
53	13.5	13.5	66.46	66.46
75	9.45	9.45	79.96	79.96
106	5.19	5.19	89.41	89.41
150	3.16	3.16	94.6	94.60
212	1.15	1.15	97.76	97.76
300	0.56	0.56	98.91	98.91
425	0.53	0.53	99.47	99.47
Total	100	100		

Table C 3: PSD data for the sample after 30mins of grinding

screen size (µm)	mass retained (g)	mass % retained	cum mass passing (g)	cum mass% passing
0	57.90	57.89	0.00	0.00
38	26.52	26.51	57.90	57.89
53	6.62	6.62	84.42	84.40
75	5.27	5.27	91.04	91.02
106	1.68	1.68	96.31	96.29
150	1.06	1.06	97.99	97.97
212	0.46	0.46	99.05	99.03
300	0.27	0.27	99.51	99.49
425	0.24	0.24	99.78	99.76
Total	100.02	100		

Table C 4: AAS results for the feed samples

Screen size	Mass retained (g)	Mass of sample digested (g)	C1 (ppm)	C2 (ppm)	Average conc (ppm)	Mass of copper in digested sample(g)	Mass % of copper in digested sample	Mass of copper in retained sample (g)	Mass % of copper in retained sample
0	31.84	1.012	9.16	9.19	9.18	0.00092	0.09	2.889	9.07
38	14.09	1.003	5.07	5.05	5.06	0.00051	0.05	0.711	5.04
53	13.33	1.000	4.21	4.20	4.21	0.00042	0.04	0.561	4.21
75	13.16	1.002	2.65	2.65	2.65	0.00027	0.03	0.348	2.64
106	11.07	1.001	1.99	2.00	2.00	0.00020	0.02	0.221	1.99
150	10.65	1.000	1.49	1.51	1.50	0.00015	0.02	0.160	1.50
212	3.22	1.001	1.27	1.25	1.26	0.00013	0.01	0.041	1.26
300	1.54	1.002	1.24	1.24	1.24	0.00012	0.01	0.019	1.24
425	1.43	1.002	1.20	1.20	1.20	0.00012	0.01	0.017	1.20
Total	100.33					0.00283		4.963	

Table C 5: AAS results for the samples after 10 minutes of grinding

Screen size	Mass retained (g)	Mass of sample digested (g)	C1 (ppm)	C2 (ppm)	Average conc (ppm)	Mass of copper in digested sample(g)	Mass % of copper in digested sample	Mass of copper in retained sample(g)	Mass % of copper in retained sample
0	49.92	1.002	8.20	8.30	8.25	0.00083	0.08	4.110	8.23
38	16.54	1.000	3.50	3.51	3.51	0.00035	0.04	0.580	3.51
53	13.50	1.001	2.23	2.22	2.23	0.00022	0.02	0.300	2.22
75	9.45	1.000	1.70	1.70	1.70	0.00017	0.02	0.161	1.70
106	5.19	1.001	1.59	1.58	1.59	0.00016	0.02	0.082	1.58
150	3.16	1.000	1.50	1.60	1.55	0.00016	0.02	0.049	1.55
212	1.15	1.001	1.50	1.50	1.50	0.00015	0.01	0.017	1.50
300	0.56	0.487	0.77	0.77	0.77	0.00008	0.02	0.009	1.58
425	0.53	0.482	0.69	0.69	0.69	0.00007	0.01	0.008	1.43
Total	100					0.00218		5.315	

Table C 6: AAS results for the samples after 30 minutes of grinding

Screen size	Mass retained (g)	Mass of sample digested (g)	C1 (ppm)	C2 (ppm)	Average conc (ppm)	Mass of copper in digested sample(g)	Mass % of copper in digested sample	Mass of copper in retained sample (g)	Mass % of copper in retained sample
0	57.90	1.001	7.40	7.50	7.45	0.00075	0.07	4.309	7.44
38	26.52	1.000	3.28	3.27	3.28	0.00033	0.03	0.869	3.28
53	6.62	1.001	2.34	2.33	2.34	0.00023	0.02	0.154	2.33
75	5.27	1.001	2.16	2.15	2.16	0.00022	0.02	0.113	2.15
106	1.68	1.001	2.34	2.33	2.34	0.00023	0.02	0.039	2.33
150	1.06	0.902	2.16	2.15	2.16	0.00022	0.02	0.025	2.39
212	0.46	0.398	0.98	0.97	0.98	0.00010	0.02	0.011	2.45
300	0.27	0.271	0.54	0.54	0.54	0.00005	0.02	0.005	1.99
425	0.24	0.226	0.37	0.37	0.37	0.00004	0.02	0.004	1.64
Total	100.02					0.00216		5.531	

APPENDIX D: MILL ENERGY CONSUMPTION DURING MILLING

Table D 1: Energy used for grinding with 50% solids content

Grinding times (mins)	0	5	10	15	30	60	90	120
Speed setting	0	60	60	60	60	60	60	60
Actual speed (RPM)	0	68.2855	68.2855	68.2855	68.2855	68.2855	68.2855	68.2855
Voltage	0	4.7167	4.7167	4.7167	4.7167	4.7167	4.7167	4.7167
Torque	0	-5.7125	-5.7125	-5.7125	-5.7125	-5.7125	-5.7125	-5.7125
Gross power	0	-40.8678	-40.8678	-40.8678	-40.8678	-40.8678	-40.8678	-40.8678
No load power	0	-3.9950	-3.9950	-3.9950	-3.9950	-3.9950	-3.9950	-3.9950
Net power	0	36.8728	36.8728	36.8728	36.8728	36.8728	36.8728	36.8728
Energy used (kJ)	0	11.0619	22.1237	33.1855	66.3711	132.7422	199.1132	265.4843

Table D 2: Energy used for grinding with 33% solids content

Grinding times (mins)	0	5	10	15	30	60	90	120
Speed setting	0	60	60	60	60	60	60	60
Actual speed (RPM)	0	68.2855	68.2855	68.2855	68.2855	68.2855	68.2855	68.2855
Voltage	0	4.5979	4.5979	4.5979	4.5979	4.5979	4.5979	4.5979
Torque	0	-5.1906	-5.1906	-5.1906	-5.1906	-5.1906	-5.1906	-5.1906
Gross power	0	-37.1337	-37.1337	-37.1337	-37.1337	-37.1337	-37.1337	-37.1337
No load power	0	-3.7245	-3.7245	-3.7245	-3.7245	-3.7245	-3.7245	-3.7245
Net power	0	33.4093	33.4093	33.4093	33.4093	33.4093	33.4093	33.4093
Energy used (kJ)	0	10.0228	20.0456	30.0684	60.1367	120.2734	180.4101	240.5468

Table D 3: Energy used for grinding with 25% solids content

Grinding times (mins)	0	5	10	15	30	60	90	120
Speed setting	0	60	60	60	60	60	60	60
Actual speed (RPM)	0	68.2855	68.2855	68.2855	68.2855	68.2855	68.2855	68.2855
Voltage	0	4.5810	4.5810	4.5810	4.5810	4.5810	4.5810	4.5810
Torque	0	-5.1164	-5.1164	-5.1164	-5.1164	-5.1164	-5.1164	-5.1164
Gross power	0	-36.6027	-36.6027	-36.6027	-36.6027	-36.6027	-36.6027	-36.6027
No load power	0	-3.9522	-3.9522	-3.9522	-3.9522	-3.9522	-3.9522	-3.9522
Net power	0	32.6505	32.6505	32.6505	32.6505	32.6505	32.6505	32.6505
Energy used (kJ)	0	9.7952	19.5903	29.3855	58.7710	117.5419	176.3129	235.0839

Table D 4: Energy used for grinding with 20% solids content

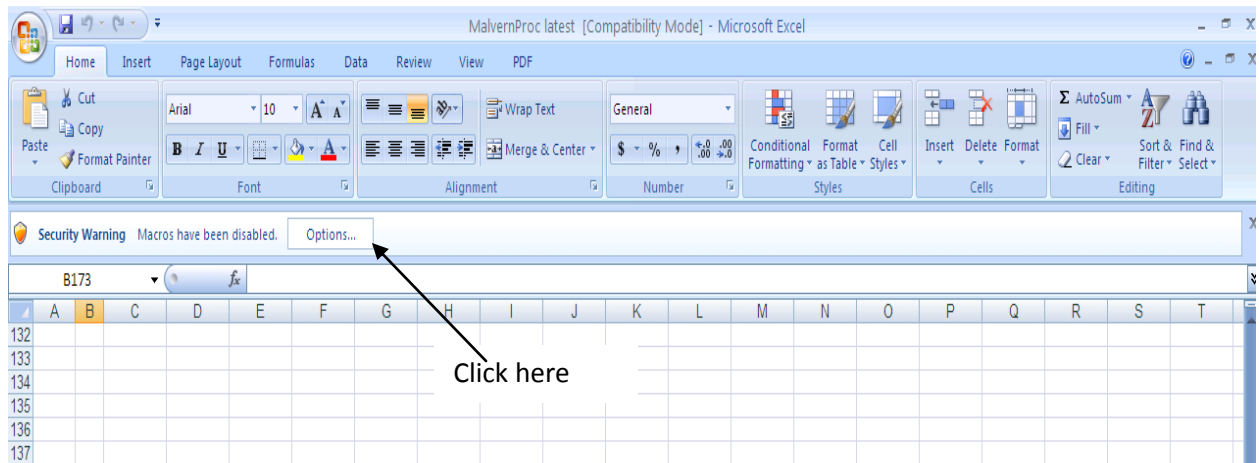
Grinding times (mins)	0	5	10	15	30	60	90	120
Speed setting	0	60	60	60	60	60	60	60
Actual Speed (RPM)	0	68.2855	68.2855	68.2855	68.2855	68.2855	68.2855	68.2855
Voltage	0	4.5662	4.5662	4.5662	4.5662	4.5662	4.5662	4.5662
Torque	0	-5.0515	-5.0515	-5.0515	-5.0515	-5.0515	-5.0515	-5.0515
Gross power	0	-36.1389	-36.1389	-36.1389	-36.1389	-36.1389	-36.1389	-36.1389
No load power	0	-3.9825	-3.9825	-3.9825	-3.9825	-3.9825	-3.9825	-3.9825
Net Power	0	32.1564	32.1564	32.1564	32.1564	32.1564	32.1564	32.1564
Energy used (kJ)	0	9.6469	19.2938	28.9407	57.8814	115.7628	173.6443	231.5257

APPENDIX E: THE AR PROGRAMME OPERATING PROCEDURE

Consider a feed (-600 μ m) of 500g mass of pre-milled platinum ore charged into a 0.302 by 0.295m mill run at 80% of the critical speed. 7.8kg (fractional ball filling of 8.2%) of single sized 10mm stainless steel balls used as grinding media. The mill is run for grinding times ranging from 5 to 120 minutes. After each specific test grind time, the mill contents are emptied followed by separation of the product slurry from the grinding media, on a wire mesh. The milled product is analyzed in a Malvern Hydro 2000MU particle size analyzer and classified into three size classes. The feed size class chosen to be the mass fraction of material for particle sizes above 45-microns in diameter, the intermediate size class as the mass fraction of material for particle sizes between 15 and 45-microns and the fines size class as the mass fraction for particle sizes below 15-microns. Outlined below is a step by step procedure of how to operate the programme to get an example AR plot.

Prepare the data source file in the same format as one shown in Appendix F. This is a volume below based cumulative data file. The first column shows the particle size classes, and subsequent columns show the cumulative volume percent of material below a certain size for different periods of grinding starting from the feed material.

1. Double click the 'AR Software' workbook to access the program. Enable 'Macros' by clicking on the 'Options' tab on the Information bar and selecting the 'Enable this content' box and Ok. Userform1 inter-phase appears on the screen.



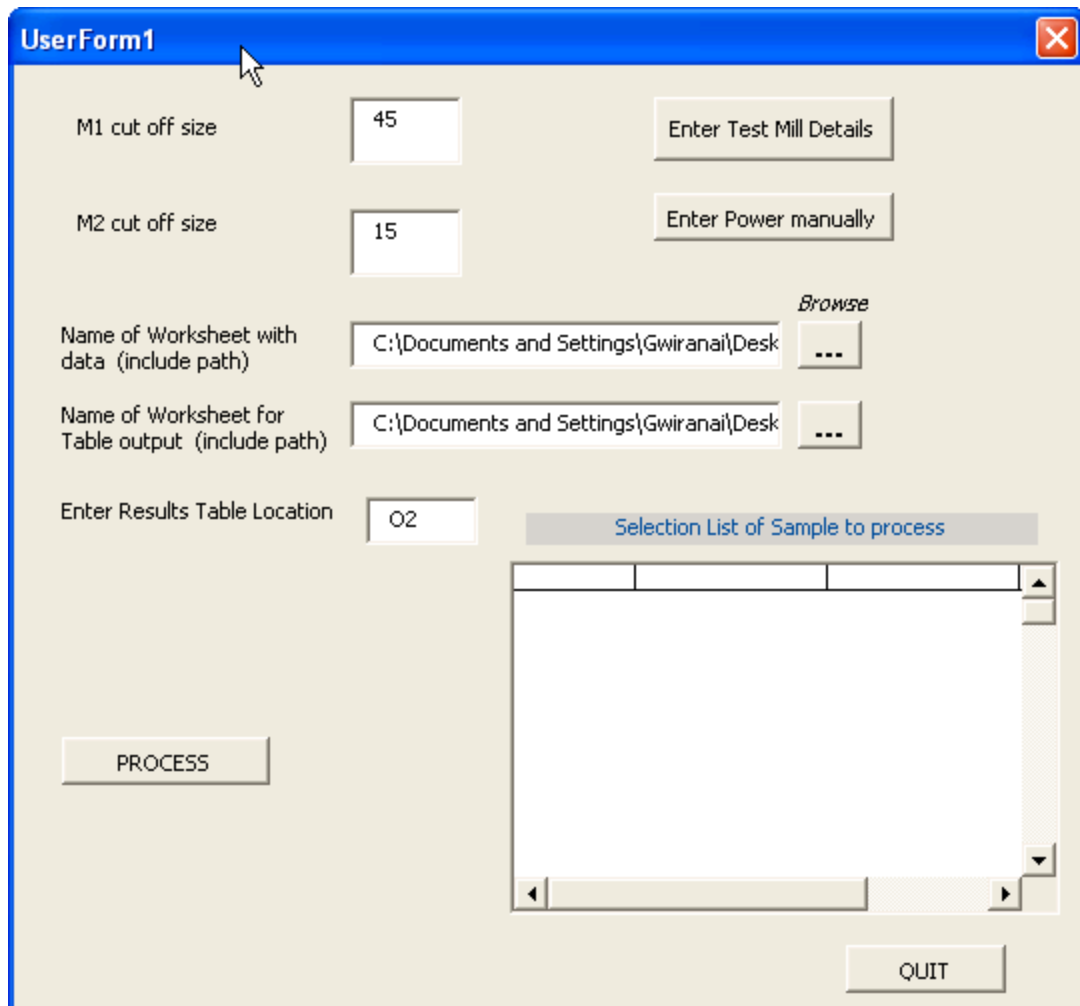


Figure E 1: Userform1 inter-phase

2. Specify the M1 (feed size class) and M2 (intermediate size class) separation size or cut off points.
3. Some laboratory scale ball mills can record power, if that is your case, then 'Enter power manually'.
4. Otherwise, if you want the programme to calculate power, click the 'Enter test mill details' box and specify the mill, feed material and operating parameters. After entering test mill details, click 'Back to Main' tab, to go back to userForm1.

Parameter	Value	Parameter	Value
Mill Diameter (m)	0.457	Mill Length (m)	0.381
% Mill Fill (J)	35	% of Nc	74
% Solids in Slurry	100	Ball Density (kg/m ³)	7750
Sample Mass (kg)	11.1	Sample Density (kg/m ³)	2800
Estimated Lift Angle	35		
Voidage	Charge: 0.4	Sample: 0.4	

Figure E 2: Mill details inter-phase

5. 'Browse' and double click on the name of worksheet with data to be processed.
Here, you are loading the data source file
6. 'Browse' and double click on the name of worksheet for table output or where results will be exported to.
7. 'Enter results table location'. This specifies the cell where you want the results table to appear.
8. Click two times in the white space under 'selection list of samples to 'process' and highlight the samples you want processed.

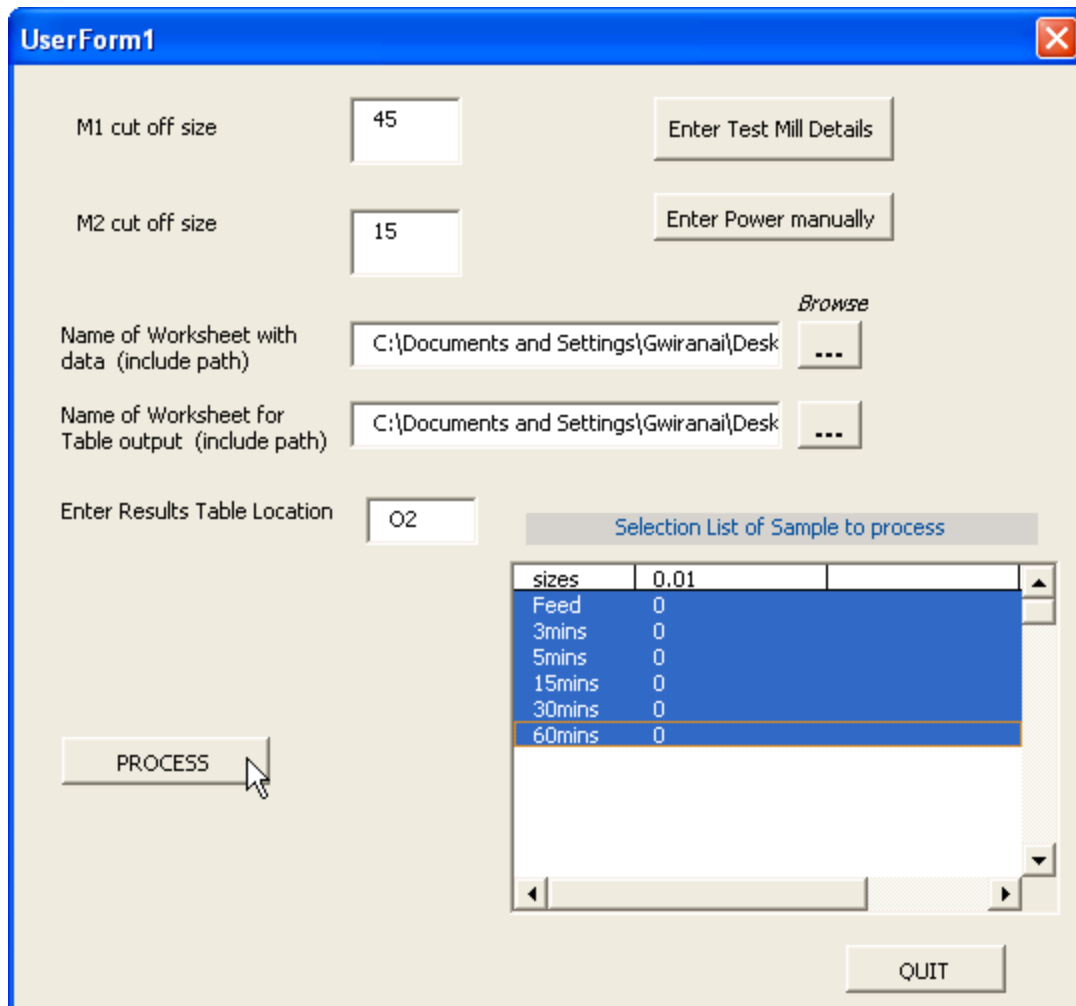


Figure E 3: Userform1 inter-phase with selected samples to be processed

9. Process the data by clicking the 'process' knob
10. Quit the programme and view the results output in the worksheet you specified in procedure number 7.
11. You can use the results table to draw the AR plots.

APPENDIX F: DATA SOURCE FILE

Sizes	Feed	5mins	10mins	15mins	30mins	60mins	90mins	120mins
0.01	0	0	0	0	0	0	0	0
0.011	0	0	0	0	0	0	0	0
0.013	0	0	0	0	0	0	0	0
0.014	0	0	0	0	0	0	0	0
0.016	0	0	0	0	0	0	0	0
0.018	0	0	0	0	0	0	0	0
0.021	0	0	0	0	0	0	0	0
0.024	0	0	0	0	0	0	0	0
0.027	0	0	0	0	0	0	0	0
0.03	0	0	0	0	0	0	0	0
0.034	0	0	0	0	0	0	0	0
0.038	0	0	0	0	0	0	0	0
0.043	0	0	0	0	0	0	0	0
0.049	0	0	0	0	0	0	0	0
0.055	0	0	0	0	0	0	0	0
0.062	0	0	0	0	0	0	0	0
0.07	0	0	0	0	0	0	0	0
0.08	0	0	0	0	0	0	0	0

0.09	0	0	0	0	0	0	0	0
0.102	0	0	0	0	0	0	0	0
0.115	0	0	0	0	0	0	0	0
0.13	0	0	0	0	0	0	0	0
0.147	0	0	0	0	0	0	0	0
0.166	0	0	0	0	0	0	0	0
0.187	0	0.05	0.07	0.05	0.01	0.07	0.14	0.13
0.211	0.06	0.16	0.19	0.17	0.29	0.25	0.49	0.49
0.239	0.18	0.35	0.4	0.39	0.63	0.62	1.03	1.05
0.27	0.34	0.61	0.68	0.68	1.09	1.14	1.77	1.84
0.305	0.54	0.93	1.03	1.05	1.66	1.83	2.71	2.86
0.345	0.78	1.32	1.44	1.49	2.35	2.66	3.83	4.1
0.389	1.06	1.76	1.91	2	3.14	3.65	5.13	5.53
0.44	1.36	2.26	2.44	2.57	4.03	4.76	6.59	7.16
0.497	1.69	2.8	3.01	3.2	5	6	8.19	8.95
0.561	2.05	3.4	3.63	3.89	6.05	7.35	9.91	10.9
0.634	2.43	4.03	4.3	4.62	7.18	8.81	11.74	12.97
0.717	2.84	4.71	5.01	5.41	8.38	10.35	13.67	15.17
0.81	3.27	5.43	5.76	6.24	9.64	11.99	15.69	17.46
0.915	3.72	6.2	6.55	7.13	10.98	13.72	17.79	19.85
1.034	4.2	7.01	7.4	8.07	12.39	15.54	19.98	22.33

1.168	4.71	7.88	8.29	9.06	13.87	17.44	22.23	24.88
1.32	5.24	8.79	9.23	10.11	15.43	19.43	24.56	27.5
1.491	5.8	9.75	10.23	11.22	17.05	21.5	26.94	30.17
1.684	6.39	10.77	11.27	12.38	18.75	23.63	29.37	32.87
1.903	7.01	11.82	12.36	13.6	20.5	25.83	31.84	35.58
2.15	7.64	12.92	13.48	14.85	22.3	28.06	34.32	38.28
2.429	8.29	14.05	14.63	16.15	24.14	30.32	36.8	40.95
2.745	8.96	15.2	15.81	17.48	26.01	32.59	39.26	43.56
3.101	9.64	16.38	17.01	18.83	27.9	34.86	41.69	46.12
3.503	10.33	17.58	18.23	20.22	29.81	37.13	44.1	48.62
3.958	11.02	18.79	19.47	21.63	31.74	39.39	46.47	51.06
4.472	11.73	20.03	20.73	23.07	33.69	41.64	48.81	53.46
5.053	12.46	21.29	22.02	24.55	35.67	43.91	51.15	55.84
5.709	13.2	22.58	23.34	26.08	37.7	46.19	53.48	58.23
6.45	13.98	23.93	24.72	27.68	39.78	48.51	55.84	60.66
7.287	14.79	25.33	26.16	29.36	41.92	50.89	58.26	63.14
8.233	15.63	26.8	27.68	31.13	44.15	53.35	60.75	65.72
9.302	16.53	28.35	29.28	33.01	46.47	55.91	63.34	68.4
10.51	17.48	30	30.99	34.99	48.9	58.58	66.05	71.19
11.874	18.48	31.75	32.8	37.1	51.46	61.39	68.89	74.09
13.416	19.55	33.6	34.72	39.32	54.15	64.34	71.85	77.05

15.157	20.67	35.55	36.75	41.65	57	67.44	74.91	80.05
17.125	21.85	37.59	38.87	44.11	60	70.65	78.02	83.02
19.348	23.09	39.72	41.1	46.67	63.17	73.97	81.14	85.9
21.86	24.39	41.93	43.43	49.36	66.49	77.32	84.18	88.61
24.698	25.75	44.21	45.86	52.17	69.93	80.66	87.09	91.09
27.904	27.19	46.55	48.4	55.11	73.46	83.9	89.78	93.28
31.527	28.72	48.95	51.06	58.18	77	86.97	92.18	95.13
35.62	30.37	51.42	53.85	61.4	80.49	89.78	94.25	96.65
40.244	32.16	53.96	56.8	64.76	83.84	92.27	95.96	97.82
45.469	34.13	56.6	59.93	68.26	86.96	94.39	97.31	98.67
51.371	36.31	59.34	63.24	71.85	89.78	96.13	98.32	99.26
58.041	38.73	62.19	66.72	75.49	92.24	97.48	99.04	99.63
65.575	41.39	65.16	70.34	79.11	94.3	98.49	99.51	99.85
74.089	44.29	68.23	74.03	82.61	95.95	99.18	99.79	99.95
83.707	47.41	71.35	77.71	85.9	97.21	99.63	99.94	100
94.574	50.7	74.47	81.26	88.85	98.1	99.88	99.99	100
106.85	54.11	77.52	84.57	91.4	98.67	99.98	100	100
120.72	57.59	80.44	87.55	93.47	99	100	100	100
136.4	61.12	83.15	90.12	95.06	99.1	100	100	100
154.1	64.7	85.61	92.23	96.19	99.12	100	100	100
174.11	68.33	87.8	93.9	96.93	99.19	100	100	100

196.71	72.06	89.72	95.16	97.35	99.31	100	100	100
222.25	75.9	91.38	96.09	97.58	99.45	100	100	100
251.11	79.84	92.83	96.76	97.7	99.6	100	100	100
283.7	83.84	94.1	97.27	97.81	99.75	100	100	100
320.54	87.78	95.23	97.68	97.96	99.87	100	100	100
362.15	91.49	96.26	98.07	98.21	99.95	100	100	100
409.16	94.76	97.22	98.48	98.54	99.99	100	100	100
462.28	97.37	98.11	98.91	98.95	100	100	100	100
522.3	99.16	98.88	99.34	99.37	100	100	100	100
590.1	99.98	99.5	99.71	99.74	100	100	100	100
666.71	100	99.95	99.97	99.98	100	100	100	100
753.27	100	100	100	100	100	100	100	100
851.06	100	100	100	100	100	100	100	100
961.54	100	100	100	100	100	100	100	100
1086.4	100	100	100	100	100	100	100	100
1227.4	100	100	100	100	100	100	100	100
1386.8	100	100	100	100	100	100	100	100
1566.8	100	100	100	100	100	100	100	100
1770.2	100	100	100	100	100	100	100	100
2000	100	100	100	100	100	100	100	100